

WL-TR-93-2099

AD-A274 149



**Spectroscopy and Dynamics of  
Molecular and Ionic Impurities  
Embedded In Solid Hydrogen**



Takeshi Oka  
Professor of Chemistry and  
Astronomy and Astrophysics  
The University of Chicago  
5735 S. Ellis Avenue  
Chicago, IL 60637

DTIC

DEC 23 1993

August 1993

Final Report for 13 April 1990 - 12 April 1993

Approved for public release; distribution is unlimited

Aero Propulsion & Power Directorate  
Wright Laboratory  
Air Force Materiel Command  
Wright-Patterson Air Force Base, Ohio 45433-7650

93-30740



93 12 21 087

**Best  
Available  
Copy**

## NOTICE

When Government drawings, specifications, or other data are used for any purpose other than in connection with a definitely Government-related procurement, the United States Government incurs no responsibility or any obligation whatsoever. The fact that the government may have formulated or in any way supplied the said drawings, specifications, or other data, is not to be regarded by implication, or otherwise in any manner construed, as licensing the holder, or any other person or corporation; or as conveying any rights or permission to manufacture, use, or sell any patented invention that may in any way be related thereto.

This report is releasable to the National Technical Information Service (NTIS). At NTIS, it will be available to the general public, including foreign nations.

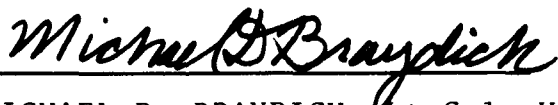
This technical report has been reviewed and is approved for publication.



ALAN GARSCADDEN  
Research Physicist  
Advanced Plasma Research Section  
Power Components Branch  
Aerospace Power Division  
Aero Propulsion and Power Directorate



JERRELL M. TURNER  
Chief, Advanced Plasma Research Section  
Power Components Branch  
Aerospace Power Division  
Aero Propulsion and Power Directorate



MICHAEL D. BRAYDICH, Lt Col, USAF  
Deputy Chief  
Aerospace Power Division

If your address has changed, if you wish to be removed from our mailing list, or if the addressee is no longer employed by your organization please notify WL/POOC, WPAFB, OH 45433-6563 to help us maintain a current mailing list.

Copies of this report should not be returned unless return is required by security considerations, contractual obligations, or notice on a specific document.

REPORT DOCUMENTATION PAGE			Form Approved OMB No. 0704-0188	
<small>Public reporting burden for this collection of information is estimated to average 1 hour per response, including the time for reviewing instructions, searching existing data sources, gathering and maintaining the data needed, and completing and reviewing the collection of information. Send comments regarding this burden estimate or any other aspect of this collection of information, including suggestions for reducing this burden, to Washington Headquarters Services, Directorate for Information Operations and Reports, 1215 Jefferson Davis Highway, Suite 1204, Arlington, VA 22202-4302, and to the Office of Management and Budget, Paperwork Reduction Project (0704-0188), Washington, DC 20503.</small>				
1. AGENCY USE ONLY (Leave blank)	2. REPORT DATE SEPT 1993	3. REPORT TYPE AND DATES COVERED Final, 4/13/90 --04/12/93		
4. TITLE AND SUBTITLE  Spectroscopy and Dynamics of Molecular and Ionic Impurities Embedded in Solid Hydrogen		5. FUNDING NUMBERS  C F33615-90-C-2035 PE 61102F PR 2301 TA S2 WU 10		
6. AUTHOR(S)  Takeshi Oka				
7. PERFORMING ORGANIZATION NAME(S) AND ADDRESS(ES)  Department of Chemistry University of Chicago 5735 S. Ellis Avenue Chicago, IL 60637		8. PERFORMING ORGANIZATION REPORT NUMBER		
9. SPONSORING / MONITORING AGENCY NAME(S) AND ADDRESS(ES)  Aero Propulsion and Power Directorate Wright Laboratory Air Force Materiel Command Wright-Patterson Air Force Base, OH 45433-6553		10. SPONSORING / MONITORING AGENCY REPORT NUMBER  WL-TR-93-2099		
11. SUPPLEMENTARY NOTES				
12a. DISTRIBUTION / AVAILABILITY STATEMENT  Approved for public release; distribution unlimited		12b. DISTRIBUTION CODE		
13. ABSTRACT (Maximum 200 words)  The research involved high resolution infrared spectroscopy to measure 1.) the crystalline field and intermolecular interactions in solid hydrogen coupled with a variety of methods (bombardment by high energy electrons and gamma-ray irradiation) to energize and ionize solid hydrogen and obtain solid plasmas. Simultaneous absorption and stimulated Raman measurements are reported. 2.) the infrared spectrum of the trimer hydrogen ion (protonated hydrogen). A review was completed of the spectroscopy of H <sub>3</sub> <sup>+</sup> and of its occurrence and importance in laboratory and space plasmas.				
14. SUBJECT TERMS Condensed Phase Spectroscopy, Parahydrogen Intermolecular Interactions, Infrared Spectroscopy Trimer Hydrogen Ion, Space Plasmas			15. NUMBER OF PAGES 73	
			16. PRICE CODE	
17. SECURITY CLASSIFICATION OF REPORT  Unclassified	18. SECURITY CLASSIFICATION OF THIS PAGE  Unclassified	19. SECURITY CLASSIFICATION OF ABSTRACT  Unclassified	20. LIMITATION OF ABSTRACT  Unclassified	

## TABLE OF CONTENTS

<b>1. INTRODUCTION .....</b>	<b>1</b>
<b>2. CRYSTALLINE FIELD AND INTERMOLECULAR INTERACTION .....</b>	<b>5</b>
2.1. $W_0(0)$ Transition and Crystal Field Splitting .....	5
2.2. $Q_1(1)$ Transitions and Pair Splitting .....	6
2.3. $W_1(0)$ Transitions and Pair Splitting .....	7
<b>3. PURE VIBRATIONAL SPECTRUM <math>Q_1(0)</math> .....</b>	<b>8</b>
3.1. Stimulated Raman Spectroscopy .....	8
3.2. $D_2$ Impurity Spectroscopy .....	10
3.3. Electric Field Induced Spectroscopy and Stark Modulation .....	11
<b>4. ENERGY TRANSFER IN SOLID HYDROGEN .....</b>	<b>13</b>
4.1. Exciton Band ; Energy Exchange .....	13
4.2. $T_1$ Relaxation ; Energy Dissipation .....	14
<b>5. ENERGIZED AND IONIZED SOLID HYDROGEN .....</b>	<b>16</b>
5.1. Bombardment by High Energy Electrons .....	16
5.2. $\gamma$ -Ray Irradiation .....	16
<b>6. <math>H_3^+</math> IONS IN SPACE PLASMAS .....</b>	<b>20</b>
<b>PUBLICATIONS .....</b>	<b>22-23</b>
Appendix A. High Resolution Spectroscopy of Solid Hydrogen (to be published in Ann. Rev. Phys. Chem. 44 (1993)) .....	24
Appendix B. The Infrared Spectrum of $H_3^+$ in Laboratory and Space Plasmas (Rev. Mod. Phys. 64 (1992)) .....	59

## LIST OF FIGURES

Fig. 1	The tetrahexacontapole ( $2^6$ -pole) induced $W_0(0)$ ( $J = 6 \leftarrow 0$ ) transition of $H_2$ in a para- $H_2$ crystal. ....	6
Fig. 2	The $Q_1(1)$ transition at $2.41\mu m$ . ....	7
Fig. 3	Stick diagram of the observed $W_1(0)$ ( $v = 1 \leftarrow 0$ , $J = 6 \leftarrow 0$ ) transitions. ....	8
Fig. 4	Apparatus for simultaneous spectroscopy of infrared and stimulated Raman transitions. ....	9
Fig. 5	Stimulated Raman spectrum of the $Q_1(0)$ transition in para- $H_2$ crystal. ..	10
Fig. 6	Intensity variation of a quartet $Q_1(0)$ transitions of $D_2$ impurity in a para- $H_2$ crystal. ....	11
Fig. 7	Stark modulation spectroscopy of the $Q_1(0)$ transition of para- $H_2$ crystal. ....	12
Fig. 8	Low resolution FTIR spectrum of the $Q_1(0)$ exciton band at $\sim 4153\text{ cm}^{-1}$ . ....	14
Fig. 9	Variations of the transition frequencies and the linewidth of the $Q_1(0)$ field induced transition when temperature of the para- $H_2$ crystal is varied. ....	15
Fig. 10	Low resolution ( $\sim 0.1\text{ cm}^{-1}$ ) spectrum of para- $H_2$ crystal before (upper trace) and after (lower trace) the ionization. ....	17
Fig. 11	Two typical examples of the $\gamma$ -ray induced spectral line under high resolution. ....	18
Fig. 12	The $H_3^+$ emission lines in the ionospheres of Jupiter and Saturn observed in July 1992. ....	21

## LIST OF TABLES

Table 1	Graduate students and post doctorate fellows supported by the grants .....	2
Table 2	Chronological summary of events .....	3-4

Accession For	
NTIS CRA&I	<input checked="" type="checkbox"/>
DTIC TAB	<input checked="" type="checkbox"/>
Unannounced	<input type="checkbox"/>
Justification .....	
By .....	
Distribution /	
Availability Codes	
Dist	Avail and/or Special
A-1	



## 1. Introduction

The purpose of this project was to study the static and dynamical behavior of hydrogen molecules in nearly pure para-hydrogen crystals using high resolution and high sensitivity laser spectroscopy. This was a continuation of the previous AFOSR support F04611-86-K-0069. Graduate students and a postdoctoral fellow who worked in the previous project period, Mitchio Okumura, Mounqi Bawendi, Brent Rehfuss, Li-Wei Xu and Man-Chor Chan, left the group. A new blood of graduate students and a postdoctoral fellow, David Weliky, Karen Kerr, Teri Byers, Rob Dickson and Takamasa Momose, worked in this period. A list of personnel supported by the two Air Force grants are given in Table 1.

During the previous project period we unexpectedly observed that many spectral lines of hydrogen molecule are extremely sharp in properly prepared solid hydrogen. Some spectral lines are narrower than the gaseous lines by orders of magnitude! During the period of this report, we have fully utilized the high resolution capability of laser spectroscopy to study the intermolecular and crystal field interaction and energy transfer in solid hydrogen. Some of the major technical advances during this period are: (1) temperature controlled crystal preparation using continuous gas flow, (2) introduction of new laser sources, the color center laser and the InGaAsP communication diode lasers, (3) introduction of the technique of the stimulated Raman gain spectroscopy, (4) introduction of Stark modulation which increased the sensitivity by 2 orders of magnitudes, and (5) use of  $\gamma$ -ray irradiation for spectroscopy of ionized crystals. These new techniques together with those used earlier have enabled us to observe a whole variety of novel spectra of  $H_2$  and impurities in solid hydrogen. A summary of the sequence of events during this project is given in Table 2. A review article has been drafted on high resolution spectroscopy of solid hydrogen for the Annual Review of Physical Chemistry. This article is given in Appendix A. There has been an exciting development on the  $H_3^+$  emission spectrum in astronomical objects.



**A review article on this subject written for the Review of Modern Physics is given in Appendix B.**

**Altogether it has been a very inspiring and fruitful 3 years. Some highlights of the research are sketched in the following.**

**Table 1**

**Graduate Students and Postdoctoral Fellows Supported by  
Air Force Grants F04611-8G-K-0069 and F33615-90C-2035**

	<b>Current position</b>	<b>Affiliation</b>
<b>Mitchio Okumura</b>	<b>Assistant Professor</b>	<b>California Institute of Technology</b>
<b>Moungi G. Bawendi</b>	<b>Assistant Professor</b>	<b>Massachusetts Institute of Technology</b>
<b>Takamasa Momose</b>	<b>Assistant Professor</b>	<b>Kyoto University</b>
<b>Brent D. Rehfuss</b>	<b>Researcher</b>	<b>Sterling Winthrop, Inc.</b>
<b>Man-Chor Chan</b>	<b>Research Associate</b>	<b>Herzberg Institute of Astrophysics</b>
<b>Steven S. Lee</b>	<b>Postdoctoral Fellow</b>	<b>Harvard University</b>
<b>Li-Wei Xu</b>	<b>Postdoctoral Fellow</b>	<b>University of Michigan</b>
<b>Mary-Frances Jagod</b>	<b>Postdoctoral Fellow</b>	<b>University of Chicago</b>
<b>Charles M. Gabrys</b>	<b>Graduate Student</b>	<b>University of Chicago</b>
<b>David P. Weliky</b>	<b>Graduate Student</b>	<b>University of Chicago</b>
<b>Karen E. Kerr</b>	<b>Graduate Student</b>	<b>University of Chicago</b>
<b>Teri J. Byers</b>	<b>Graduate Student</b>	<b>University of Chicago</b>
<b>Rob Dickson</b>	<b>Graduate Student</b>	<b>University of Chicago</b>

**Table 2**  
**Chronological Summary of Events**  
**April 13, 1990–April 12, 1993**

---

<b>April 13, <u>1990</u></b>	<b>HEDM Model Contract Started.</b>
<b>May</b>	<b>Table of the <math>Q_1(1)</math> transitions completed.</b>
<b>June</b>	<b>Graduate student Karen Kerr joined group.</b>
<b>July</b>	<b>Infrared-Microwave double resonance planned.</b>
<b>August</b>	<b>HEDM main contract started. Theoretical discussions with Berlinsky and Harris.</b>
<b>Sep–Dec</b>	<b>Design of new crystal preparation method.</b>
<b>December</b>	<b>Paper on the <math>Q_1(1)</math> spectrum sent to the <i>Physical Review Letters</i>.</b>
<b>January <u>1991</u></b>	<b>Graduate student Teri Byers joined group.</b>
<b>February</b>	<b>Crystal growing with continuous gas flow completed. HEDM meeting at Albuquerque.</b>
<b>March</b>	<b>Paper on the <math>W_0(0)</math> spectrum sent to the <i>Journal of Chemical Physics</i>.</b>
<b>April–May</b>	<b>Double resonance cell designated.</b>
<b>June</b>	<b>Postdoctoral fellow T. Momose joined group.</b>
<b>July</b>	<b>Temperature tunable crystal making system designed.</b>
<b>August</b>	<b>InGaAsP diode introduced to measure the <math>Q_1(1)</math> transitions. Solid <math>Q_1(1)</math> radiolysis calculated.</b>
<b>September</b>	<b>Graduate student M.-C. Chan left group. Paper on <math>D_2</math> impurity spectrum sent to the <i>Journal of Chemical Physics</i>.</b>
<b>October</b>	<b>Color center laser was introduced to solid <math>H_2</math> spectroscopy.</b>
<b>November</b>	<b><math>Q_1(0)</math> transitions of <math>D_2</math> observed using frequency stabilized color center laser.</b>

December	Stimulated Raman spectrum of $Q_1(0)$ transition was observed. A paper was sent to the <i>Journal of Molecular Spectroscopy</i> .
January 1992	Design of a new crystal cell. Extension of Dewar ordered.
Feb-April	Temperature controlled crystal growing completed. Stimulated Raman spectroscopy.
April	HEDM meeting at Lancaster. Review paper "The Infrared Spectrum on $H_3^+$ in Laboratory and Space Plasmas" was sent to the <i>Review of Modern Physics</i> . $H_3^+$ emission discovered in Uranus.
May	Theoretical calculations on fine structures.
June	$\beta$ -ray calculations; graduate student Rob Dickson joined group. Gave lectures at the International School of Physics "Enrico Fermi".
July	$H_3^+$ emission discovered in Saturn.
Aug-Sep	Worked with J.L. Hall at JILA Boulder, Colorado on stimulated Raman Spectroscopy.
October	Attempted to use para- $H_2$ crystal as non-linear optical element.
Nov-Dec	Planning for $\gamma$ -ray bombardment experiment.
January 1993	Review paper "High Resolution Spectroscopy of Solid Hydrogen" was sent to the <i>Annual Review of Physical Chemistry</i> .
February	$\gamma$ -ray experiment successfully operated. A sharp feature assignment to charge induced spectrum.
March	Electric field induced spectrum observed in para- $H_2$ crystal. Stark modulation increased the sensitivity of orders of magnitude.
April	Ti:Sapphire laser introduced to spectroscopy.

---

## 2. Crystalline Field and Intermolecular Interaction

The high resolution of laser infrared spectroscopy enables us to resolve energy splittings resulting from interaction of molecules with crystalline field and neighboring molecules. Such splitting occurs for excited rotational levels of molecular hydrogen with angular momentum  $J$  equal or greater than 1. The general formula for angularly dependent intermolecular interaction can be expressed as:

$$V_i = \sum_{l'm} B_{lm}''(R_i) C_{lm}(\omega) C_{l'm}(\omega_i) \quad (1)$$

Where  $\omega$  and  $\omega_i$  are angular orientations of the central and interacting molecule ( $i$ ), respectively, and  $R_i$  is their distance. For crystal field interaction we sum over  $i$  for  $l' = 0$  and using angular orientation  $\Omega$  with respect to crystal field axis:

$$V_c = \sum_{l,m} C_{lm}(\Omega) \left[ \sum_i B_{lm}(R_i) C_{lm}^*(R_i) \right] \quad (2)$$

where  $C_{lm}^*(R_i)$  is the Racah spherical harmonics for the angular orientation of the  $i$ -th molecule with respect to the central one.

### 2.1 $W_0(0)$ Transition and Crystal Field Splitting

The presence of crystal field splitting has been long assumed in solid hydrogen but its measurement was limited to the indirect method of temperature dependent NMR intensity. We could observe the splitting directly in the tetrahexacontapole  $2^6$ -pole induced  $W_0(0)$  ( $J = 6 \leftarrow 0$ ) transition. The observed splitting is shown in Fig. 1. The assignment of the  $M$  values was done from symmetry considerations in which an extended group of the crystal point group and the molecular symmetry group was used. Using Eq. (2) and the symmetry, the crystal field can be written as:

$$V_c = \epsilon_{2c} C_{20}(\Omega) + \epsilon_{4c} C_{40}(\Omega). \quad (3)$$

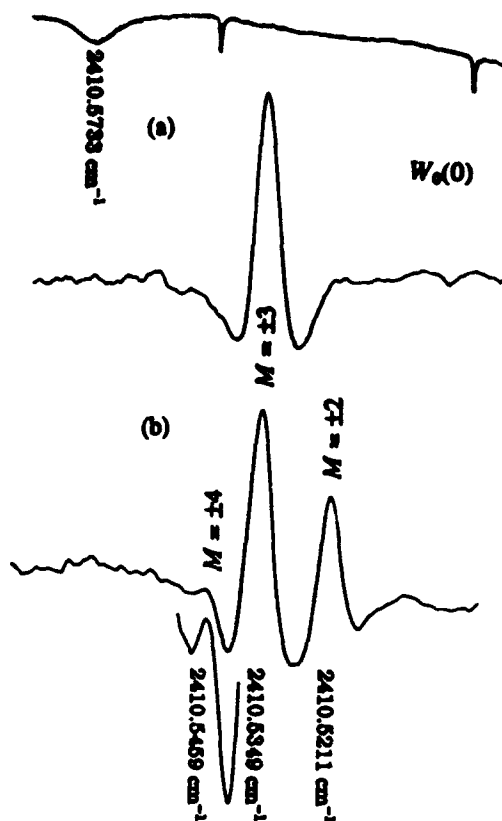


Figure 1. The tetrahexacontapole ( $2^8$ -pole) induced  $W_0(0)$  ( $J = 6 \leftarrow 0$ ) transition of  $H_2$  in a para- $H_2$  crystal. The upper trace gives the spectral line when the electric field of the laser radiation is parallel to the crystal axis and the lower trace perpendicular. The crystal field (Davidov) splitting is clearly observed. The markers above the traces are separated by 1500 MHz.

The observed splitting led us to determine  $\epsilon_{4c}$  which is the dominating term. This gives understanding on the behavior of molecules in the crystal field.

## 2.2 $Q_1(1)$ Transitions and Pair Splitting

When we make the nearly pure para- $H_2$  crystals, we can control the concentration of the ortho- $H_2$  impurity by adjusting the temperature of the catalyst used to convert ortho- $H_2$  to para- $H_2$ . Usually the conversion is made at liquid  $H_2$  temperature which gives crystals with 0.2% of ortho- $H_2$ . Among the randomly distributed  $J = 1$   $H_2$ , some happen to lie close to other  $J = 1$   $H_2$ . When this happens they interact with each other through electric quadrupole-quadrupole interaction and

their  $3 \times 3$  fold degeneracy is split. We see these splitting as intricate spectral patterns. An example is shown in Fig. 2. The extremely rich structure results from the nine-fold multiplicity in the excited state as well as in the ground state. The strongest central line

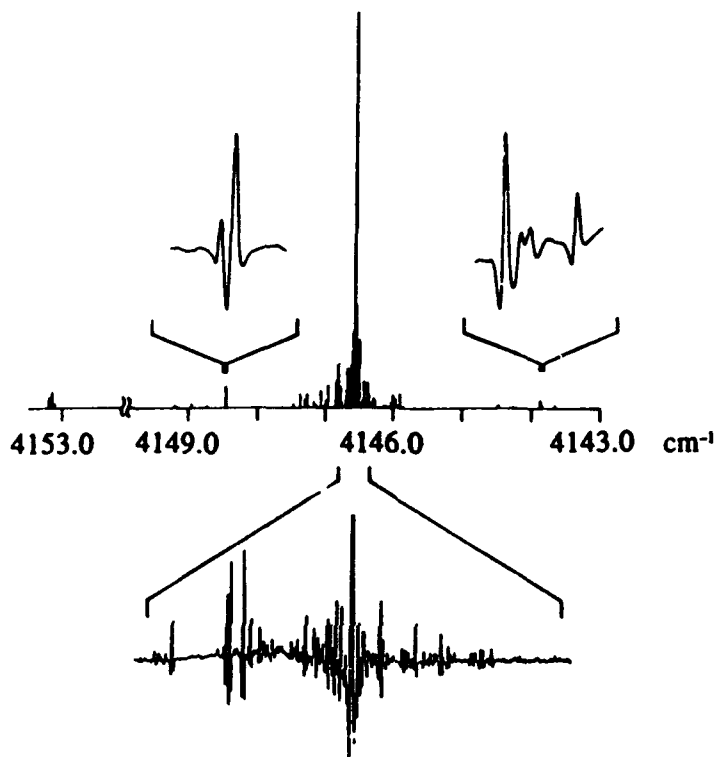


Figure 2. The  $Q_1(1)$  transition at  $2.41\mu\text{m}$ . The upper figure gives a computer generated stick diagram of the observed spectral lines and the lower trace and insets give observed lines. The rich structure of the transition is caused by the pair splitting of  $J = 1$  pair in the ground and excited states.

is due to the  $Q_1(1)$  ( $\nu = 1 \leftarrow 0$ ,  $J = 1 \leftarrow 1$ ) transition of the isolated ortho- $\text{H}_2$ . This line is accompanied by a great number of satellite lines resulting from ortho pairs in a variety of relative positions. In effect we have resolved the inhomogeneous broadening due to multipole interactions. We have yet to understand the structure but its overall pattern has been characterized.

### 2.3 $W_1(0)$ Transitions and Pair Splitting

The introduction of the InGaAsP communication diode as an infrared radiation source has allowed us to study the  $2^{\text{nd}}$ -pole induced  $W_1(0)$  transition ( $\nu = 1 \leftarrow 0$ ,

$J = 6 \leftarrow 0$ ) in the region of  $1.55\mu\text{m}$ . In addition to the crystal field splitting discussed earlier in (1.1), we could also observe fine structure due to the interaction between  $\text{H}_2$  in the  $J = 6$  level in the excited state and neighboring  $J = 1$   $\text{H}_2$ . This pattern is easier to understand than the  $Q_1(1)$  pattern because the splitting is limited to the excited state. The observed spectrum is given in Fig. 3. A least square fitting is in progress.

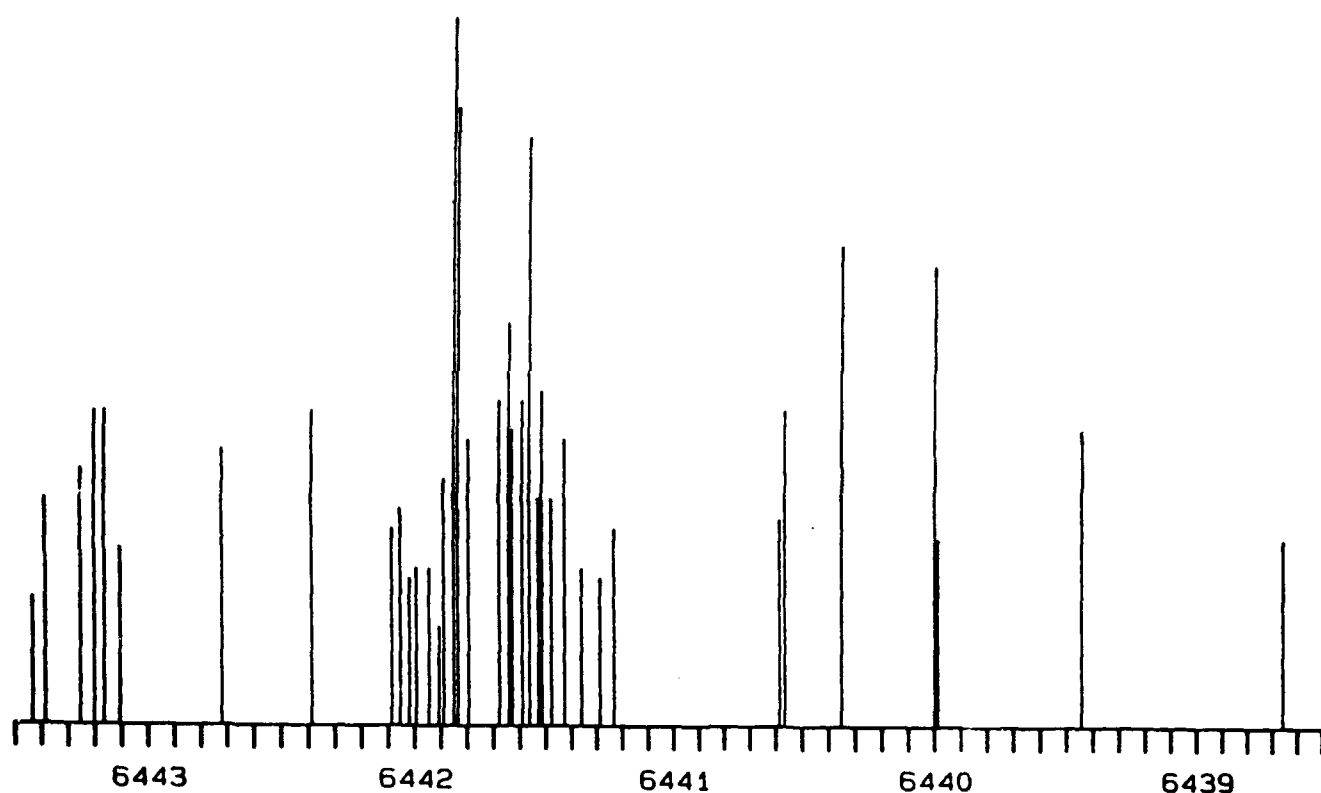


Figure 3. Stick diagram of the observed  $W_1(0)$  ( $\nu = 1 \leftarrow 0$ ,  $J = 6 \leftarrow 0$ ) transitions. The structure of the pattern is due to the interaction between  $J = 6$  level and  $J = 1$  impurity. The central position at  $6441.73 \text{ cm}^{-1}$  corresponds to the pure  $W_1(0)$  transition. The widely split lines are due to interactions between nearest neighbors while closely spaced satellites are due to farther neighbors.

### 3. Pure Vibrational Spectrum $Q_1(0)$

In para- $H_2$  crystals used in our experiments, 99.8% of the  $H_2$  molecules are in the ground molecular level  $J = 0$ ,  $\nu = 0$ . In this level all spin quantum numbers are also zero,  $S = 0$ ,  $I = 0$ . Almost all molecules in the crystal with the density of  $2.6 \times 10^{22} \text{ cm}^{-3}$  are in this single state without any angular momentum. The  $Q_1(0)$  transition ( $\nu = 1 \leftarrow 0$ ,  $J = 0 \leftarrow 0$ ) is the simplest transitions from this state which appears at  $2.41 \mu\text{m}$  for  $H_2$  and  $3.35 \mu\text{m}$  for  $D_2$ . We have studied this pure vibrational transition using a variety of methods.

#### 3.1 Stimulated Raman Spectroscopy

The  $J = 0 \leftarrow 0$  transition is strictly forbidden in a single photon transition regardless of the nature of transition moments. Therefore, some induction mechanism is needed to cause such a transition. In the 2-photon Raman process, the extra radiation induces the transition. In order to fully exploit the high resolution of laser spectroscopy, we used the stimulated Raman gain spectroscopy. A diagram of the apparatus is given in Fig. 4.

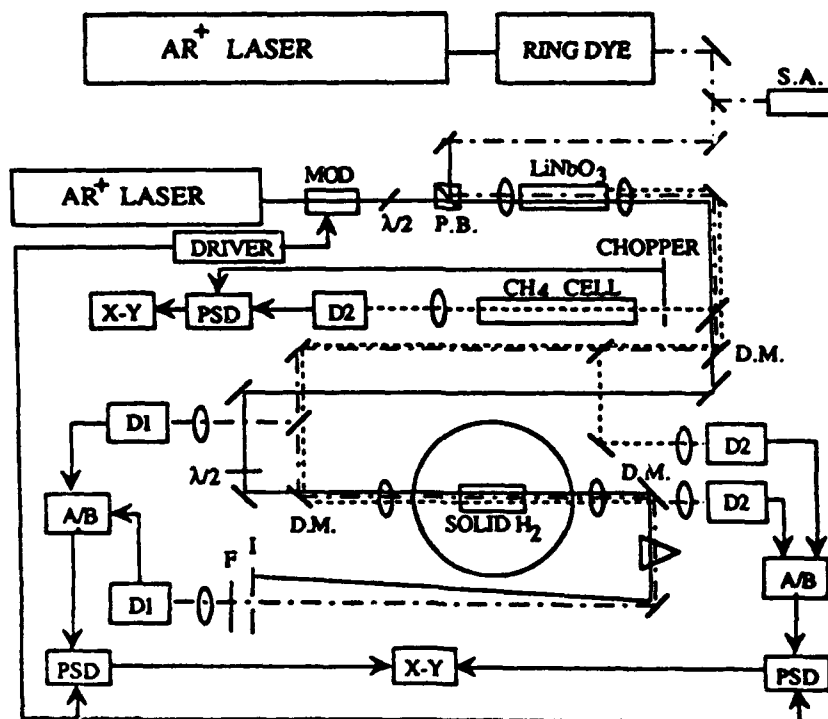


Figure 4. Apparatus for simultaneous spectroscopy of infrared and stimulated Raman transitions. The optical nonlinearity of  $LiNbO_3$  is used for the former and that of solid  $H_2$  is used for the latter. An argon laser and a dye laser are used for radiation sources.



We have used a variety of combinations of lasers such as (Ar-Dye), (Ti:Sapph-NdYag), (Kr-Ti:Sapph) but the first worked the best. Observed signal is given in Fig. 5. The sharpness of the signal ( $\Delta\nu \sim 7$  MHz) demonstrates that the  $\Delta k = 0$  exciton momentum selection rule is well obeyed. The symmetry of the observed spectral line and absence of any other features indicate that the crystal has pure hcp structure and is fairly free of strain. When the ortho concentration is increased, the spectrum shows interesting variations. Theoretical explanation for such observations is being attempted.

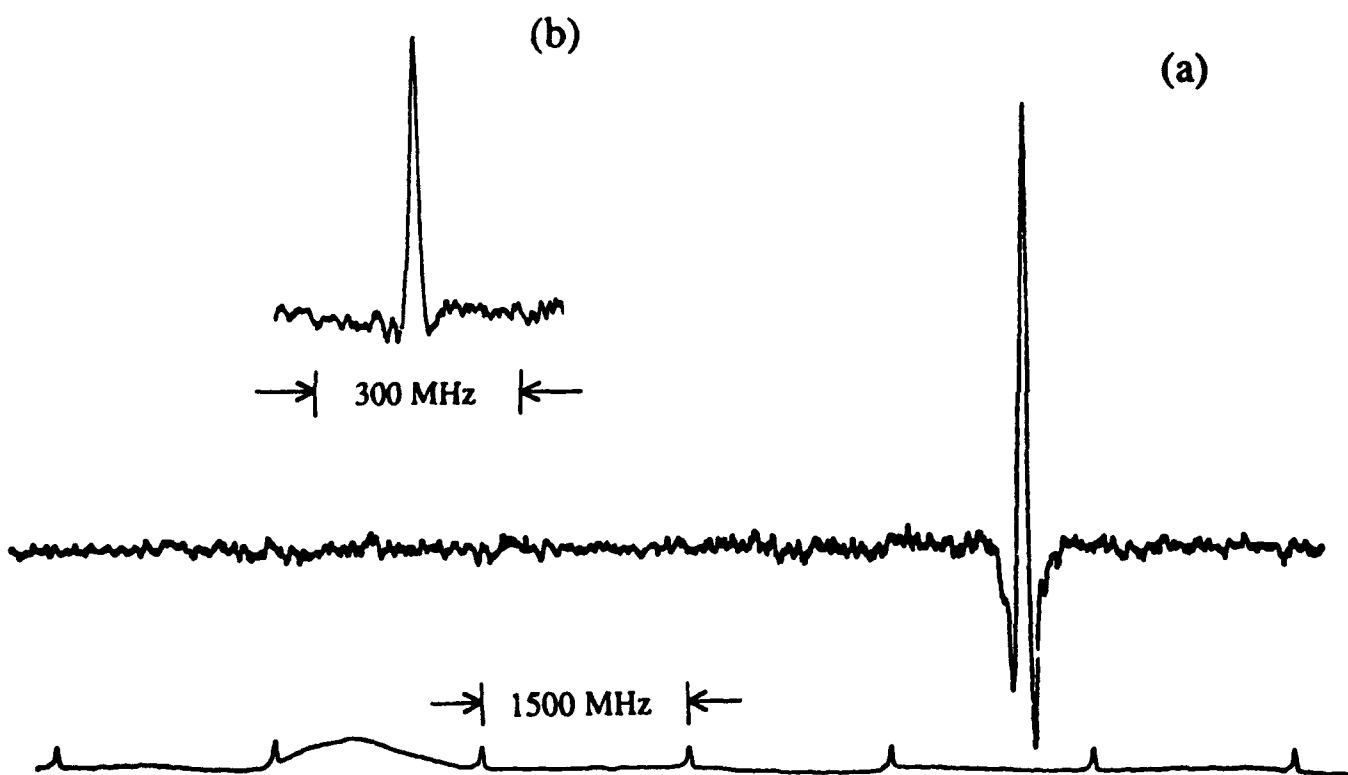


Figure 5. Stimulated Raman spectrum of the  $Q_1(0)$  transition in para- $H_2$  crystal. A combination of a single mode Ar laser and a dye laser were used as coherent radiation sources. The sharpness of the line is due to the exciton momentum selection rule  $\Delta k = 0$ . Trace (a) gives a tone burst signal with radiofrequency of 80 MHz and (b) of 6 MHz. The symmetric lineshape and the absence of other features demonstrates purity of the crystal.

### 3.2 $D_2$ Impurity Spectroscopy

The  $Q_1(0)$  transition is also induced by the local electronic field due to the  $J = 1$   $H_2$  impurity in the crystal. The  $Q_1(0)$  transition of  $H_2$  caused by such effect is

broadened by the exciton band (discussed in 4.1). However if we use  $D_2$  impurity in a para- $H_2$  crystal, excitons are localized and sharp spectral lines are observed. A frequency stabilized color center laser ( $\Delta\nu \sim 0.5$  MHz) has allowed us to observe this transition with great sharpness ( $\Delta\nu \sim 2$  MHz) and clarity. The beautiful quartet pattern and its variation with the direction of the laser electric field are shown in Fig. 6.

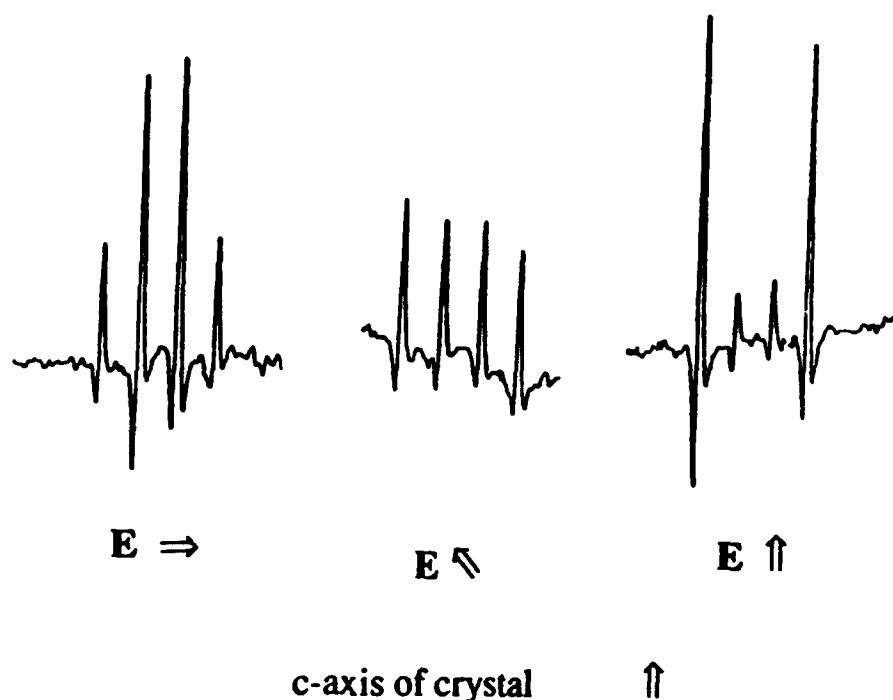


Figure 6. Intensity variation of a quartet  $Q_1(0)$  transitions of  $D_2$  impurity in a para- $H_2$  crystal. A color center laser is used for its observation. The linewidths of the signals are 2 MHz (half width at half maximum) and their spacing is  $\sim 54$  MHz. The sharpness of the signal demonstrates well localized exciton and its long life time.

### 3.3 Electric Field Induced Spectroscopy and Stark Modulation

The  $Q_1(0)$  transition can be induced also by an external electric field as initially predicted theoretically by Condon. This may be considered as Raman transition in which one "radiation" is the D.C. electric field. We have observed the electric field induced  $Q_1(0)$  transitions of  $H_2$  and  $D_2$ . Since the spectral intensity is proportional to the square of the applied electric field, we can use this effect as Stark modulation. An

example of the spectrum detected by the Stark modulation method is shown in Fig. 7. The modulation method provides the long sought-for molecular

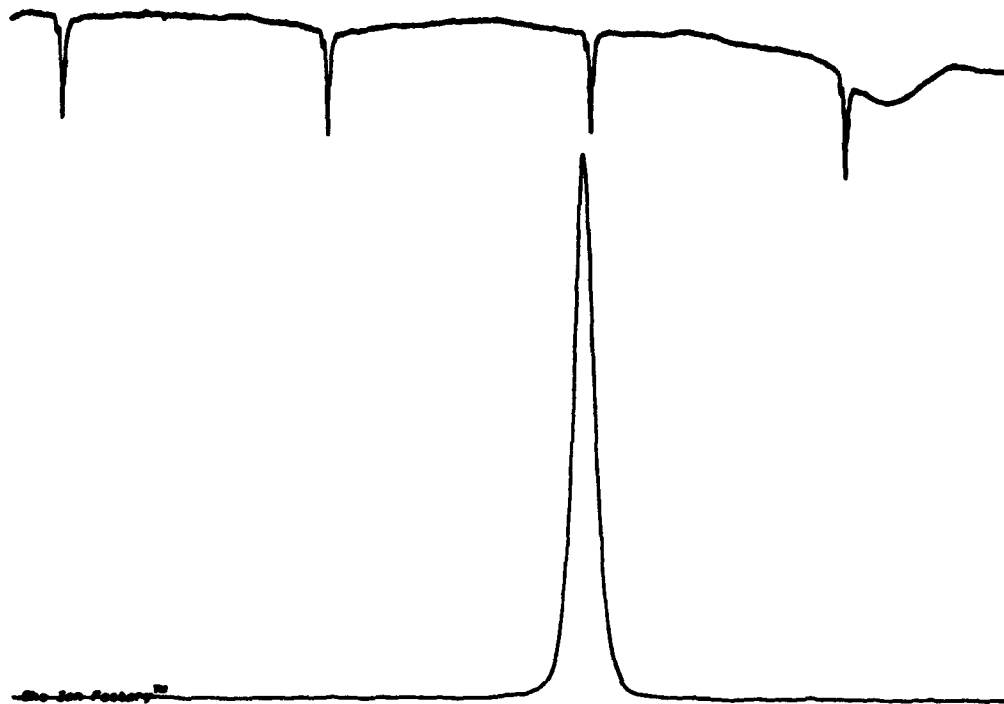


Figure 7. Stark modulation spectroscopy of the  $Q_1(0)$  transition of para- $H_2$  crystal. An AC electric field of 6kv/cm peak to peak with the frequency of 10 kHz was used as the modulation field and the signal was detected by 2f mode of the phase sensitive detector. The detection sensitivity has been increased by more than 2 orders of magnitude to  $\sim 2 \times 10^{-8}$ .

modulation applicable to solid hydrogen spectroscopy. By using this method, the sensitivity of the spectroscopy has increased by 2 orders of magnitude from  $5 \times 10^{-4}$  to  $2 \times 10^{-6}$ . This is obviously a great progress. This method has allowed us to measure the shift and broadening of the spectral lines as temperature of the crystal was varied from 4.2K to the triple point 13.6K.

#### **4. Energy Transfer in Solid Hydrogen**

The vibrational excitation energy introduced into the crystal by laser radiation tends to stay in the crystal for some time. Our observation of the very sharp spectral lines indicates that the relaxation time of the excitation is much longer than in ordinary condensed phase systems. The excitation energy hops around in the crystal till it is dissipated in the crystal through exciton-phonon interaction. We can obtain information on these dynamical effects from spectroscopy.

##### **4.1 Exciton Band ; Energy Exchange**

The vibrational excitation (vibron) introduced in a molecule may hop to a neighboring molecule through resonant exciton exchange process. This produces the exciton band which forms a most beautiful example of Bloch state. Such a band is directly observed in the  $Q_1(0)$  transition induced by the  $J = 1$   $H_2$  impurities. A low resolution FTIR spectrum of the band is shown in Fig. 8. The width of the band and theoretical calculations indicates that the exchange of excitation occurs with a hopping time of  $\sim 100$  ps. The inset of the figure shows theoretical exciton band calculated by Bose and Poll. A different part of the band corresponds to different values of the exciton momentum  $k$ . By using high resolution spectroscopy we may be able to study key positions of the band. For example, the stimulated gain spectrum given in Fig. 5 appears at the low frequency end of the band at  $4149.7\text{ cm}^{-1}$  corresponding to  $k = 0$ . We also observe sharp features at the high frequency end of the exciton band which presumably corresponds to the singularity resulting from the high degeneracy of the corresponding energy levels. Stimulated Raman spectrum with increased ortho- $H_2$  concentration shows broadening and structure due to dephasing of the Bloch state because of the impurity. We also obtain much information on localization of excitons on a variety of impurities. For example, as we increase the concentration of the  $D_2$  impurity, we see broadening and structure of the spectrum corresponding to hopping of excitons between randomly distributed impurity molecules.

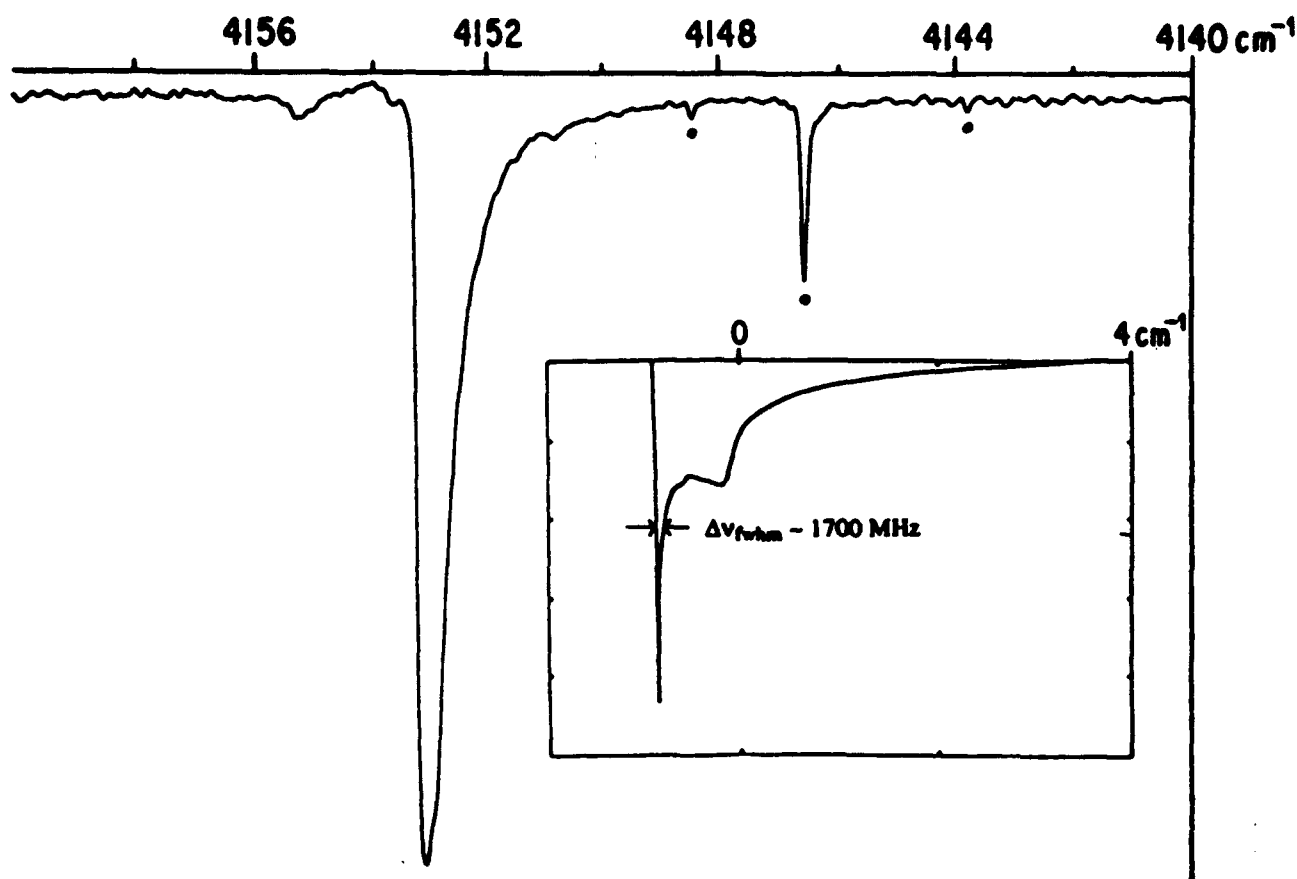


Figure 8. Low resolution FTIR spectrum of the  $Q_1(0)$  exciton band at  $\sim 4153 \text{ cm}^{-1}$ . This spectrum is induced by  $J = 1$  impurities and therefore does not follow the  $\Delta k = 0$  rule. Inset shows the theoretical exciton band calculated by Bose and Poll. The dotted lines are  $Q_1(1)$  structure given in Fig. 2 under high resolution.

#### 4.2 $T_1$ Relaxation ; Energy Dissipation

Many observed spectral lines are so sharp because the excitation has a long longitudinal  $T_1$  relaxation time. This long relaxation time is due to the large mismatch between the excitation energy ( $4150 \text{ cm}^{-1}$  for example) and the phonon energy (the phonon Debye temperature is  $\sim 100 \text{ K}$ ). However, this situation depends critically on the observed transitions. For example, the  $Q_1(0)$  lines of impurity  $D_2$  are extremely sharp ( $\sim 2 \text{ MHz}$ ) while the  $S_1(0)$  line ( $v = 1 \leftarrow 0, J = 2 \leftarrow 0$ ) is broader ( $\Delta\nu \sim 0.1 \text{ cm}^{-1}$ ) by a factor of  $\sim 1500$ . This is because molecules in the excited state with  $J = 2$  may relax to  $J = 0$  in the excited vibrational state through the roton ( $J = 2 \leftarrow 0$ )—phonon interaction where the energy mismatch between the roton ( $\sim 180 \text{ cm}^{-1}$ ) and phonon is

much smaller.<sup>7</sup> We also note that the linewidths vary with temperature of the crystal because of the excitation of phonons. Thus for example the electric field induced  $Q_1(0)$  transition changes its width as the crystal is heated from 4.2 K He temperature to 13.5 K just below the hydrogen triple point. An observed example is shown in Fig. 9.

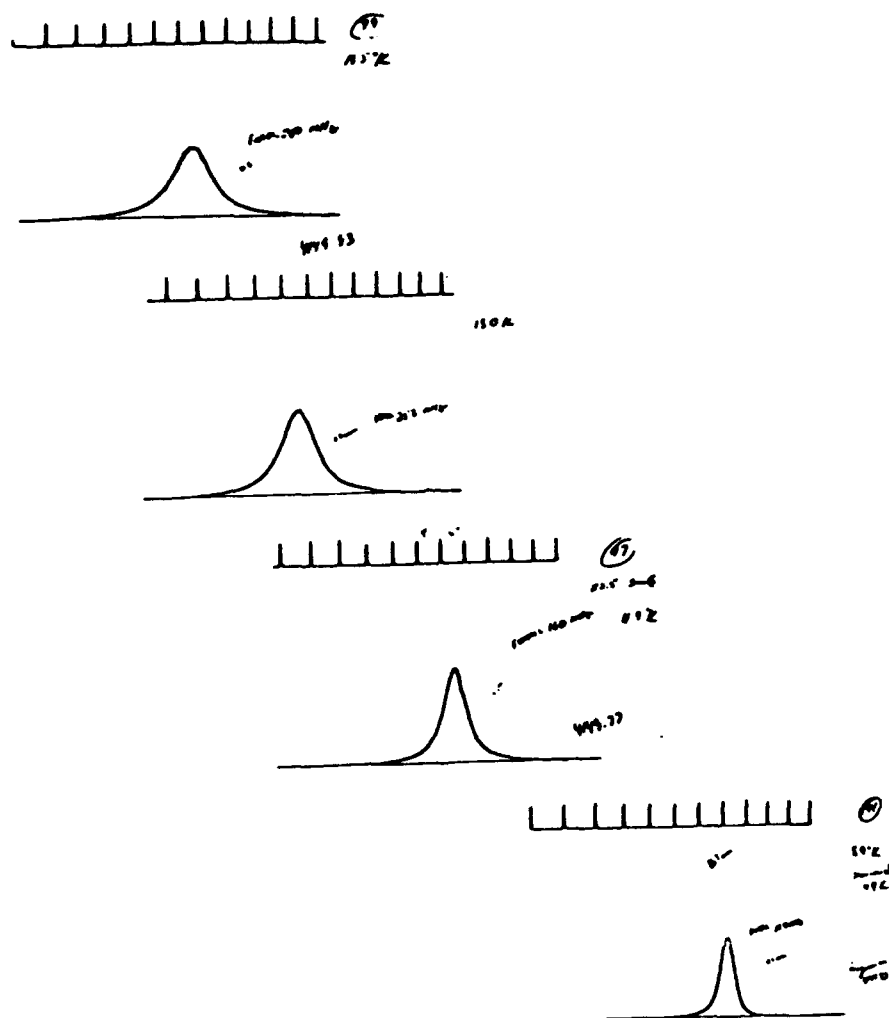


Figure 9. Variations of the transition frequencies and the linewidth of the  $Q_1(0)$  field induced transition when temperature of the para- $H_2$  crystal is varied. The top trace corresponds to  $T=13.5$  K just below the triple point while the bottom  $T=8.9$  K. The frequency markers are separated by 150 MHz. The total shift is about 3 GHz.

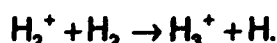
The observation of the lineshift as well as the broadening of the spectrum gives clear cut experimental evidence for variation of molecular vibration and crystal phonon with temperature.

## 5. Energized and Ionized Solid Hydrogen

We have attempted a whole variety of methods to energize and ionize solid hydrogen to study solid plasmas and possibly to excavate new directions in the physics of high energy density matter. We have attempted a variety of methods such as electron bombardment, excimer laser irradiation,  $\beta$ -ray bombardment from radioactive isotopes, and  $\gamma$ -ray irradiation. The methods of excimer irradiation and radioactivity (Promethium 147) were not effective. The electron bombardment worked but the experiment was difficult, inconvenient, and expensive. We were delighted to find after all these that the  $\gamma$ -ray irradiation is most powerful and effective. This method will be used hereafter.

### 5.1 Bombardment by High Energy Electrons

A beam of 3 MeV electrons from a Van de Graaf acceleration at Argonne National Laboratory was used to bombard solid hydrogen crystals (1 cm  $\phi$ , 2.5 cm long). The electrons ionized hydrogen molecules and the  $H_3^+$  molecular ions are produced through the efficient ion-neutral reaction:



The resultant  $H_3^+$  attract surrounding  $H_2$  molecules by Langevin force and form clusters and stabilize. Spectrum of the cluster ions have been observed. In addition we observed a sharp feature near the  $Q_1(0)$  transition. This feature was subsequently studied using  $\gamma$ -ray irradiation as described below.

### 5.2 $\gamma$ -Ray Irradiation

A crystal of nearly pure para- $H_2$  was prepared in a cylindrical copper cell (1.7 cm  $\phi$ , 10 cm long) and was irradiated with  $\gamma$ -ray from a Cobalt 60 source at Argonne National Laboratory. The irradiation was for ~1 hour and the dose was ~1 Mrad, which

corresponds to  $\sim 3.5 \times 10^{17}$  ionizations  $\text{cm}^{-3}$  in solid hydrogen. This method has been found to be very reliable and efficient since the ionization is uniform. It is also very convenient for spectroscopy because the ionization lasts nearly permanently so that the irradiated sample can be brought back to the laboratory to conduct the state-of-the-art spectroscopy. A low resolution FTIR spectrum of a para- $\text{H}_2$  crystal before and after  $\gamma$ -ray irradiation is shown in Fig. 10. When the sharp induced feature was examined

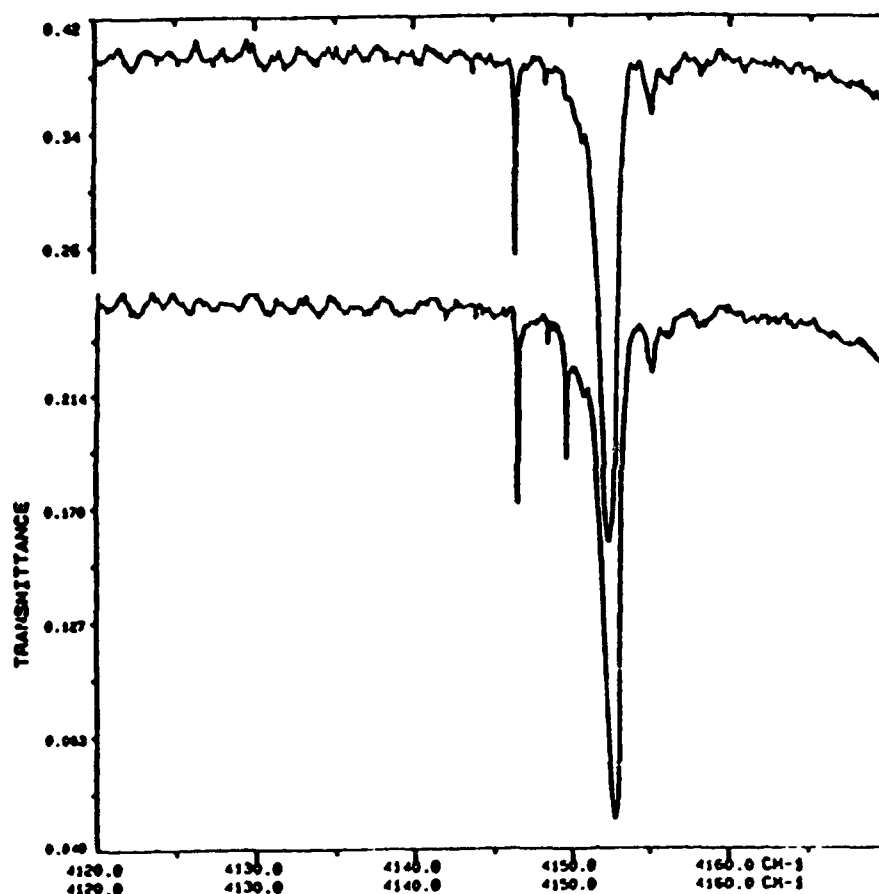
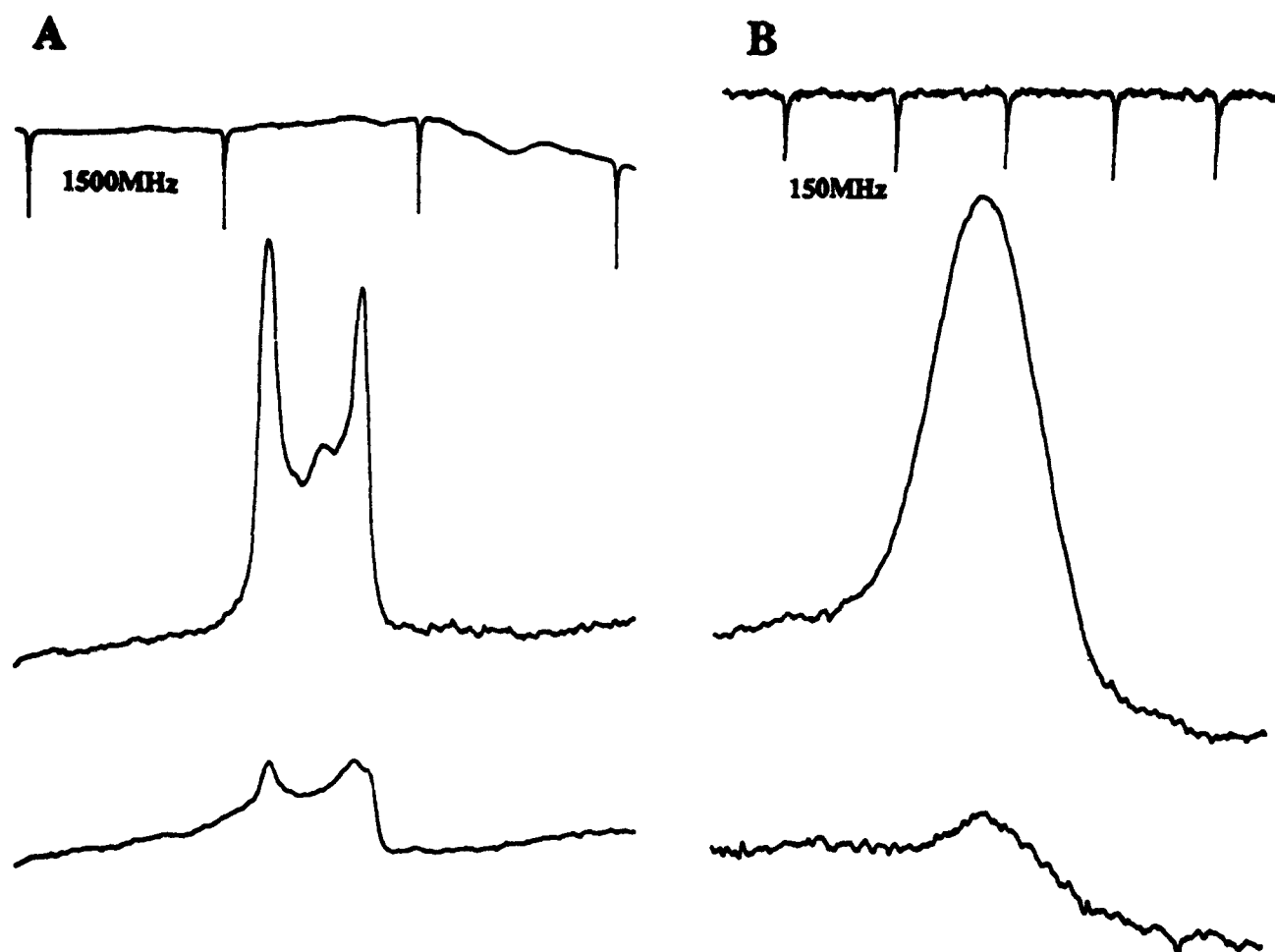


Figure 10. Low resolution ( $\sim 0.1 \text{ cm}^{-1}$ ) spectrum of para- $\text{H}_2$  crystal before (upper trace) and after (lower trace) the ionization. The sharp induced feature at  $4150 \text{ cm}^{-1}$  is studied under high resolution in Fig. 11.

under high resolution using laser spectroscopy, we found a sharp feature with the width of 100–900 MHz whose shape varies depending on the crystal as shown in Fig. 11. The frequency of the main feature, however, is always at the position of the  $Q_1(0)$





**Figure 11.** Two typical examples of the  $\gamma$ -ray induced spectral line under high resolution. Trace A was recorded by the difference frequency laser system. The position of the absorption maximum agrees well with that of the  $Q_1(0)$  Raman line of unionized crystal. Trace B was recorded by a color center laser on a different run of the  $\gamma$ -ray radiolysis. Upper traces are for laser field normal to the wall while for lower trace it is parallel.

transition with  $\Delta k = 0$ , that is,  $4149.696 \text{ cm}^{-1}$ . This spectrum is interpreted as due to charges caused by  $\gamma$ -ray and localized in the crystal. The intensity of the induced feature gives an estimate of average electric field in the crystal from which the charge density is calculated to be  $\sim 10^{16} \text{ cm}^{-3}$ . One remarkable outcome of the experiment is that the charges in the crystal are extremely stable; the feature lasts many days without appreciable decrease and survives temperature cycles as long as the temperature is below the melting point. Based on these observations the following sequence of

events were inferred. The  $\gamma$ -ray (1.17 MeV, 1.33 MeV) ionizes  $H_2$  through Compton scattering. The secondary electrons ejected from  $H_2$  have energy on the order of a fraction of MeV and cause cascades of ionizations through electron bombardment. The ionized  $H_2^+$  thus produced are converted to  $H_3^+$  and form clusters  $H_3^+(H_2)_n$ . The ejected electrons lose their energy while they migrate through the crystal. Many of them recombine with cations but some are stabilized on hydrogen atoms produced by bombardment to form  $H^-$ . The hydrogen anions  $H^-$  form clusters  $H^-(H_2)_n$  and stabilize. Our experimental results indicate that once stabilized and localized both the cluster cations and anions survive through temperature cycles. This robustness of the energized and ionized solid hydrogen was quite unexpected and may have practical applications.

## 6. $H_3^+$ Ions in Space Plasmas

In addition to the study of molecular ions in solid states, our studies of hydrogenic molecular ions in hot plasmas both in the laboratory and in space continued. In particular, in astronomical  $H_3^+$  spectroscopy, this last 4 years will be long remembered as the most inspiring discovery period. The laboratory spectroscopy and observational spectroscopy conducted by my students and myself and supported by AFOSR have contributed greatly to this development. The  $4\mu$   $\nu_2$   $H_3^+$  emission detected by us has since been detected also in Uranus and Saturn; it has become a very powerful general tool to study plasma activities in planetary ionospheres. It is truly amazing that our laboratory spectroscopy which was conducted from our curiosity on the quantum mechanical and dynamical behavior of  $H_3^+$  in laboratory plasmas is now so useful in astronomy. This inspiring development is summarized in The Review of Modern Physics article attached here as Appendix B. Fig. 12 shows a portion of the  $H_3^+$  emission in Jupiter and in Saturn discovered by us last summer. The purity of the spectrum, i.e., the strong spectral emission with virtually zero background and free of other spectral lines is truly breathtaking. So far the plasma activity of Jovian magnetosphere has been studied by satellite vehicles Pioneers and Voyagers but now the  $H_3^+$  emission spectrum allows us to study them from ground-based observation sites.

In a remarkable paper Miller *et al.* claimed discovery of the  $H_3^+$  emission in the envelope of supernova 1987A. It is very likely that further exciting discoveries await us in the next several years.

# SATURN and JUPITER

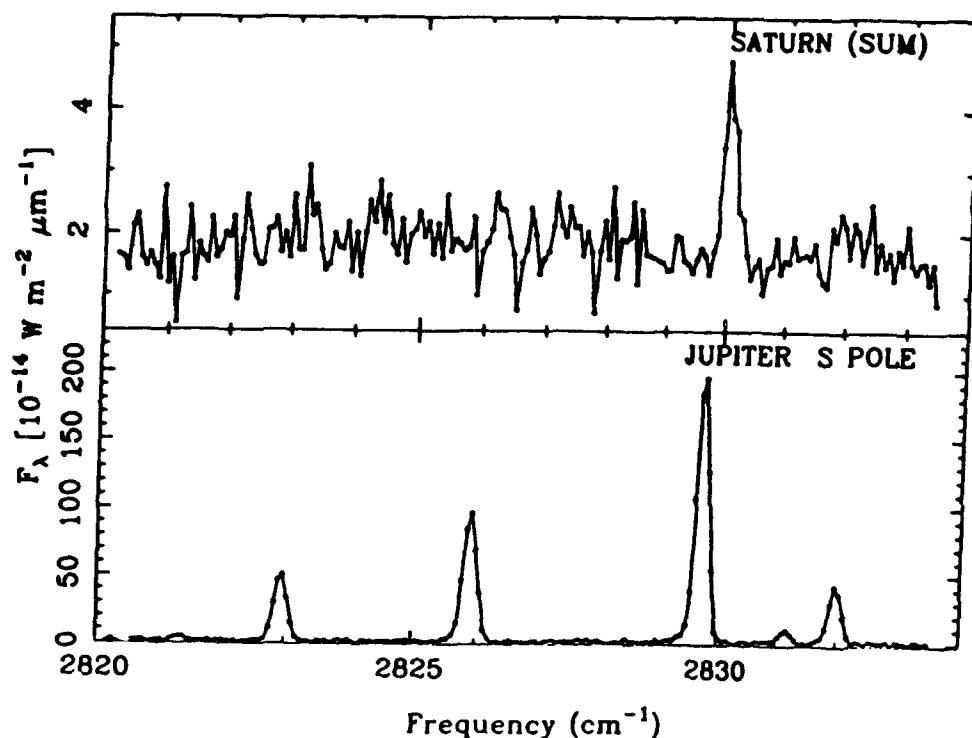


Figure 12. The  $\text{H}_3^+$  emission lines in the ionospheres of Jupiter and Saturn observed in July 1992. The five emission lines in the Jupiter south pole are (from the right to left): J, G, U  $\rightarrow$  J, K = 4, 2,  $-1 \rightarrow 3$ , 2 (2832.197  $\text{cm}^{-1}$ ), 4, 1,  $-1 \rightarrow 3$ , 1 (2831.340  $\text{cm}^{-1}$ ), 4, 3,  $-1 \rightarrow 3$ , 3 (2829.923  $\text{cm}^{-1}$ ), 3, 1,  $+1 -1 \rightarrow 2$ , 1 (2826.113  $\text{cm}^{-1}$ ), and 3, 2,  $+1 \rightarrow 2$ , 2 (2823.133  $\text{cm}^{-1}$ ), for the  $\nu_2 \rightarrow 0$  fundamental band. The weak emission feature at 2821.518  $\text{cm}^{-1}$  is due to the hot band  $2\nu_2(0) \rightarrow \nu_2$  with J, K  $\rightarrow$  J, G, U = 9.9  $\rightarrow$  8, 9,  $-1$ . The emission is remarkably free from background infrared radiation.

## Publications\*

1. "Observation of the 4 Micron Fundamental Band of  $H_3^+$  in JUPITER," T. Oka and T.R. Geballe, *Astrophys. J.* **351**, L53 (1990).
2. "Observation of the  $U_1(1)$  transition of Solid Deuterium," M.-C. Chan and T. Oka, *J. Chem. Phys.* **93**, 979 (1990).
3. "Observation of the Hot Bands of  $H_3^+$ ," M.B. Bawendi, B.D. Rehfuss and T. Oka, *J. Chem. Phys.* **93**, 6200 (1990).
4. "Observation of the  $2\nu_2(l=2) \leftarrow 0$  Overtone Band of  $H_3^+$ ," L.-W. Xu, C.M. Gabrys and T. Oka, *J. Chem. Phys.* **93**, 6210 (1990).
5. "High Resolution Infrared Spectroscopy of Solid Hydrogen," M.-C. Chan, M. Okumura, C.M. Gabrys, L.-W. Xu, B.D. Rehfuss and T. Oka, *Phys. Rev. Lett.* **66**, 2060 (1991).
6. "A Table of Astronomically Important Ro-Vibrational Transitions for the  $H_3^+$  Molecular Ion," L. Kao, T. Oka, S. Miller and J. Tennyson, *Astrophys. J. Suppl.* **77**, 317 (1991).
7. "Laser Spectroscopic Studies of the Pure Rotational  $U_0(0)$  and  $W_0(0)$  Transitions of Solid Parahydrogen," M.-C. Chan, S.S. Lee, M. Okumura and T. Oka, *J. Chem. Phys.* **95**, 88 (1991).
8. "High Resolution Infrared Spectroscopy of Deuterium in  $p-H_2$  Matrix," M.-C. Chan, L.-W. Xu, C.M. Gabrys and T. Oka, *J. Chem. Phys.* **95**, 9404 (1991).
9. "The Stimulated Raman Gain Spectrum of the  $Q_1(0)$  Transition of Solid Parahydrogen," T. Momose, D.P. Weliky and T. Oka, *J. Mol. Spectrosc.* **153**, 760 (1992).
10. "The Infrared Spectrum of  $H_3^+$  in Laboratory and Space Plasmas," T. Oka, *Rev. Mod. Phys.* **64**, 1141 (1992).
11. "Infrared Spectrum of  $H_3^+$  as an Astronomical Probe," T. Oka and M.-F. Jagod, *J. Chem. Soc. Faraday Transaction* **89**, in press.
12. "Application of Laser Spectroscopy to Fundamental Molecular Species:  $H_3^+$  and Solid  $H_2$ ," T. Oka, Proceedings of the International School of Physics "Enrico Fermi," Nuoro Cimento, in press.

13. "High Resolution Spectroscopy of Solid Hydrogen," T. Oka, *Ann. Rev. Phys. Chem.* **44**, 299 (1993).
14. "Infrared Absorption of Solid Hydrogen Ionized by 3 MeV Electrons," M.-C. Chan, M. Okumura and T. Oka, manuscript in preparation.
15. "Charge Induced Spectrum in  $\gamma$ -Ray Irradiated para-H<sub>2</sub> Crystals," T. Momose, K.E. Kerr, C.M. Gabrys, D.P. Weliky, A.M. Dickson and T. Oka, *Phys. Rev. Lett.*, submitted.
16. "Observation of the  $3\nu_2$  Overtone Band of H<sub>3</sub><sup>+</sup>," B.F. Ventudo, D.T. Cassidy, Z.Y. Guo, S.W. Joo, S.S. Lee and T. Oka, manuscript in preparation.
17. "Observation of the Infrared Spectra of H<sub>3</sub><sup>+</sup> with High Rotational Energy," D. Uy, C.M. Gabrys, M.-F. Jagod and T. Oka, manuscript in preparation.
18. "Detection of H<sub>3</sub><sup>+</sup> Infrared Emission Lines in Saturn," T.R. Geballe, M.-F. Jagod and T. Oka, *Astrophys. J.* **408**, L109 (1993).

# HIGH-RESOLUTION SPECTROSCOPY OF SOLID HYDROGEN

*Takeshi Oka*

Department of Chemistry and Department of Astronomy and  
Astrophysics, the University of Chicago, Chicago, Illinois 60637

**KEY WORDS:** infrared spectrum, Raman spectrum, condensed-phase spectroscopy, parahydrogen, intermolecular interaction

## INTRODUCTION

It has generally been assumed that spectral lines in condensed-phase matter are highly broadened as a result of homogeneous and inhomogeneous interactions, and that the high resolution of laser spectroscopy cannot be fully exploited unless some special techniques are employed (1-5). Recently Okumura & Chan have observed infrared spectral line in a parahydrogen crystal, corresponding to the  $J = 6 \leftarrow 0$  rotational transition of  $H_2$ , and found that it has a linewidth much smaller than the typical Doppler-broadened and Dicke-narrowed spectral lines of gaseous hydrogen in the same wavelength region (6) (see Figure 1). Since that observation a great many infrared spectral lines of  $H_2$  and impurities embedded in solid para- $H_2$  have been observed using laser spectroscopy in the 8.0 to 1.5  $\mu m$  region. The sharpest spectral lines observed so far are the vibration-rotation transitions of  $D_2$  impurity embedded in para- $H_2$  with  $\Delta\nu \sim 2$  MHz<sup>1</sup> corresponding to a resolution of  $\Delta\nu/\nu \sim 2 \times 10^{-8}$ . This high resolution allows us to study intermolecular and crystal-field interactions with unprecedented clarity and precision, based on first principles.

This review summarizes experimental results, most of which are yet to

<sup>1</sup> The observed linewidths are given in half width at half maximum throughout the paper. Although these linewidths give spectral resolution, the quantities to be compared with  $1/2 \pi T$ , etc, should be approximately three times these values, because most lines were recorded by the tone-burst modulation, which gives second derivative lineshape.



*Figure 1* Difference frequency laser spectrum of the  $J = 5 \leftarrow 0$  rotational transition in a para- $H_2$  crystal recorded using tone-burst modulation at 90 MHz (6). The frequency is at  $2410.5349 \text{ cm}^{-1}$  and the width is 90 MHz (hwhm). The upper trace gives frequency markers of a spectrum analyzer spaced by 1500 MHz and an absorption line of  $N_2O$  used as reference.

be interpreted. In my attempt to analyze these results, my students and I are fascinated by the quantitative and qualitative difference between gaseous and solid-state spectroscopy. This difference is stressed throughout this article.

## BACKGROUND

The spectroscopic study of condensed-phase molecular hydrogen has a long history in which Canadian physicists have played major roles. Almost immediately after the discovery of the Raman effect in 1928, McLennan & McLeod at the University of Toronto (7) applied it to liquid hydrogen and observed a vibrational Raman transition  $Q_1(0)$  and two rotational transitions  $S_0(0)$  and  $S_0(1)$ .<sup>2</sup> Their results clearly showed that  $H_2$  has well-

<sup>2</sup> Vibration-rotation transitions are specified by the following convention: The capital letters Q, S, U, W, Y . . . represent  $\Delta J = 0, 2, 4, 6, 8, \dots$ , respectively. Their subscripts show the vibrational quantum number  $r$  in the upper state, and the number in parentheses represents the rotational quantum number  $J$  in the lower state. Thus  $Q_1(0)$ ,  $S_0(0)$ ,  $S_0(1)$  denote  $(r = 1 \leftarrow 0, J = 0 \leftarrow 0)$ ,  $(r = 0 \leftarrow 0, J = 2 \leftarrow 0)$ ,  $(r = 0 \leftarrow 0, J = 3 \leftarrow 1)$ , respectively.



defined rotational quantization, even in the condensed phase, and that H<sub>2</sub> at low temperature must be regarded as a mixture of effectively distinct sets of molecules, ortho ( $J = 1$ ) and para ( $J = 0$ ) hydrogen. The Toronto group led by Welsh & Van Kranendonk greatly extended these results using infrared and Raman spectroscopy. The myriad of fascinating results obtained from the 1950s to the 1970s, which constituted their life work, are summarized in a lucid and inspiring treatise by Van Kranendonk (8). Our results, described in this article, may be regarded as an extension of the Toronto group's studies using high-resolution laser spectroscopy. Patel and his colleagues have also used laser spectroscopy for a systematic study of solid H<sub>2</sub> overtone bands (9). They used the optoacoustic detection method and emphasize sensitivity.

The sharpness of the spectral lines of solid H<sub>2</sub> results from the purity of the H<sub>2</sub> quantum states and the slow relaxation between these states. This was strikingly evident in the microwave spectrum of  $J = 1$  H<sub>2</sub> pairs in nearly pure para-H<sub>2</sub> reported by Hardy & Berlinsky (10, 11). In these remarkable experiments they obtained linewidths on the order of a few megahertz. Because the Doppler effect does not cause broadening in the solid state (12), our sharp infrared spectral lines should have been anticipated from Hardy & Berlinsky's microwave experiments.

The theory for solid hydrogen spectroscopy has evolved with the experimental developments. The initial work by Pauling (13), and Nakamura's paper in 1955 (14), which according to Van Kranendonk "marks the beginning of the modern microscopic theory of the solid hydrogen" (8, p. vi), are classics. Of particular importance for solid hydrogen spectroscopy are Van Kranendonk's classic papers on optical spectroscopy (15, 16), Harris' detailed work on intermolecular and crystal-field interactions (17, 18), and the many theoretical papers that followed. These studies are summarized in Van Kranendonk's book (8). In addition to these results, we find the group theoretical treatment by Miller & Decius (19) particularly useful in discussing qualitative symmetry topics such as selection rules and interactions between states.

## PARAHYDROGEN CRYSTAL

Hydrogen forms the simplest and most fundamental molecular crystals, in which dispersion forces hold H<sub>2</sub> molecules together in the most effective packing structures, i.e. in the hexagonal close packed (hcp) or face centered cubic (fcc) structure. Fundamental properties of solid hydrogen are summarized in a review by Silvera (20) and a monograph by Souers (21). Under the conditions of our experiments, that is, at low ortho concentration and at liquid He cryogenic temperature, the crystal has exclusively the hcp

structure, as confirmed spectroscopically (see the section on the stimulated Raman spectrum below). The nearest-neighbor distance of 3.793 Å is larger than those of most other simple crystals.<sup>3</sup> The large intermolecular distance together with the small mass and binding energy ( $\sim 25 \text{ cm}^{-1}$ ) cause quantum effects to dominate the properties of solid  $\text{H}_2$ . Thus, together with helium crystal, hydrogen crystals ( $\text{H}_2$  and its isotopic species) are categorized as quantum crystals (24). For such crystals the quantum mechanical zero-point energy is comparable to the binding energy "and the root-mean-square deviation of a particle from its lattice site is not small compared to the nearest-neighbor distance. The problem is not simply that the anharmonic terms are large; it is that the harmonic approximation itself breaks down" (24, p. 120). The variety of spectral lines in solid hydrogen should provide much information about quantum crystals.

Molecules in solid hydrogen have almost free vibrational and rotational quantum states for the following reasons: (a) The hcp structure has the high symmetry of  $D_{3h}$ , and half of the intermolecular distance (1.90 Å) is well above both the internuclear distance (0.74 Å) and the van der Waals radius (1.57 Å) of  $\text{H}_2$ . (b) The electronic charge distribution in  $\text{H}_2$  is nearly spherical, as experimentally manifested by the fact that the  $g$ -value of the rotational magnetic moment (+0.88291) (25) is nearly equal to +1 (26). This minimizes the angular-dependent intermolecular interactions resulting from electron overlap and dispersion. The largest of the orientation-dependent interaction is the electric quadrupole-quadrupole (EQQ) interaction, which is on the order of magnitude of  $Q^2/R^5 \sim 2.8 \text{ cm}^{-1}$ , where  $Q$  is the electric quadrupole of  $\text{H}_2$  and  $R$  is intermolecular distance. (c) Separation of the rotational energy levels is large owing to the very large rotational constant of  $\text{H}_2$  ( $B = 59.3 \text{ cm}^{-1}$ ). Since ortho- and para- $\text{H}_2$  may be regarded as separate species, the smallest energy interval is between  $J = 2$  and 0 ( $355.87 \text{ cm}^{-1}$ ), and therefore the mixing of these levels by the EQQ interaction is less than 1%.

Parahydrogen crystals are composed almost exclusively of  $J = 0 \text{ H}_2$ , except for a small impurity ( $\sim 10^{-3}$ ) of  $J = 1 \text{ H}_2$ . It is a particularly pure system because the probability distribution of the protons and the electrons in the  $J = 0$  rotational level is spherically symmetric, and the crystal may be regarded as an atomic crystal for many applications. Both the electronic and the nuclear magnetic moments vanish ( $S = 0, I = 0$ ). This simplicity

<sup>3</sup> Nearest-neighbor distances of He (hcp), Ne (fcc), and Ar (fcc) crystals are 3.50 Å, 3.20 Å, and 3.83 Å, respectively. Those for carbon and silicon crystals are 1.54 Å and 2.35 Å, respectively (22). Note also that the intermolecular distance in the  $\text{H}_2$  crystal is 0.22 Å greater than the equilibrium distance for the isotropic pair potential of  $\text{H}_2$  (20) and 0.44 Å lower than the  $\text{H}_2\cdots\text{H}_2$  distance in a gaseous hydrogen dimer ( $\text{H}_2$ )<sub>2</sub> (23).

makes the parahydrogen crystal an ideal system for studying the nature of condensed-phase spectroscopy based on first principles. It also makes the crystal a most accommodating host for impurity spectroscopy.

We prepare crystals by introducing paraenriched H<sub>2</sub> gas<sup>4</sup> into a copper or brass sample cell. The cell is thermally attached to a liquid He reservoir through an adjustable heat conductor at a temperature of  $\sim 7$  K. Because the molar volume of para-H<sub>2</sub> varies greatly from the triple point 13.8 K (23.36 cm<sup>3</sup>/mol) to 7 K (23.07 cm<sup>3</sup>/mol) but much less from 7 K to lower temperature, we obtain transparent and fairly stress-free crystals by this procedure. This method of crystal preparation is perhaps inferior to the more elaborate single-crystal preparation method (27), but it is more flexible, especially for impurity spectroscopy. It allows us to prepare crystals of a variety of lengths up to 11.5 cm. These crystals are optically transparent, except near the center of the crystal, and give sharp spectral lines whose frequencies are reproducible. We believe that during the growth of the crystal, hydrogen molecules are liquid at surface layers due to the low stabilizing potential, and the solidification proceeds through delicate diffusion and tunneling, resulting in a well-ordered crystal.

## 2<sup>6</sup> POLE-INDUCED $W_0(0)$ TRANSITION

### *Many-Body Radiative Interaction*

When Okumura et al (6) observed the sharp spectral line of the 2<sup>6</sup> pole (tetrahexacontapole)-induced  $J = 6 \leftarrow 0$   $W_0(0)$  rotational transition, we were novices in condensed-phase spectroscopy and were surprised by the striking quantitative and qualitative differences between gaseous and solid-state spectra. First, such high  $\Delta J$  rotational transitions are highly forbidden (28) in the gas phase. In the gaseous phase at low pressures, the molecules individually interact with the applied radiation. In this case, the intensities of transitions scale by  $(a/\lambda)^2$  as we compare the dipole (2<sup>1</sup> pole)-induced transition to the quadrupole (2<sup>2</sup> pole)-induced transition, where  $a$  is the molecular dimension and  $\lambda$  is the wavelength of radiation (29). Because  $a/\lambda \ll 10^{-4}$  for H<sub>2</sub> and infrared radiation, we cannot expect to see the  $W_0(0)$  transition as it is induced by the 2<sup>6</sup> pole, and it should be weaker than the quadrupole spectrum by  $(a/\lambda)^8 \sim 10^{-37}$ . The transition is rendered

<sup>4</sup>Paraenriched H<sub>2</sub> gas is obtained by passing high-purity normal H<sub>2</sub> from a Pd H<sub>2</sub> purifier through a column of APACHI nickel silica gel that is immersed in a liquid H<sub>2</sub> bath. The fraction of ortho-H<sub>2</sub> is given by  $\epsilon \sim 9 \exp(-\Delta E/T)$ , where  $\Delta E = 170.5$  K is the energy separation of the ortho ( $J = 1$ ) and para ( $J = 0$ ) H<sub>2</sub>, and  $T$  is the temperature of the catalyst.  $\epsilon = 0.21\%$  at  $T = 20.4$  K (boiling point) and  $\epsilon = 0.0039\%$  at 13.8 K (triple point). I have used  $\epsilon = 0.20$ – $0.05\%$ . The concentration is measured with relative intensities of spectral lines.

observable in the solid state by a different absorption mechanism, as Van Kranendonk initially showed (16).

Although the probability that the electric multipole moment of hydrogen  $Q_l$  ( $l = 2, 4, 6, \dots$ ) will interact directly with radiation is small, the moment creates an electrostatic potential  $\phi(R_i)$  at positions  $R_i$  of surrounding molecules  $i$  given by

$$\phi(R_i) = -Q_l \sum_{\Omega} C_{l\Omega}(\Omega) C_{l\Omega}^*(R_i) / R_i^{l+1} \quad 1.$$

where  $C_{l\Omega}(\Omega)$  and  $C_{l\Omega}(R_i)$  are the Racah spherical harmonics<sup>5</sup> for the angular orientation  $\Omega$  of the central hydrogen molecule, and ~~these of  $R_i$~~  ~~are the harmonics~~ for the surrounding molecules  $i$  with respect to the crystal fixed coordinate system. This potential gives the electric field

$$E(R_i) = -\nabla\phi(R_i) \quad 2.$$

and induces a dipole moment in the crystal

$$\mu = -\alpha \sum_i E(R_i), \quad 3.$$

where  $\alpha$  is the isotropic polarizability<sup>6</sup> of  $H_2$ . The dipole moments induced in the surrounding  $H_2$  molecules together interact with the radiation (whose wavelength is much greater than their dimension) and send the absorbed energy to the central molecule. As a result, the central molecule acquires six units of angular momenta. Equations 1-3 show that in such a many-body absorption, the dipole scales by  $a/R$  as  $l$  increases by 1; that is, the intensity scales by  $(a/R)^2$ . Because  $a/R \sim 10^{-1}$  is much larger than  $a/\lambda$ , the higher-order multipole-induced spectrum is observable in solid-state spectroscopy. The dipole moment induced in the surrounding molecules by the  $2^6$  pole moment of  $H_2$  is on the order of  $10^{-6}$  D (30, 31). This is a small transition moment, but the column density of the absorber is enormous ( $\sim 10^{23} \text{ cm}^{-2}$ ) because practically all molecules in the optical path are in the  $J = 0$  level and are ready to absorb resonant radiation. This large column density of absorbers is a significant quantitative difference between gaseous and solid-state spectroscopy.

The many-body nature of the absorption mechanism affects not only the discussion of the quantitative orders of magnitude but also the qualitative symmetry argument. In gaseous spectroscopy, the selection rules depend

<sup>5</sup>The Racah spherical harmonics are related to the usual spherical harmonics by  $C_{l\Omega}(R) = (4\pi/2l+1)^{1/2} Y_{l\Omega}(\theta, \phi)$ .

<sup>6</sup>The isotropic polarizability of  $H_2$ ,  $\alpha = (2\alpha_{\parallel} + \alpha_{\perp})/3$  is  $5.41 \text{ au} = 0.802 \text{ \AA}^3$ . The anisotropy  $\gamma = \alpha_{\parallel} - \alpha_{\perp}$  is  $2.02 \text{ au} = 0.300 \text{ \AA}^3$ . The anisotropy does not enter into this discussion unless the simultaneous rotational transition of surrounding molecules is considered.

only on the symmetry of the molecule. In contrast, we now have to consider the symmetry of both the molecule and the crystal. The symmetry of the crystal enters into the discussion through the summation over  $i$  in Equation 3. For example, the summation vanishes for even  $l$  if the crystal has an fcc structure in which each molecular site is a center of symmetry. This is because each neighbor molecule has its counterpart at the position diametrically opposed, and their induced dipole moments cancel each other. The very fact that we see the  $W_d(0)$  transition is proof that our sample contains hcp crystals. In order to discuss selection rules in an hcp crystal, we rewrite Equation 3 by explicitly calculating the  $\nabla$  operation in Equation 2 (8).

$$\mu_k = (-1)^{l+1} \alpha Q_l [(l+1)(2l+1)]^{1/2} \sum_m C(1, l, l+1; k\bar{m}) C_{lm}(\Omega) \times \sum_i C_{l+1, m-k}^*(\mathbf{R}_i) / R_i^{l+2}, \quad 4.$$

where  $\mu_k$  ( $k = 0, \pm 1$ ) are the spherical components of the dipole operator and  $C(1, l, l+1; k\bar{m})$  is a Clebsch-Gordan coefficient. In order for the summation over  $i$  to be nonvanishing, it must be totally symmetric with respect to all symmetry operations. If we take the crystal fixed  $z$ -axis along the direction of the  $C_3$  axis, we see the symmetry properties of spherical harmonics under rotation  $C_3$  and plane reflection  $\sigma_h$  as

$$C_3 C_{LM}(\Omega) = e^{2\pi M/3} C_{LM}(\Omega) \\ \sigma_h C_{LM}(\Omega) = (-1)^{L+M} C_{LM}(\Omega). \quad 5.$$

We note that for even  $l$  the summation is nonvanishing only when

$$m-k = 3 \pmod{6}. \quad 6.$$

Thus for the  $J = 6 \leftarrow 0$  transition, the parallel transition (caused by  $\mu_0$ ) has selection rule  $\Delta M = \pm 3$  and the perpendicular transitions (caused by  $\mu_{\pm}$ ) have selection rule  $\Delta M = \pm 2$  and  $\pm 4$ ; this is quite different from the case with gaseous spectroscopy.

This symmetry argument becomes more transparent if we use the theory of Miller & Decius (19). To consider the symmetry of the molecule and the crystal simultaneously, they introduced an extended group of symmetry operations composed of the product of permutation inversion operations of the molecule and the point group operation of the crystal, excluding from them products of proper and improper operations. Thus for H<sub>2</sub> molecules of  $S_2^+$  symmetry with symmetry operations  $(E, \bar{C}_2, E^*, \bar{C}_2^*)'$  and

' $S_2^+$ ' denotes the direct product of permutation (symmetry) group  $S_2$  ( $E, C_2$ ) and inversion group  $E^*$  ( $E, E^*$ ). Bars above the operations remind the reader that these are molecular operations.

for the hcp crystal of  $D_{3h}$  symmetry with symmetry operations ( $E, 2C_3, 3C_2, \sigma_h, 2S_6, 3\sigma_v$ ), we obtain an extended group  $G_{24}$  that is isomorphic to  $D_{3h}$ . However, because ortho and para molecules behave almost completely separately, we may drop the  $\bar{C}_2$  operation and use the  $G_{12}$  group composed of ( $EE, 2C_3E, 3C_2E, \sigma_hE^*, 2S_6E^*, 3\sigma_vE^*$ ). Because this group is isomorphic to  $D_{3h}$ , we may use the  $D_{3h}$  symbol for irreducible representation. The rotational wave function for a  $J, K$  state transforms as Equation 5; hence we have the symmetry of rotational states summarized in Table 1 (32). The symmetry of  $\mu_0(A_1^2)$  and  $\mu_{\pm 1}(E')$  gives the selection rules  $\Delta M = \pm 3$  and  $\Delta M = \pm 2, \pm 4$ , respectively. If the  $J = 10 \leftarrow 0$  transition is observed, the selection rules will be  $\Delta M = \pm 3, \pm 9$  and  $\Delta M = \pm 2, \pm 4, \pm 8, \pm 10$ , respectively.

### Crystal Field Splitting

The 13  $M$  sublevels of the  $J = 6$  rotational states that are degenerate in isotropic space split into multiplets in the crystal. The symmetry of these sublevels (shown in Table 1) indicates that they split into nine levels, but the  $A_1, A_2$  splittings are extremely small and they may be regarded as degenerate.

The selection rules allow us to observe only three levels out of the seven split levels corresponding to  $M = 0, \pm 1, \dots, \pm 6$ . Laser spectroscopy allowed Chan et al to observe this splitting (32), as shown in Figure 2. The crystal field results from a variety of pair-wise intermolecular interactions between the central  $H_2$  and the surrounding molecules, such as induction and dispersion, second-order quadrupole effect, electron overlap, etc. Regardless of the nature of interaction, the effect is exhausted by the most general expression for pair-wise interactions:

Table 1 Symmetry of rotational states and dipole operators in hcp para- $H_2$  crystal

Rotational levels		Symmetry
$M = 0$	$J$ even	$A_1'$
	$J$ odd	$A_2'$
$M \neq 0$	$M = 0 \text{ (mod. 6)}$	$A_1' + A_2'$
	$M = \pm 1 \text{ ( " )}$	$E'$
	$M = \pm 2 \text{ ( " )}$	$E'$
	$M = 3 \text{ ( " )}$	$A_1' + A_2'$
Dipole operators:		
$\mu_0$		$A_2'$
$\mu_{\pm 1}$		$E'$

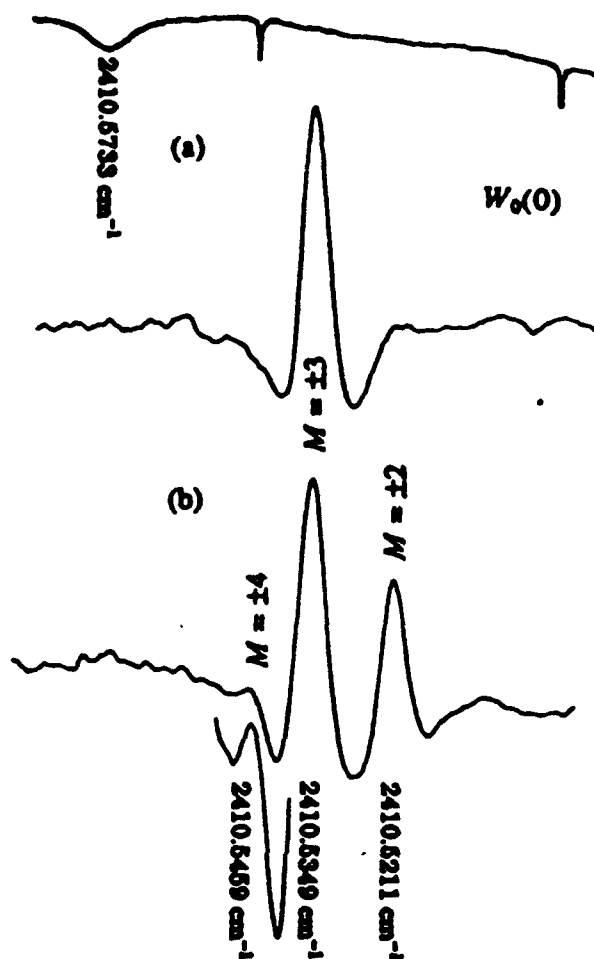


Figure 2 Crystal field splitting of the  $J = 6 \leftarrow 0$   $W_0(0)$  transition. The spectrum of para- $H_2$  crystal containing 0.06% of ortho- $H_2$  was recorded by using a difference frequency laser system with 40 MHz rf tone burst modulated at 6 kHz (32). The plane of polarization of radiation is parallel to the crystal axis for the upper trace and perpendicular for the lower.

$$V_i = \sum_{l,l'm} B_{lm}^l(R_i) C_{lm}(\omega) C_{l'm}(\omega_i), \quad 7.$$

where  $\omega$  and  $\omega_i$  are the angular orientations of the central and neighboring  $H_2$  with respect to the axis connecting them, and the coefficients  $B_{lm}^l(R_i)$  are independent of angles. The summations over  $l$  and  $l'$  are limited to even values because of the symmetry of  $H_2$ . In considering the crystal field effect we are concerned only with the  $l' = 0$  terms, and therefore,

$$V_i = \sum_{lm} C_{lm}(\Omega) \sum_l B_m(R_i) C_{lm}^0(R_i), \quad 8.$$

where now  $\Omega$  and  $R_i$  are angular orientations with respect to crystal fixed axes. Symmetry consideration, in Equation 5 shows that the summation

over  $i$  in Equation 8 is nonvanishing only when  $m = 0 \pmod{6}$ .<sup>8</sup> Considering the two lowest order terms, we obtain an effective field energy of

$$V_c = \epsilon_{2c} C_{20}(\Omega) + \epsilon_{4c} C_{40}(\Omega). \quad 9.$$

The summation over  $i$  for  $l = 2$  in Equation 8 vanishes for the nearest and next-nearest neighbors, and the sums for remaining shells of molecules are small and tend to alternate in sign. As a result of this accidental vanishing of the lattice sum, the value of  $\epsilon_{2c}$  is very small, and the observed splitting can be explained almost entirely by the  $\epsilon_{4c}$  term. If we use the value  $|\epsilon_{2c}| = 0.0058 \text{ cm}^{-1}$  reported by Schweizer et al (34) from NMR measurements with negative sign, we obtain  $\epsilon_{4c} = -0.1224 \text{ cm}^{-1}$ . This value of  $\epsilon_{4c}$  seems to agree with the sum of the induced effect (which can be expressed analytically) and the dispersion effect [obtained from the ab initio calculations of Mulder et al (35)]. Similar crystal field splitting has been observed for the vibration-rotation transition  $W_1(0)$ , discussed below.

Another mechanism of  $M$ -level splitting results from hopping of the  $J = 6$  rotational excitation (roton) in the crystal (8). This dynamic effect plays the major role in producing the large splitting ( $\sim 2 \text{ cm}^{-1}$ ) of the  $M = 0, 1$ , and 2 levels in the  $S_0(0)$  rotational Raman spectrum (36). The hopping of the  $J = 6$  roton, however, is much slower than that of  $J = 2$  rotors because the energy of the required  $2^6$  pole- $2^6$  pole interaction is much lower (by a factor of  $\sim 10^{-7}$ ) than that of a quadrupole-quadrupole interaction. The splitting that results from this mechanism is on the order of  $\sim 10 \text{ kHz}$  and is negligible compared to the static mechanism discussed above.

One qualitative feature of the observed spectrum given in Figure 2 remains unexplained. The prominence of the  $\Delta M = \pm 3$  transitions for both laser polarizations has not been clear from our intensity calculations using Equation 4, even if we consider a variety of orientations of mixed crystals.

### *Spectral Linewidths*

The spectral linewidths reported in this article are sharp for a variety of reasons. While my students and I have not yet studied this problem quantitatively, I discuss the qualitative aspects of the observed spectral widths for each transition. In general, spectral lines are sharp when inhomogeneous broadening is small and the lifetimes of population relaxation ( $T_1$ ) and phase coherence relaxation ( $T_2$ ) are long. The inhomogeneous broadening in the solid state results from interactions with impurities that are randomly distributed in the crystal and from macro-

<sup>8</sup> The small  $m = \pm 6$  term split the  $A_1^+ + A_2^+$  levels for  $M = \pm 3$  (33).



scopic nonuniformity and stress in the sample. Our observation of significantly sharper spectral lines for other transitions (discussed below) seems to exclude the latter cause of inhomogeneous broadening. This is surprising in view of our primitive method of crystal preparation. Impurities in parahydrogen crystals are ortho ( $J = 1$ ) H<sub>2</sub> ( $\sim 10^{-3}$ ), which remains unconverted, and the deuterated species HD in natural abundance ( $3 \times 10^{-4}$ ). The interaction of a  $J = 6$  H<sub>2</sub> with the nearest-neighbor  $J = 1$  H<sub>2</sub> is mainly through the EQQ interaction, and causes the  $J = 6 \leftarrow 0$  spectral line to split into a pattern of 21 components that span a region of  $\sim 5$  cm<sup>-1</sup>. As described below in connection with the  $W_1(0)$  transition, these structures, resulting from interactions not only with nearest neighbors but also with next-nearest (nn) and next-next nearest neighbors (nnn) etc, are all resolved. Only split components resulting from much farther neighbors start to pile up at the center and cause inhomogeneous width. The perturbation due to HD is probably less serious, because they are all in the  $J = 0$  level and the EQQ interaction vanishes in first order.

The  $T_1$  relaxation of the  $J = 6$  roton is expected to be slow because of the large energy mismatch between the  $J = 6 \rightarrow 4$  transition ( $1243.4$  cm<sup>-1</sup>) and the Debye temperature of phonon  $\Theta_D \sim 100$  K (37). The phonon distribution and its interaction with the  $J = 6$  roton is related to the observed phonon sideband of the  $W_0(0)$  transition recorded under low resolution, as shown in Figure 3 (32). This phonon band is induced as a simultaneous excitation of the  $W_0(0)$  transition and a phonon by a single

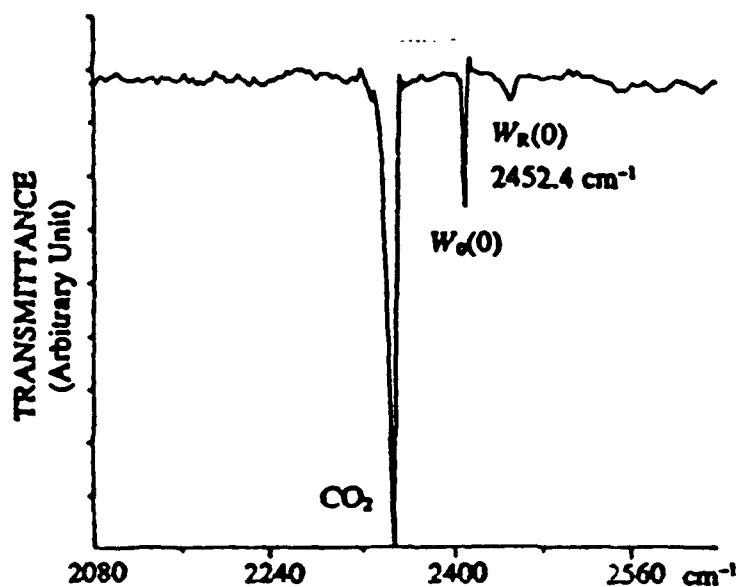


Figure 3 Low resolution ( $\sim 4$  cm<sup>-1</sup>) FTIR spectrum showing the  $W_R(0)$  phonon sideband (32). The strong absorption on the left results from a trace amount of CO<sub>2</sub> in the N<sub>2</sub> purged optical path.

photon, owing to the strong dependence of the  $2^{\text{nd}}$  pole-induced dipole moment on the intermolecular separation (38). This dependence will also cause the relaxation of the  $J = 6$  rotons, but because of the large energy mismatch, a highly nonlinear term is required. Such a term is obviously very small. The  $T_1$  relaxation will be much faster if the energy mismatch is smaller. I return to this point below in connection with the relaxation of the  $J = 2$  roton of  $D_2$ .

The  $T_2$  relaxation may occur in two ways. The dependences of  $T_2$  relaxation on ortho- $H_2$  concentration, observed for the  $v = 1$  vibron (39) and the  $J = 2$  roton (40), were ascribed to dephasing of the Bloch state and the resulting violation of the exciton momentum selection rule (41, 42). This broadening mechanism does not apply to the  $J = 6$  roton because the hopping frequency is very low. Vanhimbeeck et al (42) explained the dephasing of the  $J = 2$  rotons in ortho free crystal as resulting from second-order treatment of the EQQ interaction. How their theory applies to the  $J = 6$  roton remains to be seen.

The observed reduction in linewidth from 90 MHz (6) to 70 MHz (32) with a reduction in concentration of ortho- $H_2$  from 0.20% to 0.06% indicates that inhomogeneous broadening caused by ortho- $H_2$  through the first-order EQQ is at least partially responsible for the observed linewidth.

## $Q_1(1)$ AND $Q_1(0)$ TRANSITIONS, FINE STRUCTURE, AND EXCITON BAND

### *$J = 1$ Pair Interaction and Fine Structure of $Q_1(1)$ Transitions*

The sharp spectral line of the  $W_0(0)$  transition discussed above immediately remind me of the beautiful microwave spectrum of  $J = 1$  pairs in para- $H_2$  crystals reported by Hardy & Berlinsky in 1975 (10). We thus applied our difference frequency laser spectrometer to the observation of the  $Q_1(1)$  ( $v = 1 \leftarrow 0$ ,  $J = 1 \leftarrow 1$ ) vibration-rotation transition at  $4146.6 \text{ cm}^{-1}$  and found an incredible number of very sharp and strong spectral lines (43). We have seen over 200 lines spread over a range of  $13 \text{ cm}^{-1}$  from  $4153.2 \text{ cm}^{-1}$  to  $4140.5 \text{ cm}^{-1}$ . Figure 4 shows the central portion of  $0.7 \text{ cm}^{-1}$ . These spectral lines with linewidths of  $< 50 \text{ MHz}$  are all the result of intermolecular interactions between  $J = 1$   $H_2$  pairs that are statistically distributed in the crystal.\* With an ortho- $H_2$  concentration of  $\sim 0.06\%$ , the pair concentration is on the order of  $\sim 10^{-6}$  but the spectrum has considerable intensity.

\*Since the ortho- $H_2$  molecules diffuse in the crystal through resonant ortho-para conversion (44) but are stabilized and trapped when a pair is formed, the number of ortho pairs is higher than expected from a random distribution.

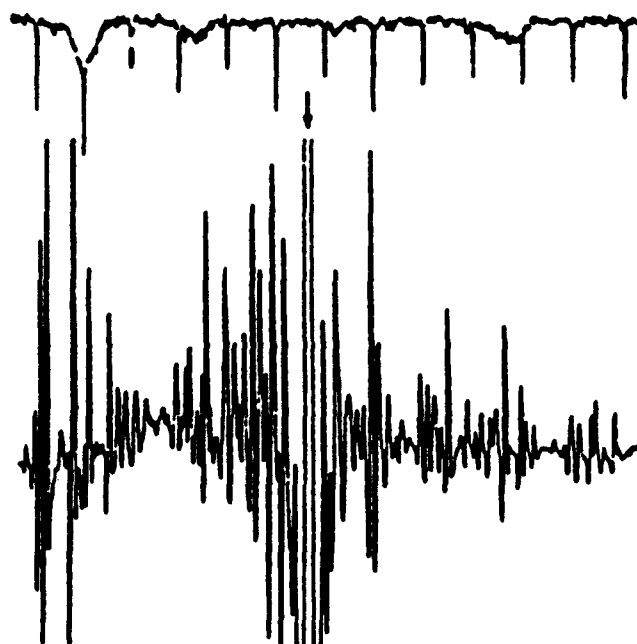


Figure 4 Highly congested region of about  $0.7 \text{ cm}^{-1}$  around the  $Q_1(1)$  central line. These structures result from the electric quadrupole-quadrupole interaction caused by relatively widely separated  $J = 1$  pairs. The central line (arrow) is saturated and does not give a sharp second-order derivative.

The  $3 \times 3$ -fold degenerate levels of a pair of  $J = 1$   $\text{H}_2$  represented by  $|M_1, M_2\rangle^{10}$  are split by a variety of intermolecular interactions, the largest of which is the EQQ interaction (14),

$$V_{\text{EQQ}} = \sqrt{70} \frac{Q_1^2}{R_{12}^3} \sum_m C(224; mm^0) C_{2m}(\omega_1) C_{2m}(\omega_2), \quad 10.$$

where  $\omega_1$  and  $\omega_2$  are the angular orientations of the two  $J = 1$   $\text{H}_2$  with respect to the intermolecular axes. This interaction splits the ninefold degenerate levels into four levels whose eigenfunctions are the bipolar spherical harmonics  $|F, M\rangle^{10}$  where  $F = 2, 1, 0$  and  $F \geq |M|$ . The split levels have energies

$$\begin{aligned} 6\Gamma & \text{ for } |2, 0\rangle \\ \Gamma & \text{ for } |2, \pm 2\rangle \\ 0 & \text{ for } |0, 0\rangle, |1, 0\rangle, |1, \pm 1\rangle \end{aligned}$$

and

$$-4\Gamma \text{ for } |2, \pm 1\rangle,$$

<sup>10</sup>  $J_1 = J_2 = 1$  are omitted in these notations for brevity.

where  $\Gamma = 6Q_2^2/25R^3 \sim 0.672 \text{ cm}^{-1}$  for nearest-neighbor pairs. The degeneracy of the  $|0,0\rangle$ ,  $|1,0\rangle$ , and  $|1,\pm 1\rangle$  states lifts when other angle-dependent interactions are taken into account. The interactions include the second-order EQQ effect, induction, dispersion, and electron overlap. The remaining double-degeneracy of the  $\pm M$  level is removed when the interaction of the pair molecules with the surrounding  $J = 0 \text{ H}_2$  is included, as initially shown by Harris (17). Because the last effect depends on the relative orientation of the pair and crystal, we have two sets of nine split levels, one for the nearest-neighbor pairs in the hexagonal plane of the crystal (in-plane pairs) and the other for those out of the plane (out-of-plane pairs). Transitions between components of these two sets of nine levels were what Hardy et al observed and analyzed in the microwave region (10, 11, 18).

The richness of the infrared spectrum of the  $Q_1(1)$  transition results from the ninefold multiplicity in the ground state as well as in the excited state. The overall spectral pattern is given in Figure 5. The strongest central line at  $4146.5606 \text{ cm}^{-1}$  is the  $Q_1(1)$  transition of isolated  $J = 1 \text{ H}_2$  in a para- $\text{H}_2$  matrix. Accompanying this line are numerous closely spaced

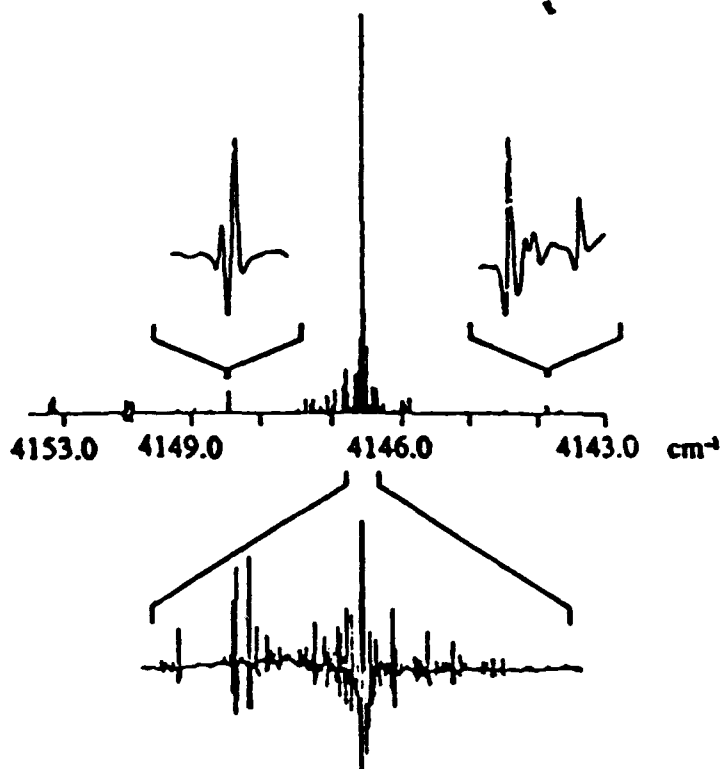


Figure 5 A computer-generated stick spectrum and some observed spectral lines of solid  $\text{H}_2$  (43). The group of lines above  $4153 \text{ cm}^{-1}$  results from the  $Q_1(0)$  transitions, and others result from the  $Q_1(1)$  transitions. The ortho  $\text{H}_2$  concentration was 0.06%.

satellite lines that result mainly from splittings caused by relatively distant  $J = 1$  H<sub>2</sub> pairs and higher clusters (45). In effect, we have resolved the inhomogeneous broadening observed earlier by classical methods (46, 47). When the ortho-H<sub>2</sub> concentration was reduced from 0.2% to 0.06%, the relative intensities of satellite lines to the central line were greatly reduced, as expected. On both sides of the highly congested central area, we observe many widely-spaced spectral lines corresponding to transitions between split levels of relatively close  $J = 1$  H<sub>2</sub> pairs. Some of them have been assigned based on Hardy & Berlinsky's spectrum in the ground state and on calculated relative intensities. The two pairs of strong doublets at 4148.5 cm<sup>-1</sup> and 4143.8 cm<sup>-1</sup> shown in Figure 5 are assigned to the pair transitions  $(1, 1)'_{\pm} \leftarrow (2, 1)_{\pm}$  and  $(2, 1)'_{\pm} \leftarrow (1, 1)_{\pm}$ , respectively for the out-of-plane  $J = 1$  pairs, where prime denotes the excited state and  $\pm$  represents symmetrized  $\pm M$  levels.

Since the infrared transition is caused by a many-body absorption mechanism resulting from the quadrupole-induced dipole moment, the intensity of the  $Q_1(1)$  transition depends on the vibrational dependence of the quadrupole moment  $Q_{10} \equiv |\langle r = 1 | Q | r = 0 \rangle|$  and of the isotropic and anisotropic polarizabilities  $\alpha_{10}$  and  $\gamma_{10}$ . A complication arises because the vibrational excitation (vibron) may hop between the two molecules of the pair. Based on the width of the vibron band for the  $Q_1(0)$  transition, this effect is expected to produce a splitting between the symmetric and antisymmetric vibrational levels on the order of 0.4 cm<sup>-1</sup>. The symmetry argument facilitates calculation of the individual transition moments by using the extended group of the  $S_2^* S_2^*$  permutation inversion symmetry of the pair and the  $C_{2v}$  (in-plane pair) and  $C_{2h}$  (out-of-plane pair) point groups of the crystal. The assignment of these 200 lines is still at a very primitive stage. A planned microwave infrared double-resonance experiment should untangle this enigma. A complete list of spectral lines is available upon request.

### *Spectral Linewidth*

The observed sharpness of the  $Q_1(1)$  spectral lines is well understood qualitatively. The inhomogeneous interactions resulting from randomly distributed ortho-H<sub>2</sub> are all resolved. The  $T_1$  relaxation from the  $v = 1$   $J = 1$  level to the  $v = 0$   $J = 1$  level is expected to be slow because of the large mismatch between their energy difference and phonon Debye temperature  $\Delta E \gg k\Theta_D$ . This relaxation rate has been reported to be 10–100 kHz (48, 49). The  $T_1$  relaxation between the split levels of the ortho pair is also small because of the energy mismatch (this time  $\Delta E \ll k\Theta_D$ ), as demonstrated by the sharp spectral lines of Hardy & Berlinsky's microwave spectrum (10, 11). The  $T_2$  relaxation of the vibron is slow because of the

energy mismatch between the  $Q_1(1)$  transition of ortho- $H_2$  and the  $Q_1(0)$  transition of the surrounding para- $H_2$ . The mismatch of  $\sim 6 \text{ cm}^{-1}$  results from the large difference between the rotational constants of  $H_2$  in the ground and excited states. The observed sharp spectral lines provide evidence for the localization of the vibron.

### *$J = 1$ -Induced $Q_1(0)$ Transition and Exciton Band*

The vibrational coupling between neighboring molecules in solid  $H_2$  and  $D_2$  broadens the excited vibrational levels into energy bands which are the simplest and most perfect examples of single-band Bloch states in all of solid state physics.

Van Kranendonk 1983 (8)

The  $Q_1(0)$  transition ( $v = 1 \leftarrow 0, J = 0 \leftarrow 0$ ) appears  $\sim 6 \text{ cm}^{-1}$  above the  $Q_1(1)$  transition. The infrared (single photon)  $J = 0 \leftarrow 0$  transition is strictly forbidden in gaseous spectroscopy regardless of the molecular symmetry and physical nature of the radiative interaction. It becomes allowed in the solid state by the presence of a neighboring ortho- $H_2$  impurity which induces the dipole moment, and itself makes a simultaneous transition. The theory of this mechanism proposed by Sears & van Kranendonk (50) satisfactorily explains the selection rules and an intensity of the observed spectrum (46). Unlike the  $Q_1(1)$  vibrons that are localized on ortho- $H_2$ , the  $Q_1(0)$  vibrons hop freely around the nearly pure para- $H_2$  crystal with a hopping time of  $\sim 100 \text{ ps}$ . Eigenstates of such hopping vibrons are expressed by Bloch waves (8).

$$U_k(R_i) = N^{-1/2} \exp(ik \cdot R_i) \quad 11.$$

where  $k$  is the exciton propagation momentum vector and  $N$  is the number of molecules in the crystal. The  $N$  eigenstates corresponding to different values of  $k$  in the first Brillouin zone form an exciton band with energy spanning several  $\text{cm}^{-1}$ . If the crystal is perfect, the exciton momentum selection rule for the  $Q_1(0)$  transition  $\Delta k = 0$  results from the equality

$$\lim_{N \rightarrow \infty} N^{-1} \sum_{i=1}^N e^{ik \cdot R_i} = \delta(k), \quad 12.$$

where  $\delta(k)$  is 1 for  $k = 0$  and 0 otherwise. Because the  $Q_1(0)$  transition results from the presence of impurity ortho- $H_2$ , however, the sum over  $i$  in Equation 10 does not extend over the crystal, and the  $\Delta k = 0$  rule is violated. Thus we can observe the whole vibron band. Figure 6 shows a low-resolution spectrum of the band recorded by Chan. The observed spectrum may be compared with theoretically calculated density of states

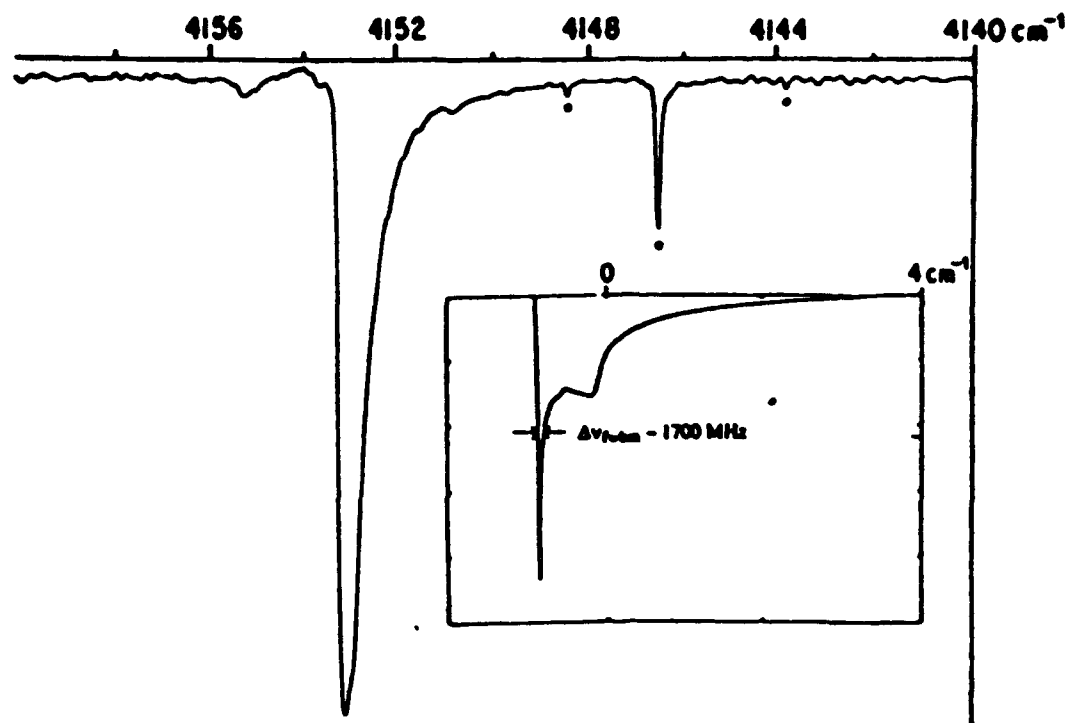


**Figure 6** Low-resolution Fourier transform infrared spectrum of the  $Q_1(0)$  exciton band (at  $\sim 4153 \text{ cm}^{-1}$ ) and the  $Q_1(1)$  structure (filled circles). Inset shows theoretical exciton band calculated by Bose & Poll (51). Other features result from simultaneous transitions not discussed in the text.

reported by Bose & Poll (51), which is shown in the inset of Figure 6. The spectrum and calculated density agree well, that is, they both have a sharp cut-off at the high-frequency end and a shoulder at about  $0.7 \text{ cm}^{-1}$  from the cut-off. The  $k = 0$  eigenstate is located at the bottom of the exciton band. The stimulated Raman spectrum of the  $Q_1(0)$  transition at  $4149.75 \text{ cm}^{-1}$ , discussed below, represents the sharp transition to this state.

Higher-resolution spectroscopy has revealed several sharp features at the high-frequency edge of the exciton band spectrum (43). These features, shown in Figure 7, are composed of three sets of closely spaced multiplets. Neither the mechanism causing such features nor the spacing of the features has been understood. The position of the sharp features with respect to the exciton band suggests that they correspond to the singularity at the edge of the theoretically calculated exciton band shown in Figure 5. This problem is related to the  $Q_1(0)$  transition of  $D_2$  impurity discussed below.

## FINE STRUCTURE IN $W_1(0)$ TRANSITION

The fine structure of a spectrum provides information on intricate intermolecular interactions in the solid and on a variety of electrical properties

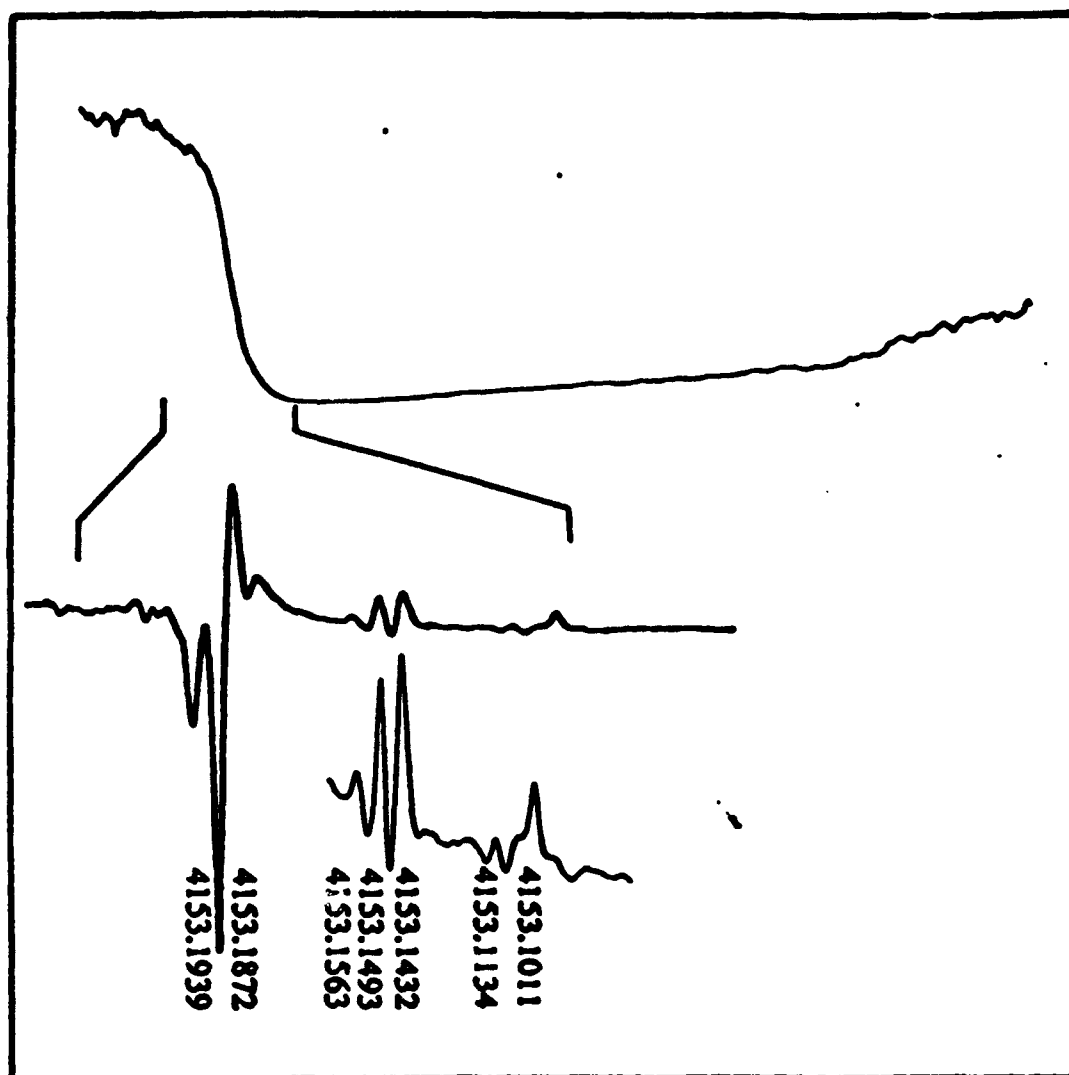


Figure 7 Low-resolution (upper trace) and high-resolution (lower trace) spectrum of the  $Q_1(0)$  transition. The upper trace shows the exciton band while the lower trace gives sharp features in the band (43).

of the molecule and crystal. The analysis of the  $Q_1(1)$  transition, however, is complicated because both the ground and excited states are split into multiplets. The splitting pattern is expected to be simpler if we use a transition starting from the unsplit  $J = 0$  level. It turns out that the  $S_1(0)$  and the  $U_1(0)$  transitions are too broad for observing such fine structure because of the fast relaxation of the  $J = 2$  and  $J = 4$  rotors (this point is discussed below). We thus attempted to observe the fine structure in the  $W_1(0)$  ( $\nu = 1 \leftarrow 0$ ,  $J = 6 \leftarrow 0$ ) transition resulting from the interaction between the  $\nu = 1$   $J = 6$   $H_2$  and neighboring  $J = 1$   $H_2$ . The transition, which appears at  $1.55 \mu\text{m}$ , is weaker than the  $W_0(0)$  transition by a factor



of  $\sim 3$  (6) as the transition moment results from the vibrational dependence of  $2^4$  pole moment  $Q_4$ . Nevertheless, the high sensitivity of spectroscopy at this wavelength afforded by the use of an InGaAsP communication diode laser has allowed Ventrudo et al to observe such fine structure in a para-H<sub>2</sub> crystal with an ortho-H<sub>2</sub> concentration of 2% (52). Figure 8 shows a computer-generated stick diagram of the observed fine structure.

The  $13 \times 3$ -fold degenerate levels of the  $J = 6$ - $J = 1$  pair are split into 21 levels because of a variety of angularly dependent interactions. In principle they further separate into 39 levels owing to the interaction between the pair molecules and the surrounding  $J = 0$  H<sub>2</sub>, but unlike the case of  $J = 1$  pairs, this splitting was not seen in the observed spectrum with the resolution of  $\sim 100$  MHz. The observed fine structure in Figure 7 is being analyzed using the theory of Harris et al (17, 18). The largest effect is the EQQ interaction between the pair molecules. The eigenvalues of this interaction are obtained by diagonalizing the  $3 \times 3$  matrix using a basis of  $|M_1 M_2\rangle$

$$\frac{\Gamma}{11} \begin{vmatrix} (M-1)^2-1 & -(2M-1)[2(7-M)(6+M)]^{1/2}/3 & [(49-M^2)(36-M^2)]^{1/2}/6 \\ & -2(M^2-14) & (2M+1)[2(7+M)(6-M)]^{1/2}/3 \\ \text{Sym.} & & (M+1)^2-14 \end{vmatrix}. \quad 13.$$

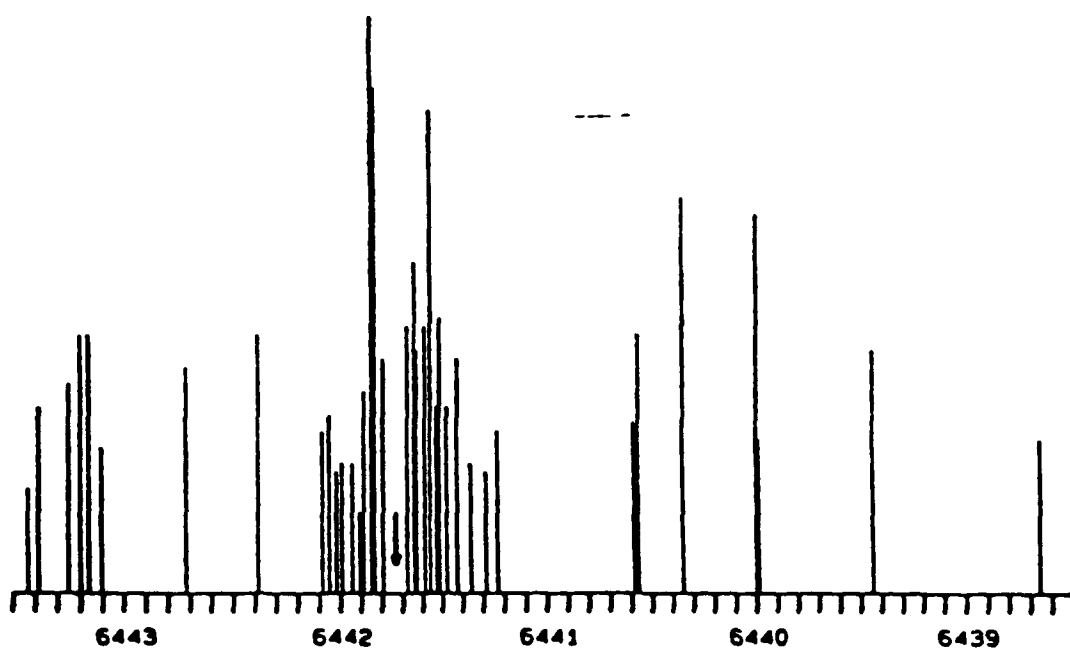


**Figure 8** Computer-generated stick spectrum for the observed  $W_1(0)$  transition. The widely split spectral lines result from the EQQ interactions between the  $J = 6$  H<sub>2</sub> and its nearest-neighbor  $J = 1$  H<sub>2</sub> impurity. The dense satellites around the central line (arrow) are caused by  $J = 1$  H<sub>2</sub> impurities that are farther from the  $J = 1$  molecule.

where  $M = M_1 + M_2$  takes the values from 0, 1, 2, . . . , 7. For  $M = 6$  and 7 the matrix is  $2 \times 2$  and  $1 \times 1$ , respectively. Unlike for the  $J = 1$  pairs, the eigenfunctions of the matrix are not the bipolar spherical harmonics. The EQQ interaction causes splitting of the levels on the order of  $Q^2/R^3 \sim 2.8 \text{ cm}^{-1}$  and explains the gross features of the overall spectrum. Interactions of the next order of magnitude are: electric quadrupole-hexadecapole interaction on the order of  $Q_2 Q_4/R^7 \sim 0.067 \text{ cm}^{-1}$ , second order EQQ interaction on the order of  $[Q^2/R^3]^2/B \sim 0.132 \text{ cm}^{-1}$ , and the polarizability effect  $\alpha[Q_2/R^4]^2 \sim 0.041 \text{ cm}^{-1}$ . The first of these interactions operates only between the  $J = 6-J = 1$  pair while the latter two involve surrounding  $J = 0$  molecules as well. To these three effects we add the crystal-field effect of Equation 9, which includes dispersion and electron overlap. In view of the large effect of phonon normalization (average over crystal oscillations), which effectively reduces these interactions by 10–20%, the terms are each treated independently and their coefficients are determined by a least-squares fitting. The final results remain to be obtained.

## SPECTROSCOPY OF D<sub>2</sub> IMPURITY

### *Fine Structure of $Q_1(0)$ Transition*

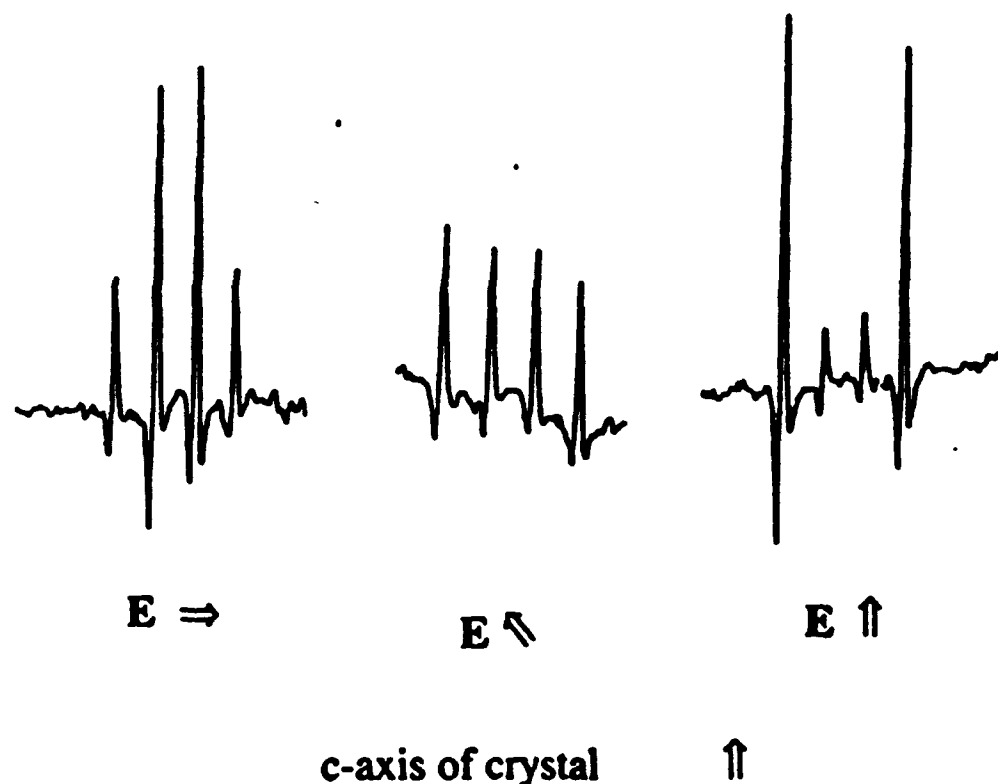
The nearly pure para-H<sub>2</sub> crystal is an excellent matrix for impurity spectroscopy. Because of the large nearest-neighbor distance and the spherical charge distribution and weak interactions in the host  $J = 0$  H<sub>2</sub>, a small impurity molecule may sit snugly in one of the crystal sites and may rotate and vibrate nearly freely. Even when the rotation is hindered by barriers, tunneling through the barriers gives the impurity molecules well-defined quantum states. The simplest impurity to start with is D<sub>2</sub>. A study of the  $Q_1(0)$  transition is of particular interest because, unlike with the transition involving H<sub>2</sub>, the large energy mismatch between the D<sub>2</sub> and the surrounding H<sub>2</sub> vibrational states causes the excitation to be well localized on the D<sub>2</sub> molecule. This allows us to study the fine structure shown in Figure 7 with more clarity.

Figure 9 shows the fine structure of the D<sub>2</sub>  $Q_1(0)$  transition recorded by Chan et al using a difference frequency laser spectrometer (53). This spectrum was taken using a sample of nearly pure (ortho-H<sub>2</sub> 0.06%) para-H<sub>2</sub> crystal in which 0.6% of normal D<sub>2</sub> ( $J = 0$  0.4%,  $J = 1$  0.2%) was embedded randomly. The spectrum is composed of ten lines arranged in four groups whose linewidths are less than 10 MHz. Although some structure was expected from the absorption mechanism of the  $Q_1(0)$  transition, the beautiful quartet on the high-frequency side of the spectrum with linewidths of 7 MHz was unanticipated. A discussion of this fine structure was given by Chan (54).



Figure 9 The  $Q_1(0)$  transition of  $D_2$  impurity in para- $H_2$  crystal (53). The linewidth was less than 10 MHz. The quartet and the singlet (strongest line) are induced by  $J = 1 H_2$ , while other features are induced by  $J = 1 D_2$ .

Weliky et al (55) studied this fine structure more thoroughly using a stabilized color center laser ( $\Delta\nu \sim 0.5$  MHz) and samples with a variety of ortho- $H_2$  and ortho- and para- $D_2$  concentrations. As discussed earlier, the usually forbidden  $Q_1(0)$  transition is induced by nearby  $J = 1 H_2$  (or  $D_2$ ). When Weliky et al used catalyst-converted  $D_2$  composed dominantly of  $J = 0 D_2$ , they observed only the quartet at the high-frequency end and the singlet at  $2986.8628 \text{ cm}^{-1}$ . This clearly demonstrated that these five lines are induced by  $J = 1 H_2$  while the other structures are induced by  $J = 1 D_2$ . When the concentration of  $J = 1 H_2$  and  $D_2$  was decreased the linewidths of the quartet were reduced to 2 MHz and the singlet to 3 MHz. These are the sharpest lines observed thus far. Apparently they continue to narrow with further reduction of ortho- $H_2$ . The fine structure shows an interesting dependence on the plane of polarization of the radiation. The orientation of the unique  $c$ -axis of the hcp crystal was known from the  $W_1(0)$  studies so that the laser electric field polarization could be labeled as either parallel or perpendicular to this axis. The ortho- $H_2$  induced quartet shows a beautiful symmetric polarization dependence (Figure 10). The two outer components are strongest with parallel polarization and the inner components with perpendicular polarization. The integrated



**Figure 10** Variation of the relative intensities of the quartet with the laser polarization. The lines were observed using a stable ( $\Delta\nu \sim 0.5$  MHz) color center laser. The linewidths are  $\sim 2$  MHz.

intensity of the quartet is approximately independent of polarization. These results clearly indicate that the quartet structure results from transitions between the various  $M$  levels of the  $J = 1$   $H_2$ , which simultaneously reorients. The singlet feature shows less pronounced polarization dependence, but its linewidth is about 20% narrower with perpendicular polarization than with parallel. The  $J = 1$   $D_2$ -induced features also exhibit polarization dependences. Even after these clear-cut observations, the exact assignment of these features is yet to be given.

With higher concentration of  $J = 0$   $D_2$  (0.4%), an exciton-band-like structure is observed superposed on each of the sharp features. Figure 11 gives a video spectrum<sup>11</sup> of an ortho- $H_2$ -induced feature at  $J = 0$   $D_2$  concentration of 0.4%. With the higher concentration of  $J = 0$   $D_2$ , a broad

<sup>11</sup> A video spectrum is obtained using the classic technique of switching the radiation on and off with a chopper and detecting the signal with a phase-sensitive detector. Such spectroscopy is less sensitive than the tone-burst method but gives high-fidelity spectral shape including the broad background.

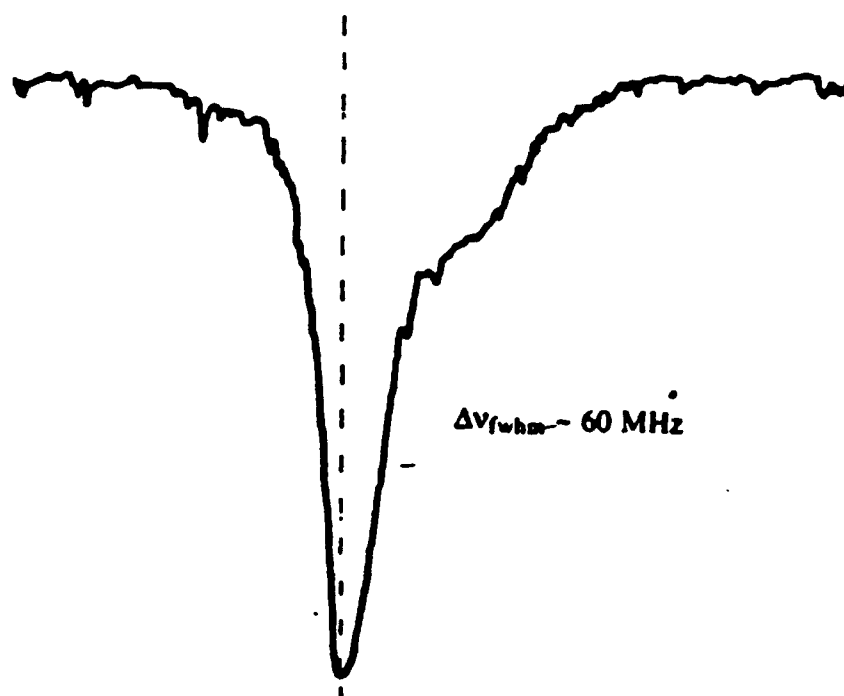


Figure 11 Exciton band for the  $Q_1(0)$  transition of the  $D_2$  impurity. The band is formed by the vibron hopping between randomly distributed  $D_2$  molecules. The basic structure shown in Figure 6 seems to be reproduced.

tail towards the lower-frequency side accompanies the sharp feature. We believe that exciton-hopping among the randomly distributed  $J = 0$   $D_2$  produces these tails. The hopping rate, which results from isotropic dispersion interaction, scales as inversely proportional to the sixth power of the intermolecular distance. The sharp feature at the high-frequency end of the exciton band with a shoulder is reminiscent of the sharp feature of para- $H_2$  spectrum in Figure 7. The exciton band of randomly distributed molecules such as  $D_2$  impurity offers an interesting theoretical problem.

### *$Q_1(1)$ Transitions, Anomalies, and Satellites*

The  $Q_1(1)$  spectrum of  $D_2$  impurities observed by Chan et al (53) exhibits much of the richness of the corresponding  $H_2$  spectrum. It is composed of a strong central line with much smaller satellites in a  $0.2\text{-cm}^{-1}$  window around the central line. Weliky et al (55) studied the central line in detail with the higher resolution of the color center laser. The video spectrum for a sample of 0.2%  $J = 1$   $D_2$  and 0.2%  $J = 1$   $H_2$  was observed to have a linewidth of 175 MHz. The line narrows to 20 MHz when the  $J = 1$   $D_2$  concentration is lowered to 0.003% and the  $J = 1$   $H_2$  to 0.060%. This

indicates that the linewidth is caused by inhomogeneous EQQ interactions with distant  $J = 1$  impurities. At these lower concentrations, the line split in the tone-burst spectrum, and the magnitude of the splitting was polarization dependent. Figure 12 shows these tone-burst spectral lines. These results were surprising because they violate the qualitative conclusion obtained from symmetry arguments. The central line is induced by  $J = 1$   $D_2$  molecules surrounded by  $J = 0$   $H_2$  through the many-body absorption mechanisms discussed earlier for the  $W_0(0)$  transition. The group theoretical argument in Table 1 shows that only  $\Delta M = \pm 2$  transitions, i.e.  $M = \pm 1 \leftarrow \mp 1$  transitions, are allowed (by radiation polarized

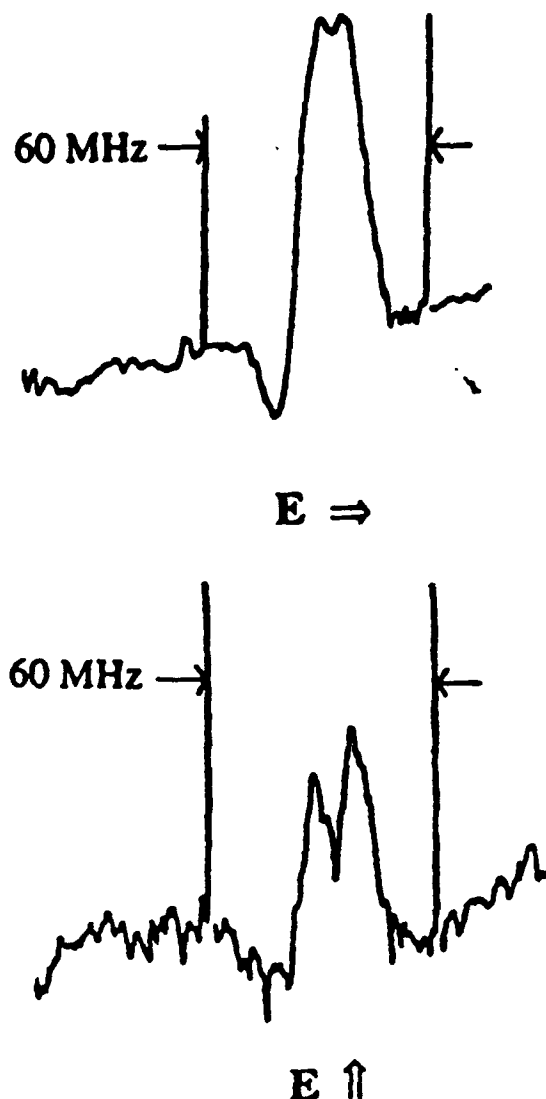


Figure 12 The anomalous splitting and polarization dependence of the  $Q_1(1)$  central line. The sample contained 0.001% of  $J = 1$   $D_2$  and 0.060% of  $J = 1$   $H_2$ . The polarization of the radiation field is perpendicular to the axis in the upper trace and parallel in the lower. The splitting is 6 MHz in the former and 11 MHz in the latter.

perpendicular to the crystal axis), and that the  $M = \pm 1$  levels belonging to the  $E''$  species are doubly degenerate. Our spectrum is not consistent with either of these predictions.

Weliky et al also extended the observation to include the full range of pair-induced fine structure. This is important for clarifying the  $D_2$   $Q_1(0)$  fine structure, which unlike the  $H_2$   $Q_1(0)$ , overlaps with the high-frequency components of the  $Q_1(1)$  structure. While the EQQ splitting of  $J = 1$  pair levels is comparable in  $H_2$  and  $D_2$ , the separation of  $Q_1(0)$  and  $Q_1(1)$  decreases by a factor of  $2^{3/2}$  because of the lower vibration-rotation constant for  $D_2$  ( $\alpha = 1.08 \text{ cm}^{-1}$ ) than for  $H_2$  ( $3.06 \text{ cm}^{-1}$ ). Using a sample with 0.7%  $J = 1$   $D_2$ , the two strong satellites  $(1, 1)' \leftarrow (2, 1)$  and  $(2, 1)' \leftarrow (1, 1)$  transition were observed at  $2987.0094 \text{ cm}^{-1}$  and  $2982.4171 \text{ cm}^{-1}$ , respectively. At this concentration, these spectral lines are broad (240 MHz) and, unlike their  $H_2$  counterparts (Figure 5), show no further structure nor polarization dependence. There should be two sets of pair splittings, one for the  $D_2$ - $D_2$  pair and the other for the  $D_2$ - $H_2$  pair, but they have not been separated thus far. A list of frequencies and intensities of all observed lines is available upon request.

### *$S_1(0)$ and $S_1(1)$ Transitions and $T_1$ Relaxation*

In contrast to the extremely sharp lines discussed so far, the linewidths of  $S_0(0)$  and  $U_0(0)$  transitions are broad. The linewidth of  $\sim 0.05 \text{ cm}^{-1}$  for the  $S_0(0)$  rotational Raman spectrum reported by Goovaerts et al (40) in a very pure para- $H_2$  crystal has been interpreted as due to the  $T_2$  dephasing of  $k = 0$  rotons. Vanhimbeeck et al (42) ascribe this observation to the second-order effect of the EQQ interaction. Their further studies (56, 57, 58) have all been interpreted on this basis. We studied  $S_1(0)$  and  $S_1(1)$  transitions of  $D_2$  at  $3159.0645 \text{ cm}^{-1}$  and  $3270.3453 \text{ cm}^{-1}$ , respectively. Because  $D_2$  impurity does not form an exciton band, the narrowing that results from the exciton momentum selection rule does not enter into the argument. Figure 13 shows the video spectral lines observed by Chan et al (53). The observed linewidths are  $0.084 \text{ cm}^{-1}$  and  $0.082 \text{ cm}^{-1}$ . While these linewidths might also be ascribed to  $T_2$  dephasing, I am tempted to consider the effect of  $T_1$  relaxation as well. Vanhimbeeck et al disregarded  $T_1$  relaxation based on the slow rate reported by Kuo et al (49) for vibrational transition. However, the energy gap rotational transitions  $J = 2 \leftarrow 0$ ,  $J = 3 \leftarrow 1$  of  $D_2$ , and  $J = 2 \leftarrow 0$  of  $H_2$  are  $172.1 \text{ cm}^{-1}$ ,  $285.5 \text{ cm}^{-1}$ , and  $355.6 \text{ cm}^{-1}$ , respectively, and are not that much higher than the phonon Debye temperature of  $\Theta_D \sim 70 \text{ cm}^{-1}$ . The fact that the linewidths of the  $S_1(1)$  and  $S_1(0)$  lines are comparable in spite of a larger mismatch with  $\Theta_D$  results from crystal field splitting. As indicated by the symmetry property of Table 1 and the selection rule of Equation 6, the

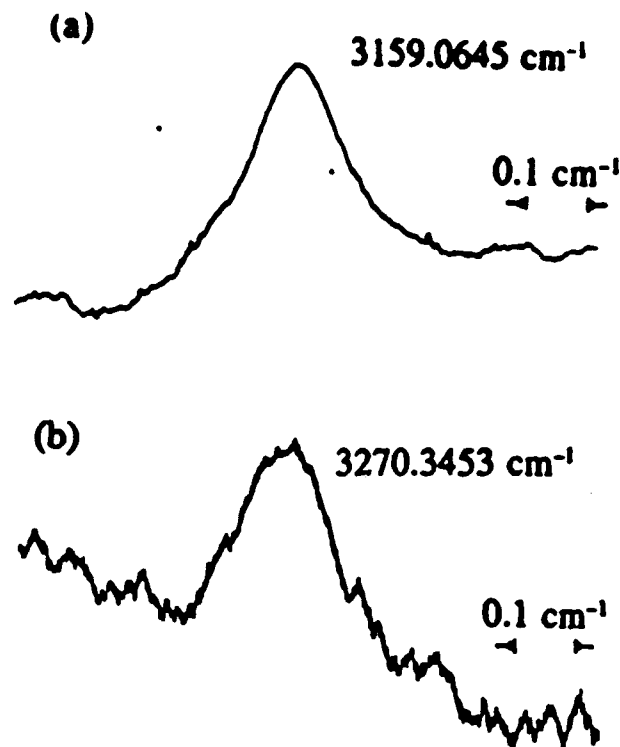


Figure 13 Video spectrum of the  $S_1(0)$  and  $S_1(1)$  transitions recorded using a difference frequency spectrometer. Unlike the  $Q_1(0)$  and  $Q_1(1)$  transitions they have large linewidths of  $0.084\text{ cm}^{-1}$  and  $0.082\text{ cm}^{-1}$ , respectively.

$S_1(0)$  transition is composed of the single line  $M = \pm 2 \leftarrow 0$ , while the  $S_1(1)$  transition is composed of five transitions,  $M = \pm 3 \leftarrow 0$ ,  $\pm 2 \leftarrow \mp 1$ ,  $\pm 2 \leftarrow 0$ ,  $\pm 3 \leftarrow \pm 1$ ,  $\mp 1$ , and  $\pm 1 \leftarrow \mp 1$ , whose maximum splitting is on the order of  $0.025\text{ cm}^{-1}$ . More theoretical studies for  $T_1$  relaxation are needed.

### STIMULATED RAMAN SPECTRUM OF $Q_1(0)$ TRANSITION

The transitions of  $H_2$  and  $D_2$  described so far have a variety of intricate spectral structure resulting from intermolecular and crystal field interactions. Even the simplest infrared transition,  $Q_1(0)$ , showed such structure, because it is caused by neighboring  $J = 1$  molecules that make simultaneous transitions. To attain the ultimate linewidth and purity of the state, observing the  $Q_1(0)$  Raman transition in pure para- $H_2$  crystal is most suitable because both levels are nondegenerate. This transition was observed under high resolution using stimulated Raman gain spectroscopy, with an Ar laser and a dye laser providing pump and probe radiations, respectively (59). Figure 14 shows the observed spectral line. The wavenumber of the line is  $4149.75\text{ cm}^{-1}$ , which corresponds to the



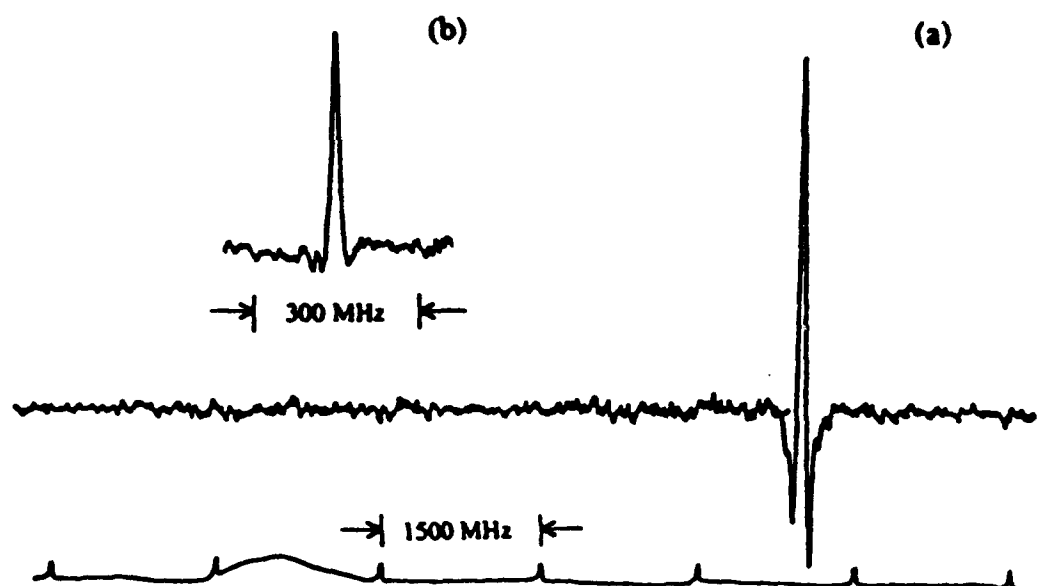


**Figure 14** Stimulated Raman gain spectrum of the  $Q_1(0)$  transition of para- $H_2$ . The 476.6-nm radiation of an Ar ion laser and 594.1-nm radiation of a dye laser were used as the pump and the signal, respectively. Trace (a) gives a tone-burst signal with the radiofrequency of 80 MHz. Trace (b) gives an 8 MHz tone-burst spectrum with a linewidth of  $\sim 7$  MHz (59).

lowest end of the exciton band given earlier in Figure 6. The clear singlet structure, without any hint of asymmetry or satellites, demonstrates that our crystal is fairly free from inhomogeneous broadening and shifts due to the complication of polycrystalline structure and stress. We have searched  $2.5\text{ cm}^{-1}$  above and below the observed line and found no other spectral features. This indicates that our crystal has a purely hcp structure. A crystal with mixed hcp and fcc structure would give an additional line.

The sharpness of the observed line does not arise from localization of the exciton, as it does for most of the infrared spectral lines discussed so far, but rather from the exciton momentum selection rule  $\Delta k = 0$ . The smallest observed linewidth of 7 MHz is most likely contaminated by laser instability because the two lasers used in the experiments were not actively stabilized. Further experiments with stabilized lasers and a purer para- $H_2$  single crystal with minimum concentration of ortho- $H_2$  and HD impurities should give a much sharper spectral line.

## IMPURITY SPECTROSCOPY

### *Neutral Molecules*

Species with low melting points can be embedded in the para- $H_2$  crystal as impurities. Chan has taken spectra of such crystals with HD,  $CH_4$ , and CO (60). Unlike  $H_2$  and  $D_2$ , the HD are all in the lowest  $J = 0$  rotational

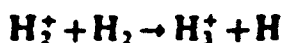
level at cryogenic temperatures. Two sharp spectral lines have been observed at  $3624.7163\text{ cm}^{-1}$  and  $3624.5793\text{ cm}^{-1}$ . The observed linewidths, relative intensities, and spacing of these two lines are reminiscent of the two features of ortho- $\text{H}_2$ -induced  $Q_1(0)$  transition of  $\text{D}_2$  (Figure 9), except that the spacing of the two features is larger by an amount approximately in proportion to their frequencies. No spectroscopy has been conducted for a solid HD crystal. If an isotopically pure HD crystal is prepared, its spectroscopy will be very interesting because the purity of the  $J = 0$  level will be higher.

$\text{CH}_4$  has three nuclear spin modifications, ortho ( $I = 1, F$ ), meta ( $I = 2, A$ ) and para ( $I = 0, E$ ) (61). However, at low temperature only the  $J = 0$  (meta) and the  $J = 1$  (ortho) levels are populated because the para species converts to an ortho through the near-degeneracy of ortho and para sublevels in  $J = 2$  (62). Observations of the rotational fine structure of  $\text{CH}_4$  in  $\text{N}_2$  and rare gas matrices have been reported (63, 64 and references therein) since the initial observation of Cabana et al (65). Chan has observed the  $\nu_3$  and  $\nu_4$  fundamentals of  $\text{CH}_4$  using a  $\text{CH}_4$  concentration of  $\sim 10^{-5}$ . As noted earlier by Nelander for  $\text{CH}_4$  in an  $\text{N}_2$  matrix, the spectrum of the  $\nu_4$  band at  $1300\text{ cm}^{-1}$  is much sharper than that of the  $\nu_3$  band at  $3015\text{ cm}^{-1}$ , reflecting that the phonons couple to a higher degree with the stretching vibration than with the bending vibration. Using diode lasers, Chan & Lee have observed an intricate structure of  $\text{CH}_4$  in a para- $\text{H}_2$  crystal that is composed of  $R(1)$ ,  $R(0)$ ,  $Q(1)$ , and  $P(1)$  transitions and their many satellites. The linewidths are  $\sim 300\text{ MHz}$ . Although we are far from a detailed analysis of the spectrum, the sharp spectral lines and the reproducible structure demonstrate that  $\text{CH}_4$  in a para- $\text{H}_2$  crystal has well-defined rotation-tunneling quantum states. The spectrum of  $\text{CO}$  in a para- $\text{H}_2$  crystal also showed an approximate rotational pattern and a few satellites. Obviously, many other molecules can be studied as impurities in para- $\text{H}_2$  crystals.

### *Ionic Species*

Our primary objective for studying solid hydrogen was to conduct cluster ion spectroscopy in the solid. We bombarded solid  $\text{H}_2$  with high-energy (3 MeV) electrons from a van de Graaf accelerator to produce the hydrogenic cation  $\text{H}_2^+$  and its clusters  $\text{H}_2^+(\text{H}_2)_n$ , and observed their infrared spectra using a medium-resolution Fourier transform spectrometer (66). This is an extension of the experiments by Souers et al, who used tritium for ionization (67 and references therein), and those by Brooks, Hunt, and coworkers who used proton bombardment (68 and references therein). Our hope was to extend this method to other protonated cations and their clusters such as  $\text{CH}_3^+$  and  $\text{CH}_3^+(\text{H}_2)_n$  etc.

The cluster ion forms in three steps. First, the high-energy primary electrons ionize H<sub>2</sub> to produce many H<sub>2</sub><sup>+</sup> in their path. Many of the ejected secondary electrons recombine with H<sub>2</sub><sup>+</sup>, but some fly away with sufficient energy to become permanently separated from H<sub>2</sub><sup>+</sup> cations. These electrons are ultimately localized on H atoms produced in the crystal through H<sub>2</sub> dissociation or ion-neutral reactions (see below). Second, the H<sub>2</sub><sup>+</sup> ions thus produced immediately react with neighboring H<sub>2</sub> through the efficient ion-neutral reaction



to produce stable H<sub>3</sub><sup>+</sup> and H atoms. Third, H<sub>3</sub><sup>+</sup> then attracts neighboring H<sub>2</sub> from their equilibrium position of 3.79 Å to the clustered position of ~1.7 Å (69) through the Langevin force to form ion clusters. We have observed four groups of eight lines. Apparently, high-resolution laser spectroscopy is applicable to some of the lines. Other methods of ionization, such as excimer laser and radioactive β-ray source, have been tried without success. γ-ray irradiation experiment is in preparation.

## SUMMARY

My feelings about the results described in this article may be summarized in two phrases: many beautiful spectra, and scarce theoretical understanding. Experimental attempts at clarifying some problems engender more questions than answers. Nevertheless, we are inspired by the prospect of understanding condensed phase spectroscopy from first principles. My purpose in writing this glaringly premature review is to seek your help. Some of the main puzzles are as follows:

1. Most of the observed fine structures have not been assigned with confidence. The complexity of the spectral pattern ranges from the simplest single-line pattern of the Q<sub>1</sub>(0) Raman transition, to the several-line pattern for the *J* = 1 molecule-induced Q<sub>1</sub>(0) infrared transition of D<sub>2</sub> impurity, to the complicated pattern of the W<sub>1</sub>(0) transition, where the fine structure results only from the excited state; to the most complicated pattern of the Q<sub>1</sub>(1) transition, where the splitting results from both the ground and excited states. In view of the fact that the analysis by Harris et al (11, 18), dealing with pair splittings between *J* = 1 molecules in the ground state only, is already fairly complex, a complete analysis may not be a simple task. Such an analysis will lead us to a better grasp of intermolecular and crystal field interactions. This is necessary before we can begin to understand the fine structure of more complicated impurities.

2. For several clear-cut experimental results, the basic physical mechanisms are not well understood. (a) The sharp features at the high-fre-

quency edge of the exciton band in the  $Q_1(0)$  transition of para- $H_2$  remain unexplained. Neither their cause nor the origin of the smaller and larger splittings has been confidently located. (b) The observed symmetric quartet and its clear-cut polarization dependence (Figure 10) suggest higher symmetry of the  $J = 0 D_2$ - $J = 1 H_2$  pair (and the surrounding  $J = 0 H_2$ ) than anticipated from localized pairs. Because the localized in-plane and out-of-plane pairs lower the symmetry of the system, and since their positions are not equivalent, one expects more spectral lines and a less symmetric pattern than is observed. Rotational diffusion of ortho- $H_2$  (8) in the hexagonal plane, for example, will restore the  $D_{3h}$  symmetry of the system, but other mechanisms may also be considered. (c) The observed small splitting of the  $Q_1(1)$  central line of the  $D_2$  impurity and its anomalous polarization remain uninterpreted. Here the symmetry argument of degeneracy and selection rules seems to be violated. (d) The polarization dependence of the relative intensities of the three  $M$  components of the  $W_0(0)$  and the  $W_1(0)$  transitions is incongruous with the theory.

3. We do not have a quantitative explanation of the observed linewidths apart from the handwaving arguments given in this article. The theory of  $T_2$  relaxation given in earlier papers (41, 42) does not seem to be the whole story. We will need more theory of the type given by Statt & Hardy (72), which includes  $T_1$  relaxation and is closely related to experimental observation. Quantitative understanding of relaxation in condensed phase is difficult, but here we have clear-cut experimental results that set upper limits to relaxation rates for a wide variety of quantum states in the most fundamental molecular crystal.

4. Experimentally determined molecular constants and crystal field splittings represent their effective values averaged over zero-point crystal vibration (renormalization). This situation is analogous to gaseous spectroscopy, in which molecular constants are an average of the inverse of the moment of inertia, etc, over zero-point vibration. However, the quantum crystal nature of solid  $H_2$ , together with the low frequencies and a great number of phonon modes, make these effects larger and more difficult to calculate. For example, the values of  $Q^2/R^3$  for the excited state and the ground state obtained from the fine structure of the  $Q_1(1)$  transition are smaller by  $\sim 10\%$  than those calculated from known values of  $H_2$  quadrupole moments and the equilibrium intermolecular distance. As explained by Harris et al (18), this observation is contrary to expectation because an average of  $1/R^3$  by any symmetric vibration will increase the effective value. The decrease was ascribed to the average of an angular dependent factor whose average decrease overrides the increase in the averaging of  $1/R^3$ . As in gaseous spectroscopy, these renormalization effects provide information on the crystalline potential energy. More theor-

etical studies of the vibrations in quantum crystals and their effect on molecular energy levels are awaited.

## FINAL REMARKS

I conclude this article with a rough projection for future experiments. What we have observed thus far is just a beginning. The signals are so strong and the sensitivity of laser spectroscopy so high that we should be able to perform many interesting experiments.

First, it will be interesting to see how narrow the spectral lines become if we eliminate instrumental width and minimize inhomogeneous broadening caused by ortho-H<sub>2</sub> and HD impurities. The transition most suitable for this purpose remains to be seen. The Q<sub>1</sub>(0)-stimulated Raman line is very promising. Because both states of this transition are  $J = 0$ , they are relatively insensitive to orientation-dependent interaction with the unavoidable impurity. We do not know, however, how rigorously the momentum selection rule  $\Delta k = 0$  is obeyed. This rule is violated by the existence of impurities, the finite wavelength of radiation, and the limited size of the crystal. If the rule holds well and the  $T_1$  relaxation is indeed as small as reported (48, 49), we should be able to narrow the line to the order of a few hundred kilohertz, i.e.  $\Delta\nu/\nu \sim 10^{-9}$ . If we can achieve this kind of linewidth and measure the absolute frequency with the accuracy of  $\sim 10^{-10}$ , we should be able to measure pressure- and temperature-dependent shifts of the spectral line. Our spectroscopy has been conducted at He temperature of 4.2 K, but cooling the crystal further to a few tens of mK is technically feasible. The infrared Q<sub>1</sub>(0) spectra of impurity D<sub>2</sub> or HD may also permit us to obtain sharp lines. The localization of excitons is the major advantage if the violation of the  $\Delta k = 0$  rule turns out to be the limiting factor for sharpness.

With the advent of new laser sources such as InGaAsP communication diodes, the Ti-Sapphire laser, the CW Nd-YAG laser, and a variety of nonlinear optical crystals, we can extend our observations to high-vibration and -rotation states of hydrogen and its isotopic species. The overtone bands of H<sub>2</sub> up to  $v = 5 \leftarrow 0$  reported by Patel et al using the optoacoustic technique can be observed with higher resolution. The exciton band for the Q(0) transition should narrow with higher vibrational states, and this will provide a clearer picture of unidentified sharp features. The 2<sup>nd</sup> pole (chilotetraeicosapole)-induced  $J = 8 \leftarrow 0$  rotational transition expected at  $\sim 4045 \text{ cm}^{-1}$  is within the sensitivity of our spectrometer. The sensitivity of our solid-phase spectroscopy at the moment is on the order of  $\Delta I/I > 10^{-4}$ , significantly less than the limit of  $5 \times 10^{-7}$  for our plasma ion spectroscopy and of  $\sim 10^{-8}$  for shot noise. There is enormous room for improvement

here. We should be able to observe a variety of transitions for isotopic species as impurity and as a crystal. The absence of spin modifications and the existence of a small dipole moment in HD may give us qualitatively new spectra.

A variety of nonlinear optical techniques, such as the stimulated Raman effect, coherent anti-Stokes Raman spectroscopy, infrared-infrared and infrared-microwave double resonance, induction decay, photon echo, etc., can be applied to this problem. Such techniques should help clarify assignments, the physical effects behind the spectral features, and relaxation mechanisms. Solid hydrogen itself may make an excellent nonlinear optical element. The extremely small linewidth compared with that of the usual pressure-broadened Raman shifting gas must be of great advantage. We may be able to make a CW Raman shifting element from the crystal. In conducting the stimulated Raman experiment, we have observed that a para- $H_2$  crystal is extremely robust against radiation. We believe this robustness results from its high thermal conductivity (21). High-purity para- $H_2$  at He temperature has a conductivity comparable to that of metals and is a few orders of magnitude higher than that of dielectrics. Observing the Stark and Zeeman shifts of spectral lines is quite feasible because of the small linewidths. The electric field-induced spectrum (73) may appear quite intense. Such an effect may be used for modulation purposes.

A para- $H_2$  crystal makes an excellent host for matrix spectroscopy. Compared with the matrices that are normally used, i.e. Ne, Ar, Xe,  $N_2$ , etc., it has the advantage of weaker intermolecular interaction, but also has the disadvantage of more complex preparation (such as the necessity for ortho-to-para conversion). Also, the relatively high vapor pressure of para- $H_2$  makes the usual technique of blowing a premixed gas onto a cooled window impractical. So far, we have used low-melting-point gases as impurities by premixing them with para- $H_2$  and passing them directly to a cooled sample cell. This method will not work for less volatile impurities, for which the mixing must be done in situ in the crystal. Ion spectroscopy in para- $H_2$  crystal is also a very interesting possibility. Because most molecules have proton affinities higher than that of  $H_2^+$ , protons are likely to localize on impurities, forming protonated ions. To carry out such an operation extensively, we must first establish a convenient method of ionization.

Finally, a question remains as to whether the para- $H_2$  crystal is the only solid that shows such sharp spectral lines. Would any other solid show similar sharpness in its spectrum? Many researchers have been pessimistic about this question, but they also felt that way about solid  $H_2$ . The answer must be tested by experiments. Even if the spectral widths are not as narrow as those of solid hydrogen, finding their limits and considering the

physical mechanism that sets the limits will be interesting. For example, it is well known that a diamond has sharp Raman lines. Suppose we take a spectrum of isotopically pure diamond cooled to He temperature: what will the width be?

### *Note Added in Proof*

After submission of this article, two significant experimental results have been obtained.

In the first experiment, ionization of a para-H<sub>2</sub> crystal has been conducted using  $\gamma$ -ray of cobalt 60, and its spectrum was studied under high resolution. The experiment resulted in two surprises:

1. The sharp feature at  $4139.66\text{ cm}^{-1}$  mentioned in the text was extremely sharp ( $\Delta\nu \sim 50\text{ MHz}$ ), and its position matched that of the stimulated Raman spectrum of the  $Q_1(0)$  transition. We interpret this line to be the Raman type transition induced by the electric field of  $\gamma$ -ray induced charges. Using Condon's theory (73) and the observed integrated intensity of the spectrum, we estimated the charge density to be  $\sim 10^{16}\text{ cm}^{-3}$ . The charges divide the crystal into islands of microcrystals in which many molecules experience approximately equal electric field. This led us to a better understanding of the relation between the size of the microcrystal and the  $\Delta k = 0$  rule.

2. The temperature variation of the spectrum showed amazing stability of charges, which we believe are localized in the form of ion clusters  $\text{H}_3^+(\text{H}_2)_n$  and  $\text{H}^-(\text{H}_2)_n$ . There was no appreciable change of the charge density when the crystal was heated from 4.2 K to 13.5 K and cooled back to 4.2 K, although the frequency of the spectrum varies considerably during the cycle. The charge-induced signal disappears only when we melt the crystal above the triple point. The experiment shows that the electric field is polarized normal to the wall of the container near the wall and is less polarized towards the center of the crystal.

In the second experiment, the method of Stark modulation has been successfully applied to the spectroscopy of solid hydrogen. Unlike the case of polar gaseous molecule, the electric field induces spectral lines rather than shifts their frequencies. Because the electric field-induced spectrum obeys the Raman type selection rules, this technique is most useful for the study of the simplest fundamental transition,  $Q_1(0)$ . We have been able to conduct accurate measurements of the variation of the frequency and the linewidth of this transition with temperature. The direction and the magnitude of the frequency shift could be accounted for as the variation of the exciton hopping rate ( $\sim 1/R^6$ ) resulting from thermal expansion of the crystal. The variation of the linewidth provides information on  $T$ ,

owing to phonon interaction. The sensitivity increase this method provides is more than two orders of magnitude, and we estimate it to be  $\Delta I/I \sim 10^{-6}$ .

The results of these two experiments have considerably deepened our understanding of solid hydrogen spectroscopy. I believe both techniques can be applied widely to other cases.

#### ACKNOWLEDGMENTS

The experiments described in this article have been conducted by a group of excellent students and postdoctoral fellows. Their names are (in the order each joined the project), M.-C. Chan, M. Okumura, D. P. Weliky, T. Byers, K. E. Kerr, T. Momose, and R. Dickson. Other students in the plasma ion spectroscopy group, C. M. Gabrys, L.-W. Xu, S. S. Lee, M.-F. Jagod, B. Ventrudo, and B. D. Rehfsuss, aided the experiments. We have profited from discussions with veterans of solid  $H_2$  spectroscopy: J. Berlinsky, W. N. Hardy, A. B. Harris, A. R. W. McKellar, J. D. Poll, K. N. Rao, I. F. Silvera, R. H. Tipping, the veteran of laser spectroscopy J. L. Hall, and the veteran of solid spectroscopy A. Szabo. When the project was initiated R. H. Hilderbrand provided much help on the treatment of liquid  $H_2$  and cryogenics. This research has been supported by Air Force grants #F04611-86-K-0069 and #F33615-90C-2035.

#### Literature Cited

1. Szabo, A. 1970. *Phys. Rev. Lett.* 25: 924
2. Yen, W. M., Selzer, P. M. 1986. *Laser Spectroscopy of Solids*, ed. W. M. Yen, P. M. Selzer, pp. 141-88. New York: Springer-Verlag
3. Moerner, W. E., ed. 1988-1989. *Persisted Spectral Hole Burning: Science and Application*. New York: Springer-Verlag
4. Moerner, W. E., Kador, L. 1989. *Phys. Rev. Lett.* 62: 2535
5. Orrit, M., Bernard, J. 1990. *Phys. Rev. Lett.* 65: 2716
6. Okumura, M., Chan, M.-C., Oka, T. 1989. *Phys. Rev. Lett.* 62: 32
7. McLennan, J. C., McLeod, J. H. 1929. *Nature* 123: 160
8. Van Kranendonk, J. 1983. *Solid Hydrogen*. New York: Plenum
9. Glatt, J., Kerl, R. J., Patel, C. K. N. 1986. *Phys. Rev. Lett.* 57: 1437
10. Hardy, W. N., Berlinsky, A. J. 1975. *Phys. Rev. Lett.* 34: 1520
11. Hardy, W. N., Berlinsky, A. J., Harris, A. B. 1977. *Can. J. Phys.* 55: 1150
12. Dicke, R. H. 1953. *Phys. Rev.* 89: 472
13. Pauling, L. 1930. *Phys. Rev.* 36: 430
14. Nakamura, T. 1955. *Prog. Theor. Phys. (Kyoto)* 14: 135
15. Van Kranendonk, J. 1959. *Physica* 25: 1080
16. Van Kranendonk, J. 1960. *Can. J. Phys.* 38: 240
17. Harris, A. B. 1970. *Phys. Rev.* B1: 1881
18. Harris, A. B., Berlinsky, A. J., Hardy, W. N. 1977. *Can. J. Phys.* 55: 1180
19. Miller, R. E., Decius, J. C. 1973. *J. Chem. Phys.* 59: 4871
20. Silvera, I. F. 1980. *Rev. Mod. Phys.* 52: 393
21. Souers, P. C. 1986. *Hydrogen Properties for Fusion Energy*. Berkeley: Univ. Calif. Press
22. Kittel, C. 1976. *Introduction to Solid State Physics*. New York: Wiley
23. McKellar, A. R. W. 1990. *J. Chem. Phys.* 92: 3261
24. Nosanow, L. H. 1966. *Phys. Rev.* 145: 120
25. Harrick, N. J., Ramsey, N. F. 1952. *Phys. Rev.* 88: 228



26. Wick, G. C. 1933. *Z. Phys.* 85: 25
27. Hardy, W. N., Silvera, I. F., McTague, J. P. 1975. *Phys. Rev. B* 12: 753
28. Oka, T. 1976. In *Molecular Spectroscopy: Modern Research II*, ed. K. N. Rao, pp. 229-53. New York: Academic
29. Heitler, W. 1960. *Quantum Theory of Radiation*. Oxford: Oxford Univ. Press
30. Balasubramanian, T. K., D'Souza, R., D'Cunha, R., Rao, K. N. 1989. *Can. J. Phys.* 67: 79
31. Ma, Q., Tipping, R. H., Poll, J. D. 1989. *Phys. Rev. B* 39: 132
32. Chan, M.-C., Lee, S. S., Okumura, M., Oka, T. 1991. *J. Chem. Phys.* 95: 88
33. Oka, T. 1967. *J. Chem. Phys.* 47: 5410
34. Schweizer, R., Washburn, S., Meyer, H. 1979. *J. Low Temp. Phys.* 37: 289
35. Mulder, F., Van der Avoird, A., Wormer, P. E. S. 1979. *Mol. Phys.* 37: 157
36. Bhatnagar, S. S., Allin, E. J., Welsh, H. L. 1962. *Can. J. Phys.* 40: 9
37. Klump, K. N., Schnepf, O., Nosanow, L. H. 1970. *Phys. Rev. B* 1: 2496
38. Poll, J. D., Van Kranendonk, J. 1962. *Can. J. Phys.* 40: 163
39. Abram, I. I., Hochstrasser, R. M., Kohl, J. E., Semack, M. G., White, D. 1980. *Chem. Phys. Lett.* 71: 1980
40. Goovaerts, E., Chen, X. Y., Bouwen, A., Schoemaker, D. 1986. *Phys. Rev. Lett.* 57: 479
41. Abram, I. I., Hochstrasser, R. M. 1980. *J. Chem. Phys.* 72: 3617
42. Vanhimbeeck, M., DeRaedt, H., Lagendijk, A., Schoemaker, D. 1986. *Phys. Rev. B* 33: 4264
43. Chan, M.-C., Okumura, M., Gabrys, C. M., Xu, L.-W., Refuss, B. D., Oka, T. 1991. *Phys. Rev. Lett.* 66: 2060
44. Amstutz, L. I., Thompson, J. R., Meyer, H. 1968. *Phys. Rev. Lett.* 21: 1175
45. Miyagi, H. 1968. *Prog. Theor. Phys. (Kyoto)* 40: 1448
46. Gush, H. P., Hare, W. F. J., Allin, E. J., Welsh, H. L. 1960. *Can. J. Phys.* 38: 176
47. Balasubramanian, T. K., Lien, C.-H., Gaines, J. R., Rao, K. N., Damon, E. K., Nordstrom, R. J. 1982. *J. Mol. Spectrosc.* 92: 77
48. Delalande, C., Gale, G. M. 1977. *Chem. Phys. Lett.* 50: 339
49. Kuo, C.-Y., Kerl, R. J., Patel, N. D., Patel, C. K. N. 1984. *Phys. Rev. Lett.* 53: 2575
50. Sears, V. F., Van Kranendonk, J. 1964. *Can. J. Phys.* 42: 980
51. Bose, S. K., Poll, J. D. 1990. *Can. J. Phys.* 68: 159
52. Kerr, K. E., Byers, T. J., Ventrudo, B. F., Momose, T., Cassidy, D. T., Oka, T. 1992. *Proceedings of the 47th Symposium on Molecular Spectroscopy*. Columbus, OH: Ohio State Univ.
53. Chan, M.-C., Xu, L.-W., Gabrys, C. M., Oka, T. 1991. *J. Chem. Phys.* 95: 9404
54. Chan, M.-C. 1992. *J. Mol. Spectrosc.* 153: 750
55. Weliky, D. P., Kerr, K. E., Momose, T., Byers, T. J., Oka, T. 1992. *Proceedings of the 47th Symposium on Molecular Spectroscopy*. Columbus, OH: Ohio State Univ.
56. Sierens, C., Bouwen, A., Goovaerts, E., De Maziere, M., Schoemaker, D. 1988. *Phys. Rev. A* 37: 4769
57. Chen, X. Y., Goovaerts, E., Schoemaker, D. 1988. *Phys. Rev. B* 38: 1450
58. Leblans, M., Bouwen, A., Sierens, C., Joosen, W., Goovaerts, E., Schoemaker, D. 1989. *Phys. Rev. B* 40: 667
59. Momose, T., Weliky, D. P., Oka, T. 1992. *J. Mol. Spectrosc.* 153: 760
60. Chan, M.-C. 1991. PhD thesis. Univ. Chicago, Chicago, Ill.
61. Herzberg, G. 1945. *Molecular Spectra and Molecular Structure II. Infrared and Raman Spectra of Polyatomic Molecules*. New York: Van Nostrand Reinhold
62. Frayer, F. H., Ewing, G. E. 1968. *J. Chem. Phys.* 48: 781
63. Nelander, B. 1985. *J. Chem. Phys.* 82: 5340
64. Jones, L. H., Ekberg, S. A., Swanson, B. I. 1986. *J. Chem. Phys.* 85: 3203
65. Cabanna, A., Savitky, G. B., Hornig, D. F. 1963. *Can. J. Phys.* 39: 2942
66. Chan, M.-C., Okumura, M., Oka, T. 1993. *J. Chem. Phys.*
67. Poll, J. D., Hunt, J. L., Souers, P. C., Fearon, E. M., Tsugawa, R. T., et al. 1983. *Phys. Rev. A* 28: 3147
68. Miller, J. J., Brooks, R. L., Hunt, J. L., Poll, J. D. 1988. *Can. J. Phys.* 66: 1025
69. Yamaguchi, Y., Gaw, J. F., Remington, R. B., Schaefer, H. F. 1987. *J. Chem. Phys.* 86: 5072
70. Poll, J. D., Hunt, J. L. 1985. *Can. J. Phys.* 63: 84
71. Okumura, M., Yeh, L. I., Lee, Y.-T. 1988. *J. Chem. Phys.* 88: 79
72. Statt, B. W., Hardy, W. N. 1980. *Can. J. Phys.* 58: 1341
73. Condon, E. U. 1932. *Phys. Rev.* 41: 759

# The infrared spectrum of $H_3^+$ in laboratory and space plasmas

Takeaki Oka

Department of Chemistry and Department of Astronomy and Astrophysics,  
The University of Chicago, Chicago, Illinois 60637

Protonated hydrogen,  $H_3^+$ , composed of three protons and two electrons, is the simplest stable polyatomic system. It is the most abundant ionic species in molecular hydrogen plasmas, and it is assumed to play a central role in the chemical evolution of molecular clouds, the birthplace of stars. The existence of this species has been known since its discovery by J. J. Thomson in 1912, but its first spectrum was observed only in 1980. The infrared spectrum has since been extended to higher vibrational and rotational states. The existence of a large amount of  $H_3^+$  in Nature was first demonstrated in the serendipitous discovery of its infrared emission bands in the polar auroral regions of the Jupiter ionosphere. The spectrum is extremely intense and pure and can be used to monitor the morphology and temporal variation of the dynamic Jovian plasmas. Early this year, an identification of  $H_3^+$  emission was claimed in Supernova 1987A. In April strong  $H_3^+$  infrared emission was detected in Uranus. These developments are reviewed and the future is projected.

## CONTENTS

I. Introduction	1141
II. Historical Background <sup>1</sup>	1142
III. The $H_3^+$ Spectrum in the Laboratory	1143
A. The $H_3^+$ $\nu_2$ fundamental band <sup>1,2</sup>	1143
B. Hot, overtone, and forbidden bands	1143
IV. The $H_3^+$ Spectrum in Space	1144
A. The $H_3^+$ emission from the Jovian auroral regions	1144
B. The colossal Jovian plasma	1145
C. $H_3^+$ in Supernova 1987A (??)	1147
D. The $H_3^+$ emission from Uranus	1147
V. Final Remarks	1148
Acknowledgments	1148
References	1148

## I. INTRODUCTION

From my point of view one of the most inspiring developments in recent science has been the unification of astronomy and chemistry. When I was a student, molecules had hardly any place in astronomy. Most of the matter in the Universe was believed to be condensed in hot stars, where nuclear physics dominates; interstellar space was viewed as a vast vacuum with an extremely low density of atoms and dust. The existence of a few unstable diatomic radicals had been reported (with hindsight, they were just the tip of the iceberg), but by and large it was assumed that stable molecules could not exist in the harsh conditions of interstellar space.

This understanding was drastically changed when Townes and his colleagues discovered the microwave emission spectrum of interstellar ammonia in Sagittarius B2, a molecular cloud located towards the center of our galaxy (Cheung *et al.*, 1968). This discovery induced an avalanche of radio-astronomical observations of many familiar molecules and also of many that were unfamiliar even to chemists, e.g.,  $HC_nN$  ( $n=5,7,9,11$ ). These discoveries and subsequent studies have created a new discipline, molecular astrophysics. Once a novel concept, the "molecular cloud" is now well established as being

the birthplace of stars; the chemical evolution of these clouds is recognized as a step in star formation.

The entry of molecules into the astrophysics not only of our own galaxy, but also of distant extragalactic objects, is best demonstrated by the infrared emission of quadrupolar transitions of molecular hydrogen. These transitions, initially observed by Herzberg (1949) in the laboratory, are extremely weak, but intense emissions appear in a variety of astronomical objects because of the enormous abundance of hydrogen in molecular form at low densities and at high temperatures. Figure 1 shows the extremely strong  $2\ \mu\text{m}$  infrared emission of  $H_2$  from the enigmatic superluminous galaxy-merger system NGC

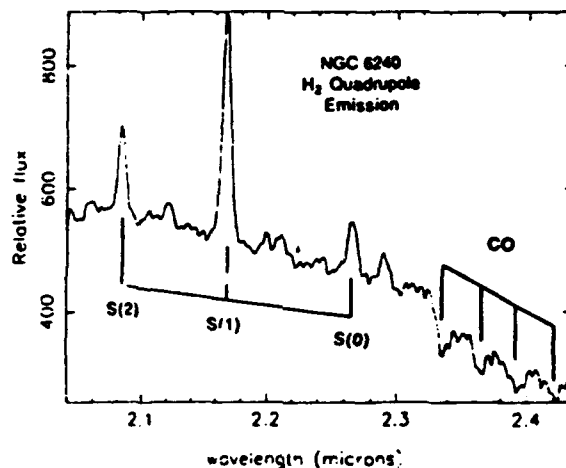


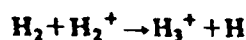
FIG. 1.  $H_2$  quadrupole emission spectrum from the superluminous galaxy NGC 6240. The single line  $S(1)$  ( $v=1 \rightarrow 0$ ,  $J=3 \rightarrow 1$  of ortho- $H_2$ ) carries the total brightness of a hundred million solar luminosities, as initially reported by Joseph, Wright, and Wade (1984). There are also weaker features corresponding to the hot band emission  $v=2 \rightarrow 1$  [ $S(1)$  at  $2.28\ \mu$ ,  $S(2)$  at  $2.20\ \mu$ , and  $S(3)$  at  $2.12\ \mu$ ]. This spectrum was recorded by Geballe, Momose, and Oka using the CGS4 grating spectrometer at the United Kingdom Infrared Telescope. Note that the spectrum is Doppler shifted by  $Z=0.0254$  (redshift of  $\sim 0.05\ \mu\text{m}$ ) due to the expansion of the universe.

6240, one of the most luminous known infrared objects, some 300 million light years away. These extremely strong molecular features correspond to the vibration-rotation transitions  $v = 1 \rightarrow 0$ ,  $J + 2 \rightarrow J$  of  $H_2$ . They are easily visible after a few minutes of integration with a modern high-resolution infrared spectrometer. The luminosity of the strongest  $H_2$  emission line  $S(1)$ , initially reported in that source by Joseph, Wright, and Wade (1984), amounts to  $\sim 1 \times 10^4 L_\odot$  ( $L_\odot$  = one solar luminosity). Can you imagine—the total luminosity of one hundred million suns in one molecular spectral line! The absorption due to the  $R$ -branch bandheads of carbon monoxide first-overtone bands ( $\Delta v = 2$ ) and its hot bands are also visible in Fig. 1. Remember these spectral lines because we shall come back to them later.

In dense clouds where a vast number of molecules at low temperature ( $\sim 30$  K) are shielded from stellar radiation, the main chemical reaction scheme is believed to be ion-neutral kinetics. The ubiquitous cosmic rays ionize  $H_2$  and He, and the subsequent ion-neutral reactions govern the chemical evolution of the clouds, as initially advocated by Klemperer (Herbst and Klemperer, 1973), Watson (1976), Dalgarno (Dalgarno and Black, 1976), and their colleagues. The theory was strongly influenced by the radio-astronomical discovery by Buhl and Snyder (1970) of the strong emission of protonated carbon monoxide  $HCO^+$  (Klemperer, 1970). Recognition of such a chemical scheme and subsequent studies on interstellar chemistry revealed a major void in our knowledge of molecular spectroscopy, a void that had previously been known to a few specialists but was not widely felt. The spectrum and thus the quantum-mechanical information on protonated hydrogen  $H_3^+$ , the simplest and the most fundamental polyatomic system, was totally absent. It is this ion which is initially produced in molecular clouds and which plays the universal role of protonator in interstellar chemistry.

## II. HISTORICAL BACKGROUND<sup>1</sup>

The existence of  $H_3^+$  has been known since the early days of mass spectroscopy. It was none other than J. J. Thomson (1912) who discovered  $H_3^+$  in his "positive rays" and noted "the existence of this substance is interesting from a chemical point of view, as it is not possible to reconcile its existence with the ordinary conceptions about valency, if hydrogen is regarded as always monovalent." Dempster (1916) soon showed that  $H_3^+$ , rather than the primary ion  $H_2^+$ , is most abundant in hydrogen discharges, a fact which applies both to laboratory and to space plasmas. Hogness and Lunn (1925) identified the celebrated reaction



<sup>1</sup>See Oka (1983) for more details.

as the origin of the production and dominance of  $H_3^+$ . This reaction, with its large Langevin rate ( $\sim 10^{-9}$  cm<sup>3</sup>s<sup>-1</sup>) and exothermicity ( $\sim 1.7$  eV), is extremely efficient. Thus the  $H_2^+$  ions initially produced in molecular clouds by the cosmic ray flux are immediately converted to  $H_3^+$ . One can interpret this reaction as "proton hopping" from an H atom (with proton affinity  $\sim 2.7$  eV) to the  $H_2$  molecule (P.A.  $\sim 4.4$  eV). More recent experiments, however, have demonstrated that this naive picture is not quite right; approximately 50% of the reaction is due to hydrogen abstraction (i.e., an H atom hopping from H to  $H_2^+$ ). The true nature of this most fundamental reaction is still under study experimentally and theoretically (see Pollard *et al.*, 1991, and references therein). The  $H_3^+$  ion thus produced acts as the universal protonator through the proton-hopping reaction  $H_3^+ + X \rightarrow HX^+ + H_2$  and initiates interstellar chemistry. This reaction is generally efficient for most molecules and atoms whose proton affinities exceed that of  $H_2$  (notable exceptions are He, Ne, Ar, N, and  $O_2$ ). Once protonated, reactions such as  $HX^+ + Y \rightarrow XY^+ + H$  proceed efficiently (contrary to the reactions  $X + Y \rightarrow XY + h\nu$ , which are extremely slow). The late Hiroko Suzuki (1989) coined the phrase " $H_3^+$  chemistry" for these chemical processes.

For many years after its discovery, the true nature of  $H_3^+$  remained an enigma. Experiments could not tell much about  $H_3^+$  other than that it existed. Eyring was quoted<sup>1</sup> as having said that the  $H_3^+$  problem was "the scandal of modern chemistry." Being the simplest polyatomic system,  $H_3^+$  presented a major challenge to quantum chemistry. It is a historical curiosity that Niels Bohr (1919) was the first to publish a theoretical paper on triatomic hydrogen. From 1936–1938 Eyring, Hirschfelder, and others published a series of five papers, concluding in Part V (Hirschfelder, 1938) that the triangular structure is more stable than the linear structure. With the advent of modern computers, the quantum mechanics of the three hydrogen system has become a major battlefield for theorists (Porter, 1982). It was shown that the equilateral configuration has the minimum energy (Christoffersen *et al.*, 1964; Conroy, 1964) and that  $H_3^+$  (protonated  $H_2$ ), like  $H^-$  (deprotonated  $H_2$ ), does not have any stable excited electronic state except for a triplet state very close to its second dissociation limit. These results indicated that the vibration-rotation spectrum associated with the infrared active degenerate vibrational mode,  $\nu_2$ , is the only possible vehicle for laboratory and astronomical observation except for weaker distortion-induced rotational transitions (Pan and Oka, 1986). Carney and Porter (1974, 1976) published classic papers predicting the frequency of the  $\nu_2$ -fundamental band to be 2516 cm<sup>-1</sup>, a value found to be only 5 cm<sup>-1</sup> off the real value. Their predictions on the electrical properties of  $H_3^+$  and on some crucial vibration-rotation constants (unpublished but made available to Oka and J. K. G. Watson) were of great help in planning the laboratory spectroscopy and in its identification. Close collabora-

tion of theorists and experimentalists has been an essential ingredient of this field ever since. Today brute force variational calculations using supercomputers predict individual vibration-rotation levels with an accuracy of  $\sim 1 \text{ cm}^{-1}$ . This truly remarkable development, in a series of many papers by Miller, Tennyson, and Sutcliffe (1990 and references therein), based on an *ab initio* potential of Meyer, Botschwina, and Burton (1986), has played a major role in the recent studies of the  $\text{H}_3^+$  spectrum in the laboratory and in space.

### III. THE $\text{H}_3^+$ SPECTRUM IN THE LABORATORY

Several papers claimed observation of the  $\text{H}_3^+$  spectrum in the early days. The spectral lines reported in the optical region, however, were subsequently all ascribed to transitions between excited electronic states of  $\text{H}_2$ . Since theory indicated that no discrete optical spectrum was likely to exist, the search for the  $\text{H}_3^+$  spectrum was shifted to the infrared region. Herzberg (1967) described his plan to find the spectrum in infrared emission. His effort over many years culminated with his discovery (Herzberg, 1980; Herzberg *et al.*, 1981; Herzberg, 1982) of a Rydberg spectrum of the important and beautiful neutral species  $\text{H}_3$ . The observation of the  $\text{H}_3^+$  spectrum, however, had to wait for the high sensitivity of laser spectroscopy.

#### A. The $\text{H}_3^+$ $\nu_2$ fundamental band<sup>1,2</sup>

The infrared absorption spectrum of  $\text{H}_3^+$  was observed using a liquid-nitrogen-cooled hydrogen plasma (Oka, 1980). Crucial for this observation were two recent technological advances: (1) the development of a widely tunable laser infrared source by Pine (1974) and (2) the use of a long positive column glow discharge introduced to microwave spectroscopy by Woods and his colleagues (Woods *et al.*, 1975). Figure 2 shows a stick diagram of the 15 observed lines. Unlike the usual vibration-rotation spectra of simple molecules, this spectral pattern shows no obvious symmetry or regularity. This is because of the large interaction between vibration and rotation, which makes the perturbation treatment difficult. J. K. G. Watson looked at this enigmatic spectrum and analyzed it overnight; his name should have appeared as a coauthor.

The most telltale feature of this spectrum is the absence of any line over an interval of more than  $100 \text{ cm}^{-1}$  at  $\sim 2600 \text{ cm}^{-1}$ . This indicates that the carrier of this spectrum cannot occupy the lowest rotational state with no angular momentum ( $J=K=0$ ), called an *S* state by physicists of other disciplines. This is the fingerprint of a system composed of the three identical fermions with

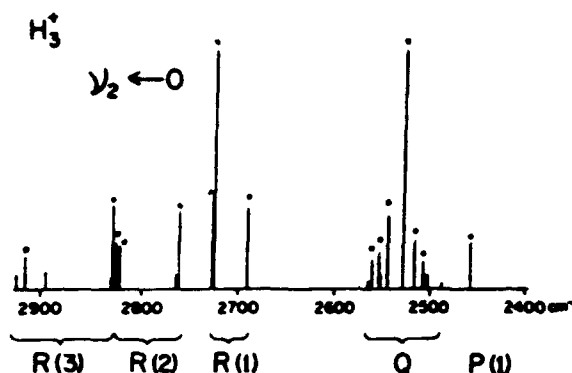


FIG. 2. Stick diagram of the first 15 lines of the  $\nu_2$  fundamental band of  $\text{H}_3^+$  observed in the laboratory (Oka, 1980). Observed lines are shown with asterisks.

spin  $\frac{1}{2}$ . An *S*-state eigenfunction is symmetric under both the odd permutation (12) and the even permutation (123) of nuclei and thus cannot satisfy the Pauli principle for the two operations simultaneously, regardless of the associated spin function. [An extra dimension of color was introduced in quantum chromodynamics to overcome this dilemma (Han and Nambu, 1965).]

Since the first observation of the  $\text{H}_3^+$  spectrum, which was made in a most primitive way, the sensitivity of molecular ion spectroscopy has been increased by at least three orders of magnitude by a variety of techniques. In particular, the velocity modulation method introduced by Gudeman, Saykally, and others (1983) has made an enormous impact on the field. A table recently published by Kao *et al.* (1991) lists 129 lines of the fundamental band, along with many more lines of other bands. Efforts are continually being made to reach higher rotational levels, anticipating their observation in some hot astronomical objects. By now we have reached the rotational state  $J=K=15$  ( $J$  and  $K$  are quantum numbers for rotational angular momentum and its projection to the  $C_3$  molecular axis) at  $5092 \text{ cm}^{-1}$  (0.63 eV) above the lowest rotational level.

One noteworthy independent development has been the laboratory observation of the  $\text{H}_3^+$  emission spectrum, which was made possible by use of a high-temperature hollow-cathode discharge ingeniously designed by Majewski, and of a high-resolution Fourier-transform spectrometer. The emission from such a discharge is dominated by the  $\text{H}_2$  emission spectrum, but Majewski, Watson, and others (1987) discriminated the  $\text{H}_3^+$  and  $\text{H}_2$  emissions through their intensity dependence on gas pressure. Majewski's spectrum contained not only the fundamental band but also overtone bands of  $\text{H}_3^+$ , and would play an important role in deciphering the  $2\text{-}\mu\text{m}$  Jovian emission spectrum (Majewski *et al.*, 1989).

#### B. Hot, overtone, and forbidden bands

The second phase of  $\text{H}_3^+$  laboratory spectroscopy was initiated in late 1987 as an attempt to detect other bands

<sup>2</sup>For an account from a different viewpoint, see Herzberg (1982).

of  $\text{H}_3^+$  which are weaker than the fundamental band by orders of magnitude. This project was motivated purely by our curiosity about the quantum mechanics of the excited vibrational states and about the dynamical behavior of  $\text{H}_3^+$  in plasmas. However, its results played a crucial role in the analysis of the then totally unexpected  $2\text{-}\mu\text{m}$  emission spectrum of Jupiter.

The vibrational energy-level structure of  $\text{H}_3^+$  is shown in Fig. 3; various observed transitions are shown by arrows. The normal vibrations of a triatomic equilateral triangle molecule are a textbook case, composed of the totally symmetric infrared-inactive  $\nu_1$  mode and the doubly degenerate infrared-active  $\nu_2$  mode. Bawendi, Reh-fuss and Oka (1990) observed the hot bands  $2\nu_2(2) \leftarrow \nu_2$ ,  $2\nu_2(0) \leftarrow \nu_2$ , and  $\nu_1 + \nu_2 \leftarrow \nu_1$ . These bands are weaker than the fundamental band by a factor of about 50 because of the Boltzmann factor for the excited vibrational states. Xu, Gabrys, and others observed the first-overtone band  $2\nu_2(2) \leftarrow 0$  (Xu *et al.*, 1990) and the forbidden bands  $\nu_1 \leftarrow 0$  and  $\nu_1 + \nu_2 \leftarrow \nu_2$  (Xu *et al.*, 1992), and Lee, Ventrudo, and others (1991) observed the second-overtone band  $3\nu_2(1) \leftarrow 0$ . These bands span the wavelength range of 5 to  $1.4\text{ }\mu\text{m}$ , requiring various laser technologies for their observation. The first principle calculations of Miller and Tennyson (Miller *et al.*, 1990, and references therein) have been indispensable for the analysis of the observed spectrum corresponding to high vibrational states.

The  $\text{H}_3^+$  emissions observed in Jupiter, corresponding to the overtone band  $2\nu_2(2) \rightarrow 0$  and to the fundamental band  $\nu_2 \rightarrow 0$ , are also indicated in Fig. 3 with bold arrows. Usually the overtone band is much weaker than the fundamental because of its smaller transition moment. The  $\text{H}_3^+$  ion is special in that, because of the large vibrational

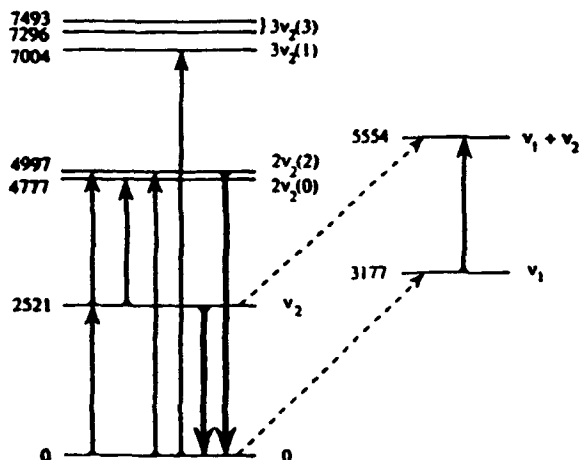


FIG. 3. Energy diagram showing the lower vibrational states of  $\text{H}_3^+$ . The bands observed in the laboratory are shown by arrows pointing upwards. The broken lines show observed forbidden transitions. Transitions observed in astronomical objects are shown by bold arrows pointing downwards. The numbers beside the levels give their energy in  $\text{cm}^{-1}$ . For example,  $3\nu_2(1)$  signifies  $\nu_2=3$  (vibrational quantum number) and  $l=1$  (vibrational angular momentum).

amplitude of its protons, the decrease of the transition moment is modest and it is compensated by the  $\nu^3$  factor in the Einstein coefficients for spontaneous emission, so much so that the value of  $A_{ij}$  for the overtone band ( $174\text{ s}^{-1}$ ) is actually larger than that for the fundamental band ( $124\text{ s}^{-1}$ ).

Experimental and theoretical efforts are being made to reach even higher vibrational and rotational states. Carrington, Buttenshaw, Kennedy, and others have observed a great many transitions of  $\text{H}_3^+$  near its dissociation limit. Their observations and many associated theoretical papers are outside the scope of this article (see Carrington and McNab, 1989, for a review).

#### IV. THE $\text{H}_3^+$ SPECTRUM IN SPACE

Immediately after the laboratory observation of the  $\text{H}_3^+$  spectrum, I attempted to detect it in absorption in the Orion Molecular Cloud and in other clouds that contain bright infrared objects (Oka, 1981). The euphoria induced by the laboratory detection made me neglect the theoretical prediction (Herbst and Klemperer, 1973) that, although the production rate of  $\text{H}_3^+$  is very high, its high reactivity, especially with CO, lowers the steady-state concentration. I was also hoping that the strong mysterious emission feature at  $3.4\text{ }\mu\text{m}$  reported by Merrill, Soifer, and Russell (1975) had something to do with  $\text{H}_3^+$ . (How naive of me; this feature is still unexplained.) The search for  $\text{H}_3^+$  in molecular clouds has continued to this day without success (Geballe and Oka, 1989; Black, van Dishoeck, and Woods, 1990). The possible detection of the submillimeter-wave rotational spectrum of  $\text{H}_2\text{D}^+$  (Phillips *et al.*, 1985) remains unconfirmed and controversial. However, the great increase in the sensitivity of spectrometers brought about by the use of multiple-diode detection arrays makes us optimistic that the discovery of  $\text{H}_3^+$  in molecular clouds is just around the corner. (Our next observation session is in July of this year. Perhaps . . .) Many theoretical papers (see Geballe and Oka, 1989, for a summary) predict  $\text{H}_3^+$  column densities on the order of  $\sim 10^{14}\text{ cm}^{-2}$ , which should be just detectable by the modern infrared spectrometer.

In the meantime the first detection of the  $\text{H}_3^+$  spectrum in Nature came from serendipitous discoveries in emission on an entirely unexpected object.

##### A. The $\text{H}_3^+$ emission from the Jovian auroral regions

Retrospectively, the first Jovian spectrum of  $\text{H}_3^+$  was recorded by Trafton and others using the McDonald Observatory infrared grating spectrometer. Their spectrum on the night of September 21, 1987 (Trafton, Lester, and Thompson, 1989) already showed the clear emission feature at  $2.093\text{ }\mu\text{m}$  which would later be assigned to the  $(J, G, U = 7, 9, +1) \rightarrow (J, K = 6, 6)$  transition of the  $2\nu_2(2) \rightarrow 0$  overtone band of  $\text{H}_3^+$ . Their spectrum, pub-

lished in 1989 as still unidentified, is shown in Fig. 4. Note the  $H_2$  S(1) quadrupole emission line at  $2.121 \mu m$  (remember the strong line in Fig. 1). These authors were primarily studying this  $H_2$  emission from Jupiter and accidentally stumbled on the rich emission features due to  $H_3^+$ .

The same emission features were observed more extensively in higher resolution at the Canada-France-Hawaii Telescope with the Fourier transform infrared spectrometer (FTIR) during the night of September 24, 1988 (Drossart *et al.*, 1989). This observation was made as a part of a systematic study of Jovian auroral activity (Kim and Maguire, 1986) during the International Jupiter Watch Week. The emission was observed only in the auroral regions at the northern and southern poles. The results were reported at the Austin DPS meeting in October 1988 (Kim *et al.*, 1988), and the possibility of emission from hydrocarbon free radicals or  $H_3^+$  was suggested. A list of the strange emission lines was sent to the Herzberg Institute of Astrophysics in late October and caused quite a sensation (which I witnessed when I gave seminars at the Institute on November 3 and 4). Majewski had recorded an extensive FTIR emission spectrum from a laboratory  $H_2$  plasma in the same wavelength region, and this spectrum contained extremely rich spectra of  $H_2$ ,  $H_3$ , and  $H_3^+$ , which are all good candidates. After a month's work J. K. G. Watson, who had earlier analyzed the first laboratory  $H_3^+$  spectrum, came to the understanding of the Jovian spectrum as due to the  $2\nu_2(2) \rightarrow 0$  band of  $H_3^+$ . Crucial to his solution were the laboratory data of the  $2\nu(2) \rightarrow \nu_2$  hot band provided by Bawendi *et al.* (1990), the analysis of which is based on the theoretical calculations of Miller and Tennyson (1989). The initial guesses, uncertainties, heated discussions, and the sudden final solution are vividly recorded in extensive E-mail correspondences between Paris (J.-P.

Maillard), Ottawa (P. A. Feldman and J. K. G. Watson), and London (S. Miller), with recurring references to Bawendi, Dabrowski, Drossart, Herzberg, Majewski, Oka, Tarrago, and Vervloet. The close collaboration of astronomers, laboratory spectroscopists, and theorists is characteristic of this field.

After the  $2\text{-}\mu m$  emission was attributed to the  $2\nu_2(2) \rightarrow 0$  overtone band of  $H_3^+$ , it was natural to expect the fundamental band  $\nu_2 \rightarrow 0$  to appear even more strongly. The observation of this band was made at the United Kingdom Infrared Telescope (UKIRT) in the morning on September 14–19, 1989 using the grating spectrometer CGS2 (Oka and Geballe, 1990). Ten strong emission lines of  $H_3^+$  corresponding to the  $Q(\Delta J=0)$  branch of the fundamental band were observed in the  $4\text{-}\mu m$  region. The previously detected  $2\text{-}\mu m$  emission was not detected, in spite of our efforts during September 9 and 10, indicating significant temporal variations of the Jovian plasmas. The much higher observed intensity of the  $4\text{-}\mu m$  fundamental band compared to that of the overtone band suggested that the observed emission does not originate from freshly produced  $H_3^+$  but from  $H_3^+$  in thermal equilibrium at temperatures of 1100 K (Drossart *et al.*, 1989) to 670 K (Oka and Geballe, 1990), collisionally excited to high vibrational states by  $H_2$  and He. This was established by Miller, Joseph, and Tennyson (1990) in their subsequent observations of the  $2\text{-}\mu m$  and the  $4\text{-}\mu m$  emissions.

The beautiful FTIR results on the  $H_3^+$  fundamental band observed by Maillard *et al.* (1990) give the best panoramic view of the band (Fig. 5). The advantage of the wide-frequency coverage due to the Fourier-transform method is clearly demonstrated. All of the stronger observed lines are assigned to the fundamental band of  $H_3^+$ . The amazing characteristic of this spectrum is that its background infrared emission is almost nonexistent. In particular, in the region of  $2600$  to  $2900 \text{ cm}^{-1}$ , the background is almost completely flat and virtually zero. Jupiter is still cooling and is radiating much of its heat in the infrared. It is also reflecting the solar radiation. However, the infrared radiation in this wavelength region is almost completely wiped out by the pressure-broadened absorption of  $CH_4$  (see, for example, Larson *et al.*, 1980).  $CH_4$  molecules exist abundantly in the low-altitude, low-temperature Jovian atmosphere and convert radiative energy to kinetic energy. Only the  $H_3^+$  emission occurring at the high altitudes of the ionosphere reaches us unabsorbed! When comparing the  $2600\text{--}2900 \text{ cm}^{-1}$  in Fig. 5 with the laboratory spectrum of Fig. 2, the agreement is breathtaking.

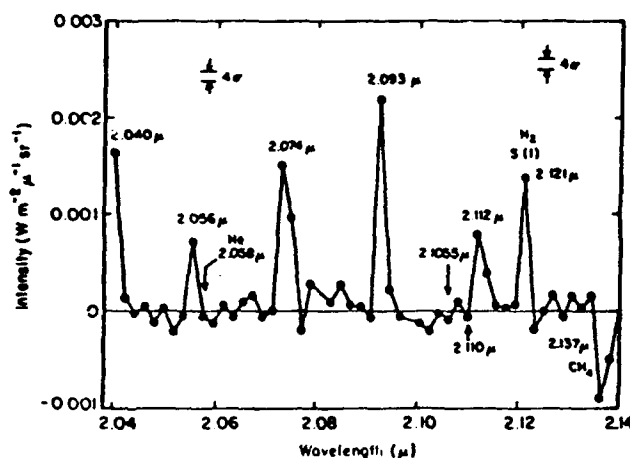


FIG. 4. The  $2\text{-}\mu m$  Jovian emission spectrum reported by Trafletton, Lester, and Thompson (1989). They were studying the S(1)  $H_2$  quadrupole emission line at  $2.121 \mu m$  (also shown in Fig. 1) and accidentally observed the other emission lines due to  $H_3^+$ . The spectrum was recorded using the McDonald Observatory infrared grating spectrometer.

#### B. The colossal Jovian plasma

The infrared emission from Jupiter is so intense that a brief integration suffices to see it very strongly. None of us was sufficiently imaginative to think about this possibility until it was discovered accidentally, providing yet

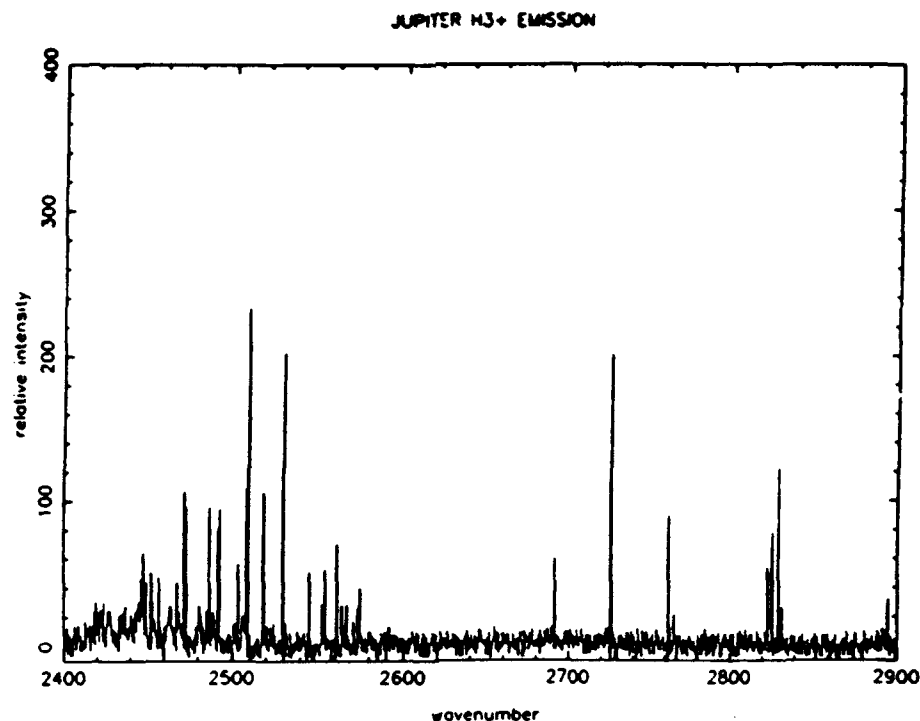


FIG. 5. The apodized  $H_3^+$  emission spectrum from the southern auroral zone of Jupiter recorded by Maillard *et al.* (1990) using the Canada-France-Hawaii Telescope Fourier-transform spectrometer. The spectral lines from 2600 to 2900  $\text{cm}^{-1}$  match perfectly with the laboratory spectrum of Fig. 2. The spectral lines in the region of 2400  $\text{cm}^{-1}$  have different relative intensities because of the higher temperature in Jupiter plasmas (1100 K) compared to the liquid-nitrogen-cooled laboratory plasmas (200 K).

another example of how we are all nitwits up against Nature. For nearly ten years I had been searching for the spectrum in objects that are thousands of light years away while the strong signal was waiting to be observed in an object only 40 light minutes away! As usual it is obvious after the fact that the auroral regions of the Jovian ionosphere provide ideal conditions for  $H_3^+$  plasmas (see Dessler, 1983). In fact,  $H_3^+$  ion had been detected *in situ* in the Jovian magnetosphere by the low-energy-charged-particle instrument on the two *Voyager* spacecraft. (Hamilton *et al.*, 1980; Krimigis and Roelof, 1983). The theoretical chemical model by McConnell and Majeed (1987) had predicted an  $H_3^+$  column density on the order of  $10^{13} \text{ cm}^{-2}$  in the Jovian ionosphere, which approximately matches the observed values (Oka and Geballe, 1990).

Jupiter is a big blob (mean radius  $\sim 70\,000 \text{ km}$ ) of supercritical fluid composed of hydrogen and helium. Because of the high gravitational pressure, hydrogen at a depth of 25 000 km from the surface into the core is believed to be metallic fluid with good electrical conductivity. Perhaps because of this (see, for example, Levy, 1989), the magnetic field of Jupiter is very high. Its magnetic moment is established (Dessler, 1983) to be  $4.3 \text{ GR}_J^3$  ( $1.4 \times 10^{30} \text{ gauss cm}^3$ ), more than four orders of magnitude higher than that of the Earth. This large magnetic field rotates along with Jupiter with a relatively short period ( $\sim 10 \text{ h}$ ), sweeping charged particles around. The charged species are trapped by the magnetic field

and corotate with Jupiter at great speed. This magnetic field not only rotates but also wobbles because the Jovian rotation axis is  $10^\circ$  off from the magnetic dipole axis. To this gigantic plasma, the ejecta from the moon Io add fuel (Fig. 6). Io's rotational period is 1.8 days, and thus Io is overtaken by the rotating field and its trapped species. The differential speed,  $v \sim 57 \text{ km s}^{-1}$  at Io ( $\sim 400\,000 \text{ km}$  from Jupiter), for a proton corresponds to the energy of  $\sim 16 \text{ eV}$ , sufficient to ionize ejecta from Io which are mostly oxygen and sulfur. The magnetic field  $B$  ( $\sim 20 \text{ mG}$ ) moving with respect to Io induces a relativistic electric field  $E = (v \times B)/c$  of  $\sim 0.11 \text{ V/m}$  along the direction from Jupiter to Io. This electric field, amounting to a potential difference of 400 kV across Io, accelerates the ion-

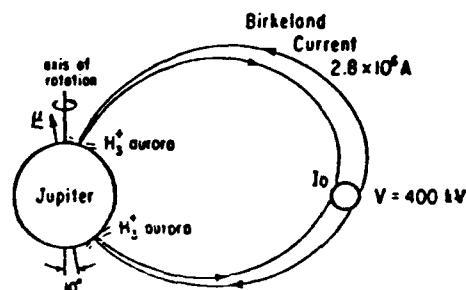


FIG. 6. Simplified schematic picture of the Jupiter-Io plasma power induction (Piddington and Drake, 1968). The diameter of Io is magnified by a factor of 10 for clarity. Other relative distances are to scale.

ized species. The ions and electrons thus accelerated move along the magnetic field and reach Jupiter (Pidgington and Drake, 1968). The field-aligned electric current has been estimated from the *Voyager 1* observation to be  $2.8 \times 10^6$  A (Acuña, Neubauer, and Ness, 1981). This enormous Birkeland current is focused onto the magnetic poles of Jupiter, flows through the ionosphere, and then returns back to Io along the magnetic field. Such a colossal Jupiter-Io plasma activity, amounting to a total power dissipation of  $\sim 1 \times 10^{12}$  W, was initially suggested from the Jovian decametric radio emission and was later observed more directly by the *Voyagers* during their close encounters with Jupiter (Dessler, 1983).

We can now monitor the infrared aurora thus produced through the  $\text{H}_3^+$  spectrum from ground-based observatories. As mentioned earlier, the Jovian infrared emission in a certain wavelength region is almost purely due to  $\text{H}_3^+$ . Thus a high-resolution spectrometer is not needed for such observation; a narrow-band filter and an infrared camera suffice. Two such papers have appeared showing detailed morphology and the fast temporal variation of the auroral activity (Kim *et al.*, 1991; Baron *et al.*, 1991).

#### C. $\text{H}_3^+$ in Supernova 1987A (17)

A most surprising paper appeared early this year in which Miller, Tennyson, Lepp, and Dalgarno (1992) claimed identification of  $\text{H}_3^+$  emission in the infrared spectrum of Supernova 1987A reported by Meikle *et al.* (1989). A comparison of the observed spectrum of SN 1987A on day 192 and a computed  $\text{H}_3^+$  fundamental spectrum is shown in Fig. 7. Here the observed spectrum is Doppler broadened by the high speed of materials in the ejecta, and it is impossible to rely on the clear fingerprint of rotational structure. Therefore the identification is nowhere near as definitive as in the Jovian spectrum discussed previously or in the Uranus spectrum to be discussed below. Nevertheless, the agreement between the observed and calculated spectrum is quite remarkable, especially for the feature at  $3.54 \mu\text{m}$  dominated by the strongest:  $4,3,1 \rightarrow 3,3$  transition. The agreement in the other wavelength region is not as impressive. Since the spectroscopic evidence is not as definitive as in other cases, other circumstantial evidence is called for: (a) no known atomic spectrum can explain the observed features, and (b) it is indeed possible that a large amount ( $\sim 1 \times 10^{-7} M_\odot$ ) of  $\text{H}_3^+$  is produced in a type-II supernova in  $\sim 100$  days.

The appearance of abundant molecular species in a supernova in such a short time interval is certainly incredible but has good observational support in the characteristic R-branch head of the  $\Delta v = 2$  CO overtone bands in emission reported by Spyromilio *et al.* (1988; remember the same bands in Fig. 1). Molecules are definitely there in 192 days. Studying the chemical evolution of a supernova in 100 days is somewhat like doing the same for the

#### Supernova 1987a

Day 192 (Meikle *et al.*)

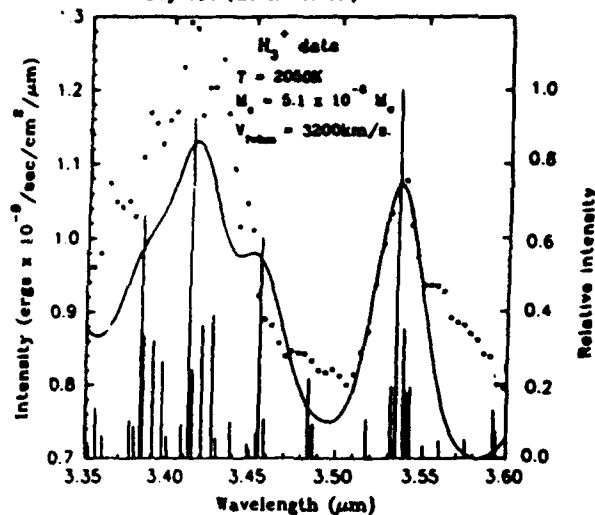


FIG. 7. Emission spectrum of Supernova 1987A on day 192: filled circles, observed results of Meikle *et al.* (1989); solid curve, computer-convoluted  $\text{H}_3^+ v_2 \rightarrow 0$  spectrum calculated by Miller *et al.* (1992).

big bang in 10 billion years. Lepp and Dalgarno applied their theory of molecular formation in primordial molecular clouds, coming up indeed with  $\text{H}_3^+$  of mass  $\sim 1 \times 10^{-7} M_\odot$  in 100 days.

One disturbing aspect of this identification is the glaring mismatch between the assumed low rotational temperature (2050 K, 1000 K) and the high kinetic temperature expected from the high expansion velocity ( $3200 \text{ km s}^{-1}$ ). The infrared and far-infrared emission through forbidden rotational transitions with lifetimes on the order of minutes to hours (Pan and Oka, 1986) will lower the rotational temperature, but whether this process is efficient enough to explain the observed results remains to be seen. Now, five years after the event, the supernova remnant is diffuse and much of the  $\text{H}_3^+$  is dissociated. The identification of  $\text{H}_3^+$  in SN 1987A will probably stay somewhat controversial. The arrival of the next bright supernova radiation (which must be on its way) is awaited. Infrared astronomers of the world, stay tuned.

#### D. The $\text{H}_3^+$ emission from Uranus

On April 1 of this year, extremely strong emission of  $\text{H}_3^+$  was detected in Uranus by Trafton, Geballe, and Miller (Geballe, private communication) using the UKIRT CGS4 spectrometer. The twelve observed features between  $3.90$  and  $4.07 \mu\text{m}$  comprise 21 Q-branch transitions of the  $v_2$  fundamental band. Uranus has a smaller diameter than Jupiter ( $\sim \frac{1}{3}$ ) and is farther from Earth ( $\sim 4\times$ ). Despite those facts, the intensity of the



$H_3^+$  spectrum is very high and suggests tempestuous plasma activity in Uranus, whose magnetic dipole axis is tilted from the axis of rotation by  $58.6^\circ$ . This is amazing in view of the small magnetic moment of Uranus ( $\sim 1/410$  that of Jupiter). By the way, the search for  $H_3^+$  emission in Saturn produced negative results in spite of good integration over two nights (Geballe and Oka, unpublished). Results of the search in Neptune are also negative thus far.

## V. FINAL REMARKS

I conclude this article with a rough projection for the future.

(1) Molecular astrophysics will grow further and will provide crucial information for our understanding of star formation. Observational infrared spectroscopy will play a major role in its development. The increasing sensitivity of spectrometers in the last few years has been phenomenal.

(2) With the new tunable-laser sources (InGaAsP communication diode, Ti-sapphire laser), laboratory  $H_3^+$  spectroscopy will reach high vibration-rotation states near or above the barrier for linearity. A new theoretical formulation will be needed to account for such states.

(3) The  $H_3^+$  spectrum will be observed in many astronomical objects and will become a common astronomical probe for the study of ionized regions. Past experience has shown that it is almost impossible to predict in precisely which object  $H_3^+$  will appear. The proposal to attempt  $H_3^+$  observation in NGC 6240 is thrilling (Draine and Woods, 1990).

(4) Following the laboratory observation of the  $H_3^+$  spectrum, spectra of many other fundamental molecular ions such as  $CH_2^+$ ,  $CH_3^+$ ,  $C_2H_2^+$ ,  $C_2H_3^+$ ,  $NH_2^+$ ,  $NH_3^+$ ,  $NH_4^+$ ,  $H_2O^+$ ,  $H_3O^+$  have been observed, all of which are key ingredients in interstellar chemistry. Their infrared spectra will also be detected in astronomical objects.

Finally, a word of caution. Space constraints and the limitations of my own training have forced me to simplify some complex subjects in this colloquium—perhaps, from the viewpoint of a specialist, to oversimplify. The reader is advised to consult the references in infrared astronomy, interstellar chemistry, theoretical astrophysics, ion kinetics, planetary science, and plasma physics for more detailed treatments of the many subfields that contribute to the fascination of this topic.

*Note added in proof.* After submission of this manuscript, we have detected the  $H_3^+$   $v_2$  band emission in Saturn (Geballe, Jagod, and Oka, unpublished). The emission observed in Saturn's polar regions is weaker than that from Jupiter by a few orders of magnitude, but the great improvement in the sensitivity of our spectrometer has led us to a clear detection of three vibration-rotation transitions:  $pR(1,0)$  at  $2725.898\text{ cm}^{-1}$ ,  $rR(1,1)$  at  $2726.923\text{ cm}^{-1}$ , and  $rR(3,3)$  at  $2829.923\text{ cm}^{-1}$ .

## ACKNOWLEDGMENTS

I wish to thank M. G. Bawendi, S. Chandrasekhar, U. Fano, P. A. Feldman, C. M. Gabrya, T. R. Geballe, G. Herzberg, M.-F. Jagod, T. Kawai, W. Klemperer, J.-P. Maillard, S. Miller, Y. Nambu, H. Sasada, K. Shimoda, K. Takagi, C. H. Townes, L. Trafton, J. K. G. Watson, and D. P. Weliky for reading this paper. Our work in this article has been supported by NSF Grants PHY-81-13097, PHY-84-08316, PHY-87-07025, PHY-90-22647 and partially also by Air Force Grants F04611-86-K-0069 and F33615-90C-2035.

## REFERENCES

- Acuña, M. H., F. M. Neubauer, and N. F. Ness, 1981, *J. Geophys. Res.* **86**, 8513.  
 Baron, R., R. D. Joseph, T. Owen, J. Tennyson, S. Miller, and G. E. Ballester, 1991, *Nature* **353**, 539.  
 Bawendi, M. G., B. D. Rehfuss, and T. Oka, 1990, *J. Chem. Phys.* **93**, 6200.  
 Black, J. H., E. F. van Dishoeck, S. P. Willner, and R. C. Woods, 1990, *Astrophys. J.* **358**, 459.  
 Bohr, N., 1919, *Medd. K. Vet.-Akad. S. Nobelinstitut* **5**, 1.  
 Buhl, D., and L. E. Snyder, 1970, *Nature* **228**, 267.  
 Carney, G. D., and R. N. Porter, 1974, *J. Chem. Phys.* **60**, 4251.  
 Carney, G. D., and R. N. Porter, 1976, *J. Chem. Phys.* **65**, 3547.  
 Carrington, A., and I. R. McNab, 1989, *Acc. Chem. Res.* **22**, 218.  
 Cheung, A. C., D. M. Rank, C. H. Townes, D. D. Thornton, and W. J. Welch, 1968, *Phys. Rev. Lett.* **21**, 1701.  
 Christoffersen, R. E., S. Hagstrom, and F. Prosser, 1964, *J. Chem. Phys.* **40**, 236.  
 Conroy, H., 1964a, *J. Chem. Phys.* **40**, 603.  
 Conroy, H., 1964b, *J. Chem. Phys.* **41**, 1341.  
 Dalgarno, A., and J. H. Black, 1976, *Rep. Prog. Phys.* **39**, 573.  
 Dempster, A. J., 1916, *Philos. Mag.* **31**, 438.  
 Dessler, A. J., 1983, Ed., *Physics of the Jovian Magnetosphere* (Cambridge University, Cambridge, England).  
 Draine, B. T., and D. T. Woods, 1990, *Astrophys. J.* **363**, 464.  
 Drossart, P., J.-P. Maillard, J. Caldwell, S. J. Kim, J. K. G. Watson, W. A. Majewski, J. Tennyson, S. Miller, S. K. Atreya, J. T. Clarke, J. H. Waite, Jr., and R. Wagoner, 1989, *Nature* **340**, 539.  
 Geballe, T. R., and T. Oka, 1989, *Astrophys. J.* **342**, 855.  
 Gudeman, C. S., M. H. Begemann, J. Pfaff, and R. J. Saykally, 1983, *Phys. Rev. Lett.* **50**, 727.  
 Hamilton, D. C., G. Gloeckler, S. M. Krimigis, C. O. Bostrom, T. P. Armstrong, W. I. Axford, C. Y. Fan, L. J. Lagerotti, and D. M. Hunten, 1980, *Geophys. Res. Lett.* **7**, 813.  
 Han, M. Y., and Y. Nambu, 1965, *Phys. Rev.* **139**, B1006.  
 Herbst, E., and W. Klemperer, 1973, *Astrophys. J.* **185**, 505.  
 Herzberg, G., 1949, *Nature* **163**, 170.  
 Herzberg, G., 1967, *Trans. R. Soc. Can.* **5**, 3.  
 Herzberg, G., 1979, *J. Chem. Phys.* **70**, 4806.  
 Herzberg, G., 1982, *Trans. R. Soc. Can.* **20**, 151.  
 Herzberg, G., H. Lew, J. J. Sloan, and J. K. G. Watson, 1981, *Can. J. Phys.* **59**, 428.  
 Hirschfelder, J. O., 1938, *J. Chem. Phys.* **6**, 795.  
 Hogness, T. R., and E. G. Lunn, 1925, *Phys. Rev.* **26**, 44.  
 Joseph, R. D., G. S. Wright, and R. Wade, 1984, *Nature* **311**,

132.  
 Kao, L., T. Oka, S. Miller, and J. Tennyson, 1991, *Astrophys. J. Suppl.* 77, 317.  
 Kim, S. J., P. Drossart, J. Caldwell, J.-P. Maillard, J. T. Clarke, and S. K. Atreya, 1988, *Bull. AAS* 20, 1125.  
 Kim, S. J., P. Drossart, J. Caldwell, J.-P. Maillard, T. Herbst, and M. Shure, 1991, *Nature* 353, 536.  
 Kim, S. J., and W. Maguire, 1986, in *The Jovian Atmospheres* (NASA Conference Publication 2441), p. 95.  
 Klemperer, W., 1970, *Nature* 227, 1230.  
 Krimigis, S. M., and E. C. Roelof, 1983, in *Physics of the Jovian Magnetosphere*, edited by A. J. Dessler (Cambridge University, Cambridge, England), p. 106.  
 Larson, H. P., U. Fink, H. A. Smith, and D. S. Davis, 1980, *Astrophys. J.* 240, 327.  
 Lee, S. S., B. F. Ventrudo, D. T. Cassidy, T. Oka, S. Miller, and J. Tennyson, 1991, *J. Mol. Spectrosc.* 145, 222.  
 Levy, E. H., 1989, in *Time-Variable Phenomena in the Jovian System*, edited by M. J. S. Belton, R. A. West, and J. Rahe, NASA SP-494.  
 Maillard, J.-P., P. Drossart, J. K. G. Watson, S. J. Kim, and J. Caldwell, 1990, *Astrophys. J.* 363, L37.  
 Majewski, W. A., M. D. Marshall, A. R. W. McKellar, J. W. C. Johns, and J. K. G. Watson, 1987, *J. Mol. Spectrosc.* 122, 341.  
 Majewski, W. A., P. A. Feldman, J. K. G. Watson, S. Miller, and J. Tennyson, 1989, *Astrophys. J.* 347, L51.  
 McConnell, J. C., and T. Majeed, 1987, *J. Geophys. Res.* 92, 8570.  
 Meikle, W. P. S., D. A. Allen, J. Spyromilio, and G. F. Varani, 1989, *Mon. Not. R. Astron. Soc.* 238, 193.  
 Merrill, K. M., B. T. Soifer, and R. W. Russell, 1975, *Astrophys. J.* 200, L37.  
 Meyer, W., P. Botschwina, and P. Burton, 1986, *J. Chem. Phys.* 84, 891.  
 Miller, S., R. D. Joseph, and J. Tennyson, 1990, *Astrophys. J.* 368, L55.  
 Miller, S., and J. Tennyson, 1989, *J. Mol. Spectrosc.* 136, 223.  
 Miller, S., J. Tennyson, S. Lepp, and A. Dalgarno, 1992, *Nature* 355, 420.  
 Miller, S., J. Tennyson, and B. T. Sutcliffe, 1990, *J. Mol. Spectrosc.* 141, 104.  
 Oka, T., 1980, *Phys. Rev. Lett.* 45, 531.  
 Oka, T., 1981, *Philos. Trans. R. Soc. London, Ser. A* 303, 543.  
 Oka, T., 1983, in *Molecular Ions: Spectroscopy, Structure and Chemistry*, edited by T. A. Miller and V. E. Bondybey (North-Holland, New York), p. 73.  
 Oka, T., and T. R. Geballe, 1990, *Astrophys. J.* 351, L53.  
 Pan, F. S., and T. Oka, 1986, *Astrophys. J.* 305, 518.  
 Phillips, T. G., G. A. Blake, J. Keene, R. C. Woods, and E. D. Churchwell, 1985, *Astrophys. J.* 294, L45.  
 Piddington, J. H., and J. F. Drake, 1968, *Nature* 217, 935.  
 Pine, A. S., 1974, *J. Opt. Soc. Am.* 64, 1683.  
 Pollard, J. E., L. K. Johnson, D. A. Lichtin, and R. B. Cohen, 1991, *J. Chem. Phys.* 95, 4877.  
 Porter, R. N., 1982, *Ber. Bunsenges. Phys. Chem.* 86, 407.  
 Spyromilio, J., W. P. S. Meikle, R. C. M. Learner, and D. A. Allen, 1988, *Nature* 334, 327.  
 Suzuki, H., 1989, in *Toward Interstellar Chemistry*, edited by N. Kaifu (University of Tokyo, Tokyo).  
 Thomson, J. J., 1912, *Philos. Mag.* 24, 209.  
 Trafton, L., D. F. Lester, and K. L. Thompson, 1989, *Astrophys. J.* 343, L73.  
 Watson, W. D., 1976, *Rev. Mod. Phys.* 48, 513.  
 Woods, R. C., T. A. Dixon, R. J. Saykally, and P. G. Szanto, 1975, *Phys. Rev. Lett.* 35, 1269.  
 Xu, L.-W., C. M. Gabrys, and T. Oka, 1990, *J. Chem. Phys.* 93, 6210.  
 Xu, L.-W., M. Rösslein, C. M. Gabrys, and T. Oka, 1992, *J. Mol. Spectrosc.* 153, 726.